# DEVELOPMENT OF POLYHIPE GRAFTS FOR GUIDED BONE REGENERATION

A Dissertation

by

MICHAEL EDWARD WHITELY JR

Submitted to the Office of Graduate and Professional Studies of
Texas A&M University
in partial fulfillment of the requirements for the degree of

DOCTOR OF PHILOSOPHY

| | |
|---|---|
| Chair of Committee, | Elizabeth Cosgriff-Hernandez |
| Co-Chair of Committee, | Akhilesh Gaharwar |
| Committee Members, | Roland Kaunas |
| | William B. Saunders |
| Head of Department, | Michael McShane |

August 2018

Major Subject: Biomedical Engineering

# ABSTRACT

A pressing need exists to develop an improved bone replacement to treat the millions of non-union fractures that occur each year as a result of severe trauma, tumor resection, spinal fusions, and joint replacements. Current bone grafts are often hindered by a lack of biodegradability, porosity or innate ability to promote regeneration. This work employs tissue engineering to design a novel bone replacement that combines the regenerative potential of autologous tissue with the tunability of synthetic grafts. This is accomplished by engineering a biodegradable scaffold with physical and mechanical properties emulating those of cancellous bone and combining this scaffold with technologies that allow for the controlled delivery of stem cells and osteoinductive factors.

In this work, polymerized high internal phase emulsions (polyHIPEs) were developed as an injectable, high porosity bone graft. Thiol-methacrylate polyHIPEs were investigated to increase resistance to oxygen inhibition and improve scaffold function under clinically relevant conditions. Methods were established to modulate and characterize scaffold porosity, cure rate, compressive properties, and degradation rates. Furthermore, cell-laden poly(ethylene glycol)-dithiothreitol hydrogels were developed to improve loading and distribution of human mesenchymal stem cells (hMSCs) within 3D printed polyHIPEs. This approach allowed for increased cell retention and supported critical markers of osteoblastic differentiation. Finally, to confer additional osteoinductive character, porous microspheres with tunable release kinetics and requisite compressive properties were fabricated using a solvent-free, in-line loading approach. Bioactivity

retention of encapsulated bone morphogenetic protein-2, along with its ability to promote osteoblastic differentiation of hMSCs, was explored.

Overall, these studies highlight the strong potential of polyHIPE scaffolds to serve as an improved bone replacement with the ability to actively guide bone regeneration. Key technologies have been developed that allow for fabrication of a bone graft with improved function in a clinically relevant setting, efficient seeding with mesenchymal stem cells, and targeted delivery of osteoinductive factors. Fundamentally, this work will be an invaluable tool in identifying and evaluating critical design requirements for future bone graft design.

# DEDICATION

To all who helped me see that where you start doesn't have to determine where you finish.

# ACKNOWLEDGEMENTS

I can't adequately express the appreciation I feel for all those who have helped me over the past five years. Graduate school has been one of the most transformative periods of my life, not just professionally, but personally as well. These experiences have opened up opportunities and ways of thinking that I could have never imagined even a few short years ago, and helped me prove to myself that our success in life is not determined by our beginnings.

First, thank you to my advisor, Dr. Elizabeth Cosgriff-Hernandez, for taking a chance and offering me an opportunity in her lab, even before I truly knew what it meant to be a graduate student. You have helped me see and appreciate my strengths and challenged me to grow and overcome my weaknesses. I will always be grateful for your patience and guidance in helping me achieve something that I had never imagined possible.

Thank you to my committee, Dr. Akhilesh Gaharwar, Dr. Roland Kaunas, and Dr. Brian Saunders, for your wonderful insight and guidance through this process. I have greatly enjoyed learning from and working alongside you. Thank you to the LSAMP community for your support, encouragement, and constant reminder of what is possible.

As challenging and rewarding as this adventure has been, it has been made so much more enjoyable being surrounded and supported by great lab mates. I'm forever indebted to Bobby Moglia and Jenny Robinson for your patience and generosity in teaching me all the basics of research. To the original IBT crew, Alysha Kishan and Allison Post, for the laughs, encouragement and research support during a time when we were all trying to

figure out how to survive in graduate school. To Nick Sears, for being a great source of knowledge and inspiring me to not just think outside the box, but to build a new box. To Thomas Wilems, for your insightful advice and mentoring as I finished up my studies. To Prachi Dhavalikar, for your tremendous help with the encapsulation work and always making me feel far more confident than I actually was. To Sahar Mohiuddin, for your steadfast reliability and patience with my inability to multitask. To Gabriel Rodriguez-Rivera for your innovative ideas and willingness to explore new directions. To all the members of the UT team, Taneidra Buie, Ziyang Lan, Siliang Wu and Megan Wancura for your willingness to always help, give new ideas and share a kind word. And to Stacy Cereceres, for leading Team College Station to the finish line with a joyous outlook, unquestionable selflessness, and most importantly, lasting friendship.

Finally, to my wife, the constant that holds my life together and the person I strive to be. I can never thank you enough for the support, sacrifice and love you have given during this process. Anything I am able to do is only because I know that I have you beside me.

## CONTRIBUTORS AND FUNDING SOURCES

This work was supported by a dissertation committee consisting of Dr. Elizabeth Cosgriff-Hernandez (chair), Dr. Akhilesh Gaharwar (co-chair) and Dr. Roland Kaunas (member) of the Department of Biomedical Engineering, and Dr. William B. Saunders (member) of the Department of Veterinary Small Animal Clinical Sciences.

Animal studies and histological analysis for Chapter II was performed by Dr. William B. Saunders. Reporter cells utilized in Chapter IV were generously provided by the lab of Dr. Daniel Alge. All other work conducted for the dissertation was completed independently.

Graduate study was supported by The Texas A&M LSAMP NSF Bridge to the Doctorate Fellowship and the Texas A&M Dissertation Fellowship.

# NOMENCLATURE

| | |
|---|---|
| APS | Ammonium Persulfate |
| BDMA | 1,4 Butane Diol Dimethacrylate |
| BMP | Bone Morphogenetic Protein |
| BPO | Benzoyl Peroxide |
| BRITIER | BMP Responsive Reporter Cell Line |
| DTT | Dithiothreitol |
| ECM | Extracellular Matrix |
| EGDMA | Ethylene Glycol Dimethacrylate |
| FBS | Fetal Bovine Serum |
| FGF | Fibroblast Growth Factor |
| GM | Growth Media |
| hMSC | Human Mesenchymal Stem Cell |
| HQ | Hydroquinone |
| IG | Iron Gluconate Dihydrate |
| IGF | Insulin-like Growth Factor |
| OM | Osteogenic Media |
| PBS | Phosphate Buffered Saline |
| PDGF | Platelet Derived Growth Factor |
| PEG | Poly(ethylene glycol) |
| PFDMA | Propylene Fumarate Dimethacrylate |

| | |
|---|---|
| PGPR | Polyglycerol polyricinoleate |
| PLA | Poly(lactic acid) |
| PLGA | Poly(lactide-co-glycolide) |
| PMMA | Poly(methyl methacrylate) |
| PolyHIPE | Polymerized High Internal Phase Emulsion |
| RGD | Arginine-Glycine-Aspartic Acid |
| TGF | Transforming Growth Factor |
| TMA | 4, N,N - Trimethylaniline |
| VEGF | Vascular Endothelial Growth Factor |

TABLE OF CONTENTS

Page

ABSTRACT ..... ii

DEDICATION ..... iv

ACKNOWLEDGEMENTS ..... v

CONTRIBUTORS AND FUNDING SOURCES ..... vii

NOMENCLATURE ..... viii

TABLE OF CONTENTS ..... x

LIST OF FIGURES ..... xii

LIST OF TABLES ..... xvi

CHAPTER I INTRODUCTION AND LITERATURE REVIEW ..... 1

1.1. Clinical Overview ..... 1
1.2. Current Treatment Options ..... 4
1.3. Tissue Engineered Scaffolds ..... 5
1.4. Mesenchymal Stem Cells in Bone Tissue Engineering ..... 9
1.5. Growth Factor Delivery in Bone Tissue Engineering ..... 17
1.6. Summary and Approach ..... 23

CHAPTER II THIOL-METHACRYLATE POLYHIPES WITH IMPROVED RESISTANCE TO OXYGEN INHIBITION ..... 25

2.1. Introduction ..... 25
2.2. Materials and Methods ..... 29
2.3. Results and Discussion ..... 40
2.4. Conclusions ..... 64

CHAPTER III IMPROVED IN SITU SEEDING OF 3D PRINTED BONE GRAFTS USING CELL-RELEASING HYDROGELS ..... 65

3.1. Introduction ..... 65
3.2. Materials and Methods ..... 69
3.3. Results and Discussion ..... 75

3.4. Conclusions ..... 92

CHAPTER IV TUNABLE RELEASE OF BMP-2 FROM POROUS POLYHIPE MICROSPHERES ..... 93

4.1. Introduction ..... 93
4.2. Materials and Methods ..... 96
4.3. Results and Discussion ..... 103
4.4. Conclusions ..... 117

CHAPTER V CONCLUSIONS ..... 118

5.1. Summary ..... 118
5.2. Significance of Work ..... 120
5.3. Challenges and Future Directions ..... 123

REFERENCES ..... 128

LIST OF FIGURES

Page

Figure 2.1. Molecular structure of propylene fumarate dimethacrylate (PFDMA) (A) and pentaerythritol tetrakis(3-mercaptoproprionate) (tetrathiol) (B). Reprinted from Whitely *et al*.[146] ..... 32

Figure 2.2. Representative scanning electron microscopy (SEM) micrographs of PFDMA (A), PFDMA-5T (B), and PFDMA-10T (C) polyHIPE pore architecture. Reprinted from Whitely *et al*.[146] ..... 41

Figure 2.3. Storage modulus during polymerization of polyHIPE (A) and work and set times (B) of polyHIPEs cured at 37 °C with 1.0 wt% initiator and reducing agent. Reprinted from Whitely *et al*.[146] ..... 43

Figure 2.4. The effect of increasing tetrathiol concentration on average gel fraction for high surface-area-to-volume ratio polyHIPEs cured under ambient and low oxygen conditions (A) and bulk cured polyHIPEs cured under ambient conditions (B). Reprinted from Whitely *et al*.[146] ..... 46

Figure 2.5. The effect of hydroquinone inhibitor (A) on average storage time (B), work and set time (C), and gel fraction (D) of thiol-methacrylate polyHIPEs. Reprinted from Whitely *et al*.[146] ..... 49

Figure 2.6. The effect of increasing tetrathiol concentration on polyHIPE compressive modulus (A) and yield strength (B). Reprinted from Whitely *et al*.[146] ..... 50

Figure 2.7. The effect of increasing tetrathiol concentration on polyHIPE degradation up to 4 weeks in 0.25 M NaOH (A) and 0.5 M NaOH (B). Reprinted from Whitely *et al*.[146] ..... 53

Figure 2.8. hMSC viability after 24 h incubation with two concentrations of PFDMA and PFDMA-10T extracts (1.0 and 0.5 vol%) (A). Micrographs illustrating live (green) and dead (red) cells cultured with respective polyHIPE extracts at 0.5 vol% (B). Reprinted from Whitely *et al*.[146] ..... 55

Figure 2.9. NMR spectrum of PFDMA and PFDMA-10T polyHIPE extracts. Reprinted from Whitely *et al*.[146] ..... 55

Figure 2.10. hMSC viability on PFDMA and PFDMA-10T polyHIPEs at 1, 3, and 7 days (A). Micrographs illustrating live (green) and dead (red) cells on the respective polyHIPE sections at 7 days (B). Reprinted from Whitely *et al*.[146] 57

Figure 2.11. Proliferation of hMSCs seeded on PFDMA and PFDMA-10T polyHIPEs at 1, 6, and 11 days as determined by DNA quantification. hMSCs were cultured in growth media (GM) and osteogenic media (OM) with an initial cell seeding density was 50,000 cells/cm$^2$. Reprinted from Whitely *et al*.[146] ..57

Figure 2.12. Alkaline phosphatase activity of hMSCs seeded on PFDMA and PFDMA-10T polyHIPEs at 1, 6, and 11 days. PolyHIPEs were cultured in growth media (GM) (A) and osteogenic media (OM) (B). Reprinted from Whitely *et al*.[146] .....59

Figure 2.13. The effect of gelatin surface modification on collagen staining (A), attached hMSC viability (B), hMSC adhesion (C), and hMSC morphology and spreading (D) of polyHIPE scaffolds.....61

Figure 2.14. Biocompatibility of polyHIPE in rat calvarial defect model. A: Negative control defects contain neovascularization (arrowheads), spindle shaped fibroblasts, and collagenous matrix. B: The polyHIPE treated defect contains similar fibrous tissue (arrowheads). C: Ordinal scoring of negative control and polyHIPE (n = 6 tissue sections) indicated no significant differences in the biologic response, except for lymphocyte infiltrate, which was increased in polyHIPEs.....63

Figure 2.15. Rabbit medial femoral condyle defect with diameter 3.5 mm and depth of 5 mm (white arrow) (A). PolyHIPE injected into the defect (B). PolyHIPE interdigitates with the bone, and solidifies (black arrow) (C). Harvested and sectioned image of the filled defect (D), and representative SEM images of the injected polyHIPE (E) and bone/graft interface (F).....63

Figure 3.1 Schematic illustrating hMSCs loading in hydrogel precursor solutions (A), injection and encapsulation in 3D printed polyHIPE scaffold (B), and protection during early stages of implantation (C). .....67

Figure 3.2. Effect of initiator concentration and reducing agent ratio on gelation onset (A) and complete network formation (B) of hydrogel carrier. The + represents a gelation and network formation time of greater than 30 minutes. The * represents a gelation onset time of less than 10 seconds. All data represents average ± standard deviation for n = 3. .....77

Figure 3.3. Percent hMSC viability following 10 min exposure to redox agents, ammonium persulfate and iron gluconate (A); 24h additional culture (B). Percent hMSC viability and cell density following carrier encapsulation with micrographs illustrating live (green) and dead (red) cells in respective hydrogel formulations (C). All data represents average ± standard deviation for n = 12. The * and ° represent significant difference ($p<0.05$) for 25 mM concentration compared to other concentrations. .....82

Figure 3.4. Micrographs illustrating live (green) and dead (red) cells 1 day post encapsulation and 7 days post release onto TCPS and polyHIPE substrates (A). Percent hMSC viability 1 day and 7 days following release and attachment onto TCPS and polyHIPE substrates (B). All data represents average ± standard deviation for n = 12. .....84

Figure 3.5. Distribution of hMSCs using carrier seeding onto multilayer polyHIPE scaffolds determined by dsDNA quantification and compared to suspension seeding control (A). Representative micrographs of top, middle and bottom layers of scaffold (B). All data represents average ± standard deviation for n = 3. The * represents significant difference ($p<0.05$) between suspension and carrier seeding at specified layer. .....86

Figure 3.6. Adhesion of hMSCs released onto TCPS and polyHIPE substrates determined by dsDNA quantification (A). Alkaline phosphatase activity of hMSCs 7D and 14D post carrier release. Cells were cultured in growth media (GM) and osteogenic media (OM) as positive control. All data represents average ± standard deviation for n = 3. The * and ° represent significant difference ($p<0.05$) for TCPS substrates compared to polyHIPEs at indicated time points. The + represents significant difference ($p<0.05$) for ALP activity on polyHIPE substrates at 14D. .....88

Figure 3.7. Alizarin red staining of hMSC cultures 4 weeks following carrier release. hMSC mineralization post release onto TCPS substrates in growth vs osteogenic media (A). Effect of release substrate (TCPS vs polyHIPE) and media conditions (growth vs osteogenic) on hMSC mineralization (B). Semi-quantitative analysis of mineralization determined by alizarin red stain recovery (C). All data represents average ± standard deviation for n = 4. The * represents significant difference ($p<0.05$) between all compositions. .....89

Figure 3.8. Effect of scaffold chemistry (PFDMA vs PLA films) and scaffold porosity (PFDMA polyHIPE vs PFDMA film) on calcium deposition in cell free conditions (A). Quantification of hMSC adhesion on varied substrate determined by dsDNA quantification (B). Effect of substrate on hMSC alkaline phosphatase activity after 14 days (C). Cells were cultured in growth media (GM) and osteogenic media (OM) as positive control. All data represents average ± standard deviation for n = 4. The * represents significant difference ($p<0.05$) for indicated composition compared to all others in respective media. .....91

Figure 4.1. Schematic of microsphere fabrication. HIPE is injected through a needle parallel to the flow of 3 wt% PVA solution and polymerized via UV irradiation. Polymerized particles are collected and filtered prior to use. .....98

Figure 4.2. Modulated particle diameter of model compositions with representative SEM micrographs (A-D). Modulated pore diameter of model compositions with representative SEM micrographs (E-H). From left to right: large particle-small pore, large particle-large pore, small particle-small pore, small particle-large pore. ..... 104

Figure 4.3. Tuning release profiles of BSA-FITC from polyHIPE microspheres. Daily and cumulative release profiles for all model compositions (A). Effect of particle size on release kinetics for large (45um) and small (15um) pore size (B). Effect of pore diameter on release kinetics for large (900um) and small (300um) particle size (C). All data represents average ± standard deviation for n = 3. ..... 109

Figure 4.4. Normalized FFLuc activity of BRITER cell line treated with releasates taken from rhBMP-2 loaded microspheres. Percent bioactivity retention determined by comparison to FFLuc of known rhBMP-2 stocks..... 111

Figure 4.5. Effect of rhBMP-2 loaded polyHIPE releasate on cell density (A) and alkaline phosphatase activity (B) of hMSCs cultured with releasate for 14 days. Cells were cultured in fresh solution of stock rhBMP-2 (BMP-2) and osteogenic media (OM) as positive control, and growth media (GM) as negative control. All data represents average ± standard deviation for n = 4. The * and ° represent significant difference ($p<0.05$) between BMP-2 or GM and indicated compositions for density or ALP activity. ..... 113

Figure 4.6. Effect of microsphere particle size and pore size on composite scaffold compressive modulus and strength for 5 wt% incorporation using four model compositions (A). Effect of increasing microsphere incorporation (5, 10 and 20 wt%) on composite scaffold compressive modulus and strength (B). All data represents average ± standard deviation for n = 3. The * and ° represent significant difference ($p<0.05$) for 20 wt% compressive modulus or strength and other indicated compositions. ..... 116

LIST OF TABLES

Page

Table 1.1. Trophic activity and therapeutic effects of mesenchymal stem cells. ..... 13

Table 1.2. Role of growth factors in bone repair. ..... 18

Table 3.1. Effect of initiator and reducing agent concentration on hydrogel compressive modulus, swelling rato, and gel fraction. ..... 79

Table 4.1. Summary table of fabrication parameters including tubing diameter, needle size, flow rate, and surfactant compositions for model compositions. ..... 98

Table 4.2. Summary table of properties for model compositions including particle diameter (n=25), pore size (n=100), and loading efficiency (n=12). All data represents average ± standard deviation. ..... 104

# CHAPTER I

# INTRODUCTION AND LITERATURE REVIEW

## 1.1. Clinical Overview

### *1.1.1. Prevalence of Nonunion Bone Defects*

Treatment of musculoskeletal injury and disease are among the most common procedures performed annually in the United States, with an estimated financial burden of greater than $200 billion.[1] Specifically, bone fractures comprise a majority of these disorders with over seven million reported cases in the United States. These defects arise from treatment of traumatic injury, congenital defect, tumor resection, and joint replacements. Unfortunately, it is estimated that up to 10 percent of these fractures will be associated with delayed or total absence of bone union during healing.[2] Several factors influence nonunion development including patient age and health, location of the injury site, damage to surrounding tissue and vasculature, and mechanical instability.[3] In cases with significantly high loss of bone tissue, proper stabilization and control of the injury site alone is not sufficient to promote healing. These defects, termed critical size, are defined as osseous defects that fail to heal spontaneously with bone during the lifetime of the patient, unless a suitable bone replacement material is placed in or onto the defect.[4] Without intervention, these defects fill primarily with fibrous connective tissue and fail to recapitulate the structure of native bone. As a result of this dependence on a secondary substrate to facilitate bone healing, critical size defects are an ideal platform to investigate novel bone replacement materials. Clinically, critical size may be determined through

radiological analysis of defect geometry. Key's hypothesis states that a segmental long bone defect greater than 1.5X the diaphyseal diameter will fail to undergo complete healing in canine models.[5] Furthermore, researchers have explored and identified similar effects of segmental defect length and diaphyseal diameter on healing in other animal models including sheep, cat and rabbit.[6]

*1.1.2. Bone Biology and Structure*

Bone is a nanocomposite of a stiff mineralized hydroxyapatite matrix and elastic collagen fibrils. Inorganic hydroxyapatite mineral comprises approximately 70% of calcified bone with 25% consisting of organic material (including cells), and 5% water.[7] Newly synthesized osteoids that have yet to be mineralized consist primarily of collagen (greater than 90%) with the remainder consisting of bone specific growth factors and proteoglycans. Cortical and cancellous bone make up the two distinct tissue architectures present in bone. The robust mechanical properties and load bearing potential is provided by the cortical layer, a primarily non-porous architecture making up 80% of skeletal tissue. Compressive modulus of cortical bone has been estimated at an impressive 17 GPa with tensile properties about 20% weaker. The inner architecture of bone consists of a spongey, honeycomb-like structure known as cancellous bone. As a result of this improved porosity (estimated up to 90%), compressive modulus values are reduced, with an estimated modulus of 20-500 MPa.[8]. Cancellous bone is typically found in the metaphysis of long bones while cortical bone makes up the diaphysis. The cortical layer of bone is surrounded by a thin membrane known as the periosteum, which contains many progenitor cells responsible for bone maintenance. Bone maintenance is governed by complex interactions

and feedback mechanisms between matrix producing osteoblasts and tissue-resorbing osteoclasts. The majority of cells in adult skeleton consist of osteocytes, fully specialized osteoblasts which facilitate extracellular calcium and phosphorus concentrations and direct osteogenesis.[9] Improved understanding of the complex processes and regulators in bone remodeling is critical to developing an optimal treatment for critical sized defects.

### *1.1.3. Natural Bone Healing*

Bone is unique among tissues as it has the ability to heal new, healthy tissue with the absence of scar tissue formation.[10] Fracture healing occurs in multiple phases, often occurring simultaneously. During the early stages of repair, disruption of the native vasculature results in formation of a hematoma, providing a matrix that encloses the wound, allows migration of inflammatory cells, fibroblasts, and progenitor cells into the wound site, and promotes granular tissue formation.[9, 11] This initial response is followed by a rapid release of angiogenic factors and cytokines to direct new blood vessel formation, as well as the release of osteoindutive factors from infiltrating stem cells and extracellular matrix.[12] The next stage is defined by the formation of a soft callus that begins to stabilize the defect. Matrix composed of Type 1 collagen and proteoglycans is produced by osteoblasts which forms the soft, internal callus, eventually undergoing mineralization and forming the bony callus. Simultaneously, intramembranous ossification occurs in the periosteum, creating an external callus. The ossification of the soft callus to bridge the broken can occur in as little as 4 weeks if properly immobilized. Finally, the hard callus is replaced with native bone, with size and vascular structure fully returning to normal over a period of several months.[13] Similar to healing in non-critical

defects, critical defect healing processes include formation of poorly organized endosteal and periosteal callus formation that proceed toward bony bridging of the gap. However, unlike non-critical healing, full bridging does not occur of the opposing callus parts, resulting instead in formation of rounded corticies.[14] This nonunion results in the loss of load transfer and mechanical stimuli that are needed to fully initiate tissue organization.[14, 15]

## 1.2. Current Treatment Options

### *1.2.1. Autografts*

Autologous grafts are currently the gold standard for bone grafting procedures due to their high healing capacities. In these procedures, tissue is harvested from a secondary location on the patient, most commonly the iliac crest of the hip or tibia, and transplanted to the injury site.[16] Advantages of autografts include high integration with surround tissue, strong osteoinductive character, and no risk of immune rejection. Multiple trials including vertebral fusions and treatment of tibial nonunion have demonstrated extremely high success rates.[17] Unfortunately, this procedure is not an option for many patients due to a lack of graft availability and complications arising from a second surgical site.[17-19]

### *1.2.2. Allografts*

Allograft bone provides a more readily available treatment option as it can be harvested from cadaveric tissue donors and easily stored.[20] As immune rejection and disease transmission can be areas of concern for allogenic transplants, decellularization processes are often introduced to reduce potential risks. Similarly to grafting with autologous tissue, the complex geometry of bone defects often makes fitting a replacement

allograft extremely difficult. As a result, donor tissue can be demineralized to form a powder or paste that allows easier implementation and is better able to match defect geometry. This processing however, severely compromises load bearing potential, further driving the need or a more viable bone replacement.[21]

### *1.2.3. Alloplastic Grafts*

Poly(methyl methacrylate) (PMMA) bone cement is the most widely utilized synthetic material in bone grafting procedures, commonly selected to stabilize implants, fill defects in tumor resection, and provide minor load bearing in spinal procedures.[22, 23] Despite widespread use, PMMA cements are not an ideal treatment option as they are nonporous, do not undergo necessary biodegradation, and often reach temperatures in excess of 100ºC during polymerization, which can lead to necrosis of the surrounding tissue. In contrast, calcium phosphate cements have been readily explored as a more cytocompatible and osteoinductive bone replacement.[1] Despite success, these grafts often exhibit low fracture toughness and fail due to fracture.[24] Combined, these limitations suggest that physicians and patients would greatly benefit from an improved bone grafting option.

## 1.3. Tissue Engineered Scaffolds

Tissue engineering aims to provide an improved tissue replacement option by combining the regenerative capacity of autologous grafts with the tunability and availability of synthetic materials.[25] The tissue engineering paradigm consists of a biomaterial scaffold that temporarily replaces tissue structure, and combining this scaffold with appropriate biochemical cues and progenitor cells to facilitate tissue regeneration.[26] As a result, this strategy has numerous advantageous over standard grafting materials.

### *1.3.1. Scaffold Requirements*

Success as a tissue engineered scaffold is dictated by the ability to support critical cell and tissue functions. To achieve this, it is necessary to have sufficiently interconnected and porous architecture to allow cellular infiltration, vascularization, and nutrient and waste transport. Multiple groups have explored optimal pore sizes needed to encourage ingrowth and osteogenesis. Broadly, a minimum pore size of 100 microns is desired, with larger pores demonstrating increased osteoblastic activity.[27-29] Native bone is unique in its ability to achieve a porous architecture while maintaining the ability to withstand high physiological loads. Typical physiological stresses have been estimated up to 50 MPa with highest stresses occurring in the femur during strenuous activities such as running.[30] Achieving this combination of porosity and strength in a synthetic material, without introducing negative stress-shielding effects, has been a major hurdle in bone grafting.[31] It is generally accepted that scaffolds with compressive properties approaching those of cancellous bone (100 MPa modulus; 10 MPa strength) are capable of supporting bone regeneration.[32] Finally, an ideal tissue engineered scaffold should degrade at a rate similar to *de novo* tissue formation, and appropriately transfer responsibility back to the healing tissue.[26] Femoral defect models in rabbits have illustrated improved healing when tissue engineered scaffolds are tuned to degrade at a rate that better matches healing.[33] Matching regeneration rates can be particular challenging however, as patient age, health, and severity of injury effect healing rates.

### *1.3.2. Scaffold Fabrication Techniques*

A multitude of fabrication techniques have been developed by tissue engineers to generate highly porous scaffolds for repair of musculoskeletal injuries. The most prominent of these include electrospinning, gas foaming, porogen leaching, and thermally induced phase separations. Electrospinning is a method utilized to generate 2-dimensional sheets of fibrous meshes that contain high SA/V ratios.[34] Tunable porosities, diameters, and alignment patterns are achieved through modulation of polymer solution and system parameters.[35] Lack of suitable compressive properties and inability to generate large constructs limit its potential in orthopedic applications. Gas foaming, or blowing, techniques are utilized to produce highly porous scaffolds with a range of pore sizes.[36] Pores are generated through gas production, typically CO2, in a polymer melt, utilizing chemical or physical processes. Elevated temperatures and post fabrication processes needed to remove a non-porous skin relegates this method to solely prefabrication applications.[37]

Dispersion, and subsequent leaching, of porogens (often salts) from a polymer solution after network formation have also yielded porous, interconnected scaffolds.[38] A common drawback to salt leached scaffolds is the presence of stress concentrations resulting from the uncontrolled shape of porogens, which can result in decreased mechanical properties.[39, 40] Inducing a change in solubility of a polymer solution can be used create polymer-rich and polymer-poor regions, that upon subsequent sublimation, yields a porous polymer scaffold. Modulating parameters in this phase separation method, including polymer type and temperature, can be used to obtain a variety of pore

geometries.[41, 42] Despite the ability of these techniques to yield porous scaffolds, fabrication parameters often introduce concerns or preclude use for *in situ* delivery, incorporation of cells, or use in growth factor delivery.

### *1.3.3. Polymerized High Internal Phase Emulsions (PolyHIPEs)*

Emulsion templating is a unique fabrication technique that is currently being studied for use in tissue engineering.[43, 44] High internal phase emulsions are defined by an internal droplet phase (greater than 74%), and an organically soluble prepolymer outer phase. Polymerization of the continuous phase locks in the internal architecture dictated by the droplet phase resulting in highly porous foams. Historically, numerous groups have reported on processing variables than can be tuned to achieve a diverse range of properties, (75-99% porosity; 1-100 μm pore size; 2 kPa- 60 MPa compressive moduli).[43, 45-49] Recently we developed a polyHIPE scaffold suitable for bone regeneration based on the biodegradable macromer, propylene fumarate dimethacrylate (PFDMA). This hydrophobic, low viscosity macromer contains ester linkages that allow for hydrolytic degradation, and reactive methacrylate end groups that undergo rapid polymerization in physiological conditions. Uniquely, we have demonstrated these injectable materials are suitable for *in situ* injection, facilitate osteogenic activity, and adaptable as 3D printable emulsion inks.

### *1.3.4. Thiol-Methacrylate Polymerization for Improved Resistance to Oxygen Inhibition*

Although traditional free radical polymerization is a robust mechanism for scaffold fabrication, use of only methacrylated macromers in our system renders it susceptible to oxygen inhibition. When polymerized under oxygen rich conditions, initiating radicals are

scavenged by molecular oxygen and converted to peroxy radicals.[50, 51] These radicals are no longer able to reinitiate polymerization of methacrylate functional groups, essentially terminating cure. This often results in reduced cure rates, poor monomer conversion, and reduced mechanical properties. Although many researchers have developed techniques to prevent oxygen inhibition in commercial settings (e.g. purging with inert gases), limited progress has been made in addressing this problem in an injectable system. Researchers have probed Michael addition-type reactions to create ideal, step-growth crosslinked networks that provide resistance to oxygen inhibition. Specifically, thiol-acrylate and thiol-methacrylate systems have been reported to have improved resistance to oxygen inhibition. O'Brient et al. illustrated that increasing thiol concentration in diacrylate systems resulted in reduced levels of oxygen inhibition.[52] In contrast to the traditional free-radical polymerization of unsaturated vinyls, thiol-methacrylate polymerization can be initiated by both cleave-type initiators and hydrogen abstraction of the thiol monomer, rendering it less susceptible to oxygen inhibition. Propagation then proceeds via thiol or methacrylic/acrylic radical addition to methacrylate/acrylate functional groups. This reduction in oxygen inhibition provided by a mixed mode polymerization mechanism could prove a major benefit in an injectable polyHIPE system.

## 1.4. Mesenchymal Stem Cells in Bone Tissue Engineering

### *1.4.1. MSC Discovery and Isolation*

One of the most exciting developments over the past 60 years in regenerative medicine is the growth of mesenchymal stem cell therapies.[53] Discovered in the 1960's through the ground breaking work of Friedenstein and colleagues, a population of stromal cells that

could be isolated from bone marrow, were plastic adherent, and could promote formation of *de novo* bone tissue were discovered.[54] Over the next two decades, significant emphasis was placed on better understanding these potent sources of healing, termed mesenchymal stem cells, and developing markers for their identification.[55, 56] Although mesenchymal stem cells represent a small portion (less than 0.01%) of total cells present in bone marrow, Pittenger *et al.* demonstrated that these cells could be expanded with high efficiency *in vitro* while retaining their multipotency.[57] These studies demonstrated that mesenchymal stem cells were capable of differentiating into adipcytic, chondrocytic, and osteocytic lineages. Exponential increase in interest led to the release of a position statement by The International Society for Cellular Therapy defining minimal criteria for classification of multipotent mesenchymal stromal cells as plastic-adherent, positive for expression of CD105, CD73, and CD90, ability to differentiate into osteoblasts, adipocytes, and chondrocytes.[58]

Harvesting of MSCs from bone marrow remains the most widely studied isolation method. In humans, the superior iliac crest of the pelvis is commonly selected, with additional isolation compartments being those of the femur, tibia, and thoracic and lumbar spine.[59-61] Large animal models typically utilize similar methods with small animal models focusing on harvest from the mid-diaphysis of the tibia or femur. Primary harvests are typically kept in culture for two weeks to allow for adherence and removal of non-adherent hematopoetic cells.[61] More recently, additional stem cell niches have been discovered, providing additional sources for tissue-specific stem cells including the periosteum, adipose tissue, and umbilical cord blood.[62-64] Yoshimura *et al.* demonstrated that solid

tissues could provide higher concentrations of mesenchymal stem cells than marrow harvests.

### *1.4.2. Trophic Activity*

The ability of mesenchymal stem cells to differentiate into specialized cell types has prompted many researchers to employ these cells in their grafts in the hopes of directly replacing the cells lost to injury and responsible for tissue remodeling. Although significant improvements in regeneration have been observed as a result of mesenchymal stem cell presence, a new school of thought has emerged suggesting an alternative therapeutic mechanism.[53, 65] It has been evidenced that in many cases, rather than specialized differentiation, MSCs were in fact creating a 'trophic effect', or that is to say, creating a regenerative microenvironment through the secretion of growth factors and bioactive molecules that promotes infiltration of native cells, angiogenesis, and tissue healing. Common trophic mechanisms are summarized in **Table 1.1**.[53] This trophic activity is achieved through the secretion of numerous growth factors to recruit and promote proliferation of native cells including transforming growth factors, insulin-like growth factor-1, basic fibroblast growth factor and epithelial growth factor.[66, 67] Furthermore, MSCs have been shown to facilitate angiogenesis through secretion of vascular endothelial growth factor and stabilizing newly formed vessels.[68, 69] Tateishi-Yuyama *et al.* demonstrated that autologous implantation of bone marrow derived cells could improve angiogenesis in patients suffering from unilateral ischemia of the leg.[70]

Another unforeseen benefit of MSC therapy is anti-inflammatory and immunomodulatory effects. Inflammation at the site of musculoskeletal injury can result

in impediment of healing processes of native progenitor cells. MSCs have been shown to secret a multitude of anti-inflammatory factors in response to injury.[71] As a result, MSCs are able to modulate function of surveilling inflammatory immune cells, including T cells, B cells, and macrophages.[72, 73] MSC delivery has also demonstrated anti-apoptotic and antimicrobial properties. Cselenyak *et al.* explored the mechanism behind bone marrow derived MSCs improving viability of ischemic cariomyoblast populations and identified the recovery to be dependent on cell-to-cell interactions.[74, 75] hCAP-18/LL-37, a peptide commonly expressed by epithelial cells and macrophages to combat bacterial infections, is secreted by MSCs in response to e coli and other infections. In an experimental colitis and sepsis model, systemic infusion of adipose derived MSCs protected from severe sepsis by reducing infiltration of inflammatory cells and by down regulation of inflammatory mediators.[76]

**Table 1.1.** Trophic activity and therapeutic effects of mesenchymal stem cells.

| Properties | Mechanism | Effect |
|---|---|---|
| **Trophic** | Release of TGF-α, TGF-β, HGF, EGF, FDF-2, IGF-1 | Direct fibroblasts, epithelial, and endothelial cells |
| | Release of VEGF, IGF-1, EGF, angiopoietin-1 | Recruit endothelial cells and facilitate vascularization |
| | Release of keratinocyte growth factor, SDF-1, macrophage inflammatory protein-1 α and β | Reduce scar tissue formation |
| **Immunomodulatory** | Release of prostaglandin 2, TGF-β1, HGF, SDF-1, nitrous oxide, indoleamine 2,3-dioxygenase, IL-4, IL-6, IL-10, IL-11 receptor antagonist, soluble tumor necrosis factor-α receptor | Inhibit function of T cells, killer cells, B cells, monocytes, macrophages and dendritic cells |
| | Express HLA Class I and HLA Class II | Avoid immune system recognition |
| **Apoptotic Rescue** | Secretion of IGF-1, IL-6, VEGF, HGF, TGF-β1 | Increase protein kinase B production to facilitate anti-apoptotic pathways |
| **Antimicrobial** | Express hCAP-18/LL-37 | Combat Gram-positive and negative bacterial infections |
| | Upregulate indoleamine 2,3-dioxygenase | Regulate T-cell activity |

### *1.4.3. Clinical Efficacy of Stem Cell Therapy*

The clinical benefits of marrow derived stem cell delivery have been widely established. Early studies focused on the percutaneous grafting of autologous bone marrow in nonunion fractures, including those of the tibia. Connolly *et al.* observed improved callus formation and defect union in eighty percent of patients stabilized with

an external cast, and one hundred percent of patients stabilized with intramedullary nails. Observed results were comparable to standard autologous grafting procedures.[77] It was later established by Hernigou and colleagues that efficacy of autologous bone marrow therapies in the treatment of nonunions was related to the number of progenitors present in the graft.[78] This work articulated that bone marrow harvesting from the iliac crest may be patient variable and not suitable for promotion of healing in the absence of concentration, emphasizing the importance of normalizing progenitor amount to reach efficacy. Finally, Bruder *et al.* demonstrated that purified and culture-expanded human MSCs could be utilized to improve regeneration in a critical sized femoral defect treated with porous hydroxyapatite/beta calcium phosphate scaffolds.[79, 80] Stem cell loaded constructs exhibited radiological and histological evidence of new bone formation after 8 weeks with improved biomechanical properties.

### *1.4.4. Natural Polymeric Cell Carriers*

Although MSC delivery holds therapeutic promise, traditional delivery methods (e.g. percutaneous grafting of stem cells via syringe or catheter) often result in limited cell engraftment and survivability, ranging between 5%-20%.[81, 82] In addition, the hostile environment of injured or diseased tissue can deprive cells of nutrients or subject them to removal by surveilling inflammatory cells, further reducing cell retention. As a result, biomaterial carriers that provide an external matrix and mechanical barrier to removal have been investigate as an improved substrate for tissue engraftment. Hydrogels, a class of biomaterials comprised of hydrophilic, water-swollen polymer networks, have emerged as a promising platform for delivering stem cells. Numerous natural and synthetic

hydrogels have been investigated for cell encapsulation.[83, 84] Natural platforms, such as those based on modified gelatin, alginate, or fibrin provide an extracellular-like matrix that is both cytocompatible during encapsulation processes, and able to promote cell attachment and migration after delivery. Encapsulation in these systems often occurs through thermal induced gelation or ionic crosslinking. Awad *et al.* investigated chondrogenic differentiation of adipose derived stem cells encapsulated in multiple natural polymer systems including agarose, alginate, and gelatin scaffolds.[85] Furthermore, Nichol *et al.* demonstrated that methacrylated gelatin, a natural derivative of collagen, can be utilized to encapsulate cells with high cell survival.[86] These constructs were advantageous as they retained native RGD binding sites and MMP-sensitive degradation sites while achieving improved mechanical properties of covalently crosslinked systems.

*1.4.5. Synthetic Polymeric Cell Carriers*

Synthetic hydrogels, specifically those based on poly(ethylene glycol) (PEG), provide an encapsulation platform with excellent cytocompatibility, and a blank slate nature that can be modified for any target tissue. Most commonly, hydrophilic precursor solutions are fabricated containing prepolymer, photoinitatior, and cell payload. These solutions are then exposed to an external UV source to facilitate free-radical polymerization of acrylate/methacrylate groups, and physical entrapment of the cell inside the polymer network. Excellent encapsulation viability, as well as the ability to promote osteogenic differentiation of MSCs was observed by Nuttleman *et al*.[87] After one week, gene expression for osteogenic markers osteonectin, ostoeopontin, and alkaline phosphatase was upregulated with mineralization present after four weeks. To improve viability of cells

encapsulated for extended periods, RGD binding sites have been covalently inserted to improve cell-matrix interactions and stimulate bone growth.[88, 89] Synthetic hydrogel platforms with improved biodegradation have also been explored for cell delivery and release. A novel *in situ* application system based on oligo(poly(ethylene glycol) fumarate) was investigated and shown to support osteogenic differentiation of encapsulate rat marrow stromal cells.[90] The redox initiation mechanism utilized in this system has the advantage of not requiring external equipment to facilitate polymerization. This system has since been modified to allow for tunable degradation and release of marrow stromal cells from the hydrogel cell carrier through incorporation of the hydrolytically degradable macromer acrylated poly(ethylene glycol)-dithiothreitol.[91] Modulating degradation profile was identified as a tool that can be utilized to control cell retention at the tissue site. Finally, hydrogel carriers provide the added advantage of being able to simultaneously deliver bioactive factors. Simmons *et al.* demonstrated that bone morphogenetic protein-2 and transforming growth factor could be combined with stem cell deliver to improve ectopic bone formation.[92]

### *1.4.6. Combination Cell Carriers*

As evidenced by the success of these varied platforms, hydrogel delivery holds strong promise in stem cell therapy. A challenge specific to bone tissue engineering is developing a cell carrier that has suitable mechanical properties for physiological loading. Recently, composite grafts have been investigated to deliver stem cells in more robust scaffolds by combining traditional bone grafting materials with hydrogel cell carriers. Zhao *et al.* demonstrated the promise of this approach by encapsulating umbilical cord mesenchymal

stem cells in alginate microbeads and incorporating them in an injectable calcium phosphate cement paste.[93] Encapsulated cells remained viable, exhibited gene markers of osteoblastic differentiation, and facilitated mineral synthesis. Similar systems, including those based on settable polyurethane scaffolds have been explored with similar promising results for chondrogenic tissue repair.[94] Combined, this work illustrates the benefits of stem cell delivery and the future promise of incorporating these cells in robust scaffold design. A primary aim of this work was to expand upon these systems by developing an injectable cell carrier that can improve seeding in patient specific grafts prepared with state of the art 3D printing modalities.

## 1.5. Growth Factor Delivery in Bone Tissue Engineering

### *1.5.1. Growth Factors in Bone Healing*

As outlined previously in this review, the stages of bone healing are well established. What is less established however, is the complex interactions and feedback loops regulating these remodeling processes. Although there are physical cues that arise from changes in mechanical properties and a loss of nutrient and oxygen supply due to fracture and damaged vasculature, the primary initiators of healing are likely the multitude of bioactive growth factors released into the fracture site.[95] These secreted proteins act as a signaling service that directs surrounding cells to carry out a specified action. Upon binding of the ligand to a target receptor on the surface of the cell, a conformational change occurs, resulting in formation of a transcription factor that travels through the cell. This transcription factor then binds nuclear DNA and facilitates new gene expression and subsequent morphological changes of the cell. The most prevalent growth factors active

in bone repair are summarized in **Table 1.2**.[95, 96] One of the most widely studied of these factors are members of the transforming growth factor-beta super family. Signaling from these proteins is activated through a transmembrane receptor complex formed by type-I and type-II serine/threonine kinase receptors. This leads to downstream activation of class of transcription factors known as SMAD proteins, which facilitate the intracellular response.[97] Other regulating factors such as platelet-drived growth factor initiate response through activation of receptor tyrosine kinases.[96] Ferguson and colleagues demonstrated that the genetic mechanisms that regulate fetal skeletal development also regulate bone healing in adults.[98] Developing platforms that allow for improved understanding of the complex overlap and cross-communication between these signaling pathways has been a driving area of study.

**Table 1.2.** Role of growth factors in bone repair.

| Factor | Activity | Source |
|---|---|---|
| **Transforming growth factor beta (TGF-β)** | Stimulate ECM production, osteoprogenitor cell proliferation, osteogenic differentiation | ECM, platelets, inflammatory cells, osteoblasts |
| **Bone morphogenetic protein (BMP)** | Promote osteoblast and chondrocyte differentiation of progenitor cells | ECM, osteoblasts, osteoprogenitor cells |
| **Fibroblast growth factor (FGF)** | Mitogenic effect of MSCs, osteoblasts and chondrocytes, promote angiogenesis | Macrophages, MSCs, chondrocytes, osteoblasts |
| **Insulin-like growth factors (IGF)** | Promote proliferation and differentiation of progenitor cells | ECM, chondrocytes, osteoblasts |
| **Platelet-drived growth factor (PDGF)** | Promote chemotaxis and proliferation of macrophages and MSCs | Platelets, osteoblasts, macrophages |

### *1.5.2. Bone Morphogenetic Proteins*

The most widely studies proteins studied for bone regeneration are members of a subset of the TGF-Beta superfamily known as bone morphogenetic proteins (BMP). Investigation into these proteins first began after the discovery that new bone could be formed as a result of intramuscular implantation of demineralized bone matrix.[99] Discovery of this 'bone induction principle' sparked numerous investigations, eventually resulting in the genetic sequencing and identification of numerous bone morphogenetic proteins.[100] Furthermore, Cheng and colleagues established a hierarchical model of osteogenisis for multiple BMPs, observing that BMP-2, -6, and -9 were able to induce alkaline phosphatase activity in pluripotent cell lines.[101] BMP-2, -4, -6, -7, and -9 were able to induce alkaline phosphatase activity in preosteoblasts, while the majority of tested factors could induce activity of differentiated osteoblasts. As a result of these collective investigations, numerous BMPs have been explored to improve bone regeneration in a clinical setting, the most promising of these being BMP-2. The therapeutic effect of BMP-2 delivery has been shown to emerge from its role in the initiation of fracture healing, chemoattactive properties, and facilitation of angiogenesis.[13, 102-106] The importance of BMP-2 in initiating fracture response is widely recognized as it is present in extracellular matrix and released into the wound environment post injury. Tsuji *et al.* reported that in the absence of BMP-2, even in the presence of other osteoindutive stimuli, limb defects in a mouse model failed to resolve with time.[102] It was critical to note that stem cell populations with upregulated expression of BMP receptors were present at the injury site, but lacked necessary signaling to facilitate healing. Furthermore, Fiedler *et al.* reported a

greater than 3-fold increase in migration of primary mesenchymal human porogenitor cells in response to BMP-2 delivery, suggesting a functional role of BMP-2 factor in the recruitment of progenitor cells in bone healing.[103] Finally, it has been reported that BMPs enhance expression of potent angiogenic factors, including vascular endothelial growth factr (VEGF) in osteoblasts.[104] This expression is not associated with osteoblastic differentiation, but rather serves to combine critical osteogenic and angiogenic processes.

*1.5.3. Clinically Available Growth Factor Delivery Systems*

Combining bone morphogenetic proteins into grafting materials has been explored as an approach to overcoming limitations in autologous bone grafting, to great success. To date, two devices have been approved for clinical treatment of bone defects.[107-110] Delivery of recombinant expressed BMP-2 in an absorbable collagen sponge was first approved for treatment of specific interbody spinal fusion procedures. It later gained approval for treatment of open tibial fractures in intramedullary nail fixation and most recently for specific craniofacial applications. In a 279 patient trial clinical trial for the treatment of degenerative disc disease, it was reported that 2-year fusion rates for the BMP/collagen sponge were greater than 88%, only marginally lower than autologous rates of 94.5%.[108] No differences in patient pain or neurological profiles were reported. In addition, complications related to secondary donor site pain and morbidity were expectedly eliminated. Furthermore, use of BMP-7, clinically known as Osteogenic Protein-1, has been granted approval by the FDA under the Humanitarian Device Exemption program for delivery in a puddy of bovine bone collagen. A clinical trial investigating repair of tibial nonunions reported that 75% of patients had radiographic confirmation of fracture

healing after nine months, only marginally lower than the autograft treatment at 84%.[110] Despite the clear ability of osteoinductive factor delivery to promote regeneration, several safety concerns have emerged. Concerns include inflammation, ectopic bone formation, and neurological deficits.[111, 112] These undesirable off-target complications often result from a bolus release of supraphysiological dosages of the factor. As the majority of protein is quickly released form the collagen carrier and removed from the injury site, high concentrations of protein are required to be initially loaded to ensure a robust therapeutic response.[113] These recent complications highlight the need to develop a delivery system that can retain the benefits of osteoinductive factor delivery, but limit safety concerns.

### *1.5.4. Controlled Growth Factor Delivery*

Numerous platforms have been investigated to provide controlled release of growth factors, aiming to achieve more physiologically relevant delivery profiles. The hydrophilic nature and mild fabrication conditions of hydrogels make them intriguing platforms for growth factor delivery. Indeed, delivery of BMPs from hydrogel platforms have been shown to promote ectopic bone formation. However, to better control release kinetics, affinity-based functionality is often required. Furthermore, growth factor delivery in calcium phosphate cements has been explored. Limited porosities and poor loading of surface coatings limits commercial potential of these systems. As a result, encapsulation of growth factors into porous, polymeric microspheres systems has emerged as a method to provide controlled release of bioactive factors.

### *1.5.5. Porous Microspheres for Growth Factor Delivery*

Significant and wide-reaching progress has been made in the development of porous microsphere fabrication techniques.[114] The most widely studied microsphere platform for drug delivery is the fabrication of porous microspheres based on the biodegradable polymer pol(lactic-co-glycolide) (PLGA).[115, 116] The ester linkages in these polymers allow for hydrolytic degradation of the polymer with degradation products that can be removed through natural processes. For fabrication, these systems often employ a double emulsion-solvent evaporation method. In this method, polymer is first dissolved in a volatile solvent, most often methylene chloride or chloroform. The polymer solution is then emulsified (water-in-oil) with an aqueous solution containing the protein, added to a secondary aqueous phase to form the double emulsion (water-oil-water), and then agitated to form the microparticles. The final step is the removal of solvent through excess stirring or vacuum drying. To control particle properties like size, emulsion parameters such as stirring conditions, solvent choice, and polymer concentration are modulated. Typical microsphere diameters fabricated with this method range from 1-200 microns with notable size distributions, and pore sizes generally remaining below a single micron.[117-119] Osmotic agents have been utilized to control pore architecture and provide porous systems for sustained growth factor release.[120] Although exposure to common solvents including methylene chloride has demonstrated minimal effect on BMP-2, stability of growth factors can vary greatly, and thus compatibility of a method should be determined with caution.

Other fabrication methods of porous microspheres mirror those used for general porous scaffold fabrication. Broadly, these include porogen leaching and gas foaming.[121]

When adapted for microsphere fabrication however, it has proven difficult to adequately control the relationship between particle and pore size. Fabrication of porous scaffolds through porogen leaching relies on the addition of salts to polymer solutions, followed by subsequent leaching of the porogen. This results in heterogeneous pore structures which may result in variable scaffold properties. Additionally, the post fabrication requirements preclude in-line loading of agents into the scaffolds. Gas foaming has also been explored to fabricate porous microsphere by addition of effervescent salts as blowing agents. Ammonium bicarbonate has been shown to create highly porous microspheres with pore sizes up to twenty microns. In this report however, the relationship between particle size and pore size was coupled, limiting the tunability of this system.[36]

To minimize manufacturing concerns resulting from costly post fabrication processes, including solvent removal and porogen extraction, spray drying has emerged as a minimal processing fabrication technique.[122] For the encapsulation of proteins, the primary water in oil emulsion is sprayed in a stream of heated air. Fabrication parameters of injection rate, temperature, and solvent choice are modulated to dictate microsphere morphology. Berkland and colleagues demonstrated that coaxial spray drying setups could be utilized to fabricate core-shell microspheres with tunable shell thickness.[123] Disadvantages of spray drying systems include suboptimal yields due to difficulties with microsphere collection and potential denaturation if elevated temperatures are utilized for fabrication.

### 1.6. Summary and Approach

Limited availability of autologous tissue, combined with inherent variability in allogenic grafts, is driving the need for an improved bone replacement material. Tissue

engineering presents a promising strategy to combine the regenerative advantages of these grafts with the availability of synthetic materials. Uniquely, emulsion templating provides a platform that can be adapted to generate highly porous scaffolds suitable for bone grafting procedure. When designing a tissue engineered polyHIPE graft, it is critical to develop a platform that can achieve requisite physical and mechanical properties inside a clinical setting. Use of a thiol-methacrylate polyHIPE allows for improved oxygen resistance and network formation. Furthermore, the tunable nature of the emulsion templating system allows for facile incorporation of injectable carrier, and controlled growth factor delivery systems. Combined, these systems provide the tools to develop a tissue engineered scaffold capable of actively guiding bone regeneration.

# CHAPTER II

# THIOL-METHACRYLATE POLYHIPES WITH IMPROVED RESISTANCE TO OXYGEN INHIBITION[1]

## 2.1. Introduction

Tissue engineers have demonstrated the importance of biomaterial scaffolds in guiding tissue regeneration.[124] Ideally, these scaffolds promote neotissue formation by providing a 3D substrate to guide cell growth, exhibiting requisite mechanical properties to restore function, and degrading at a rate that complements the rate of neotissue formation. A variety of fabrication strategies have been employed to achieve this diverse set of criterion with differing levels of success.[25, 27, 34, 36-39] Emulsion templating is a unique fabrication technique that is currently being investigated for application in tissue engineering.[125-130] High internal phase emulsions (HIPEs) are characterized by an internal droplet phase volume fraction greater than 74%. Polymerization of the continuous phase secures the architecture defined by the emulsion geometry resulting in a high porosity foam (polyHIPE). Multiple compositional and processing variables have been investigated to determine the effect on emulsion stability and the corollary impact on the resulting pore architecture and mechanical properties. Through manipulation of these variables, a diverse set of scaffolds have been fabricated with a broad range of pore sizes, porosities, and

[1] Part of the data reported in this chapter is reprinted with permission from "Prevention of oxygen inhibition of polyHIPE radical polymerization using a thiol-based cross-linker," by Michael E. Whitely, Jennifer L. Robinson, Melissa C. Stuebben, Hannah A. Pearce, Madison A. P. McEnery, and Elizabeth Cosgriff-Hernandez, ACS Biomaterials Science & Engineering 2017, 3 (3), 409-414. Copyright (2017) American Chemical Society.

mechanical properties that illustrate the utility of polyHIPEs for hard and soft tissue repair.[43, 49, 125, 126, 128, 131]

Recently, our lab developed a polyHIPE scaffold for use as an injectable bone graft based on propylene fumarate dimethacrylate (PFDMA).[126] Unlike traditional poly(methyl methacrylate) bone cements, fumarate based polyHIPEs do not exhibit significant exotherms during polymerization and allow for hydrolytic degradation *in vivo*. Uniquely, these injectable grafts cure *in situ* to compressive properties approaching cancellous bone while also promoting osteogenic differentiation of human mesenchymal stem cells.[129] No previously investigated polyHIPE graft has displayed this combination of properties while retaining the requisite properties to permit deployment as a space-filler with *in situ* cure. Although initial *in vitro* testing of these scaffolds has proved promising, additional criteria need to be addressed to permit successful implementation in the clinic. A rapidly curing polyHIPE is desired to reduce surgical times, limit infection risk, and rapidly stabilize defects.[132] We recently reported a redox initiated polymerization route that improved upon previous methods of fabricating injectable polyHIPE grafts.[128] This system permitted fabrication of an off-the-shelf graft with long term storage and cure rates similar to commonly used bone cements (<15 minutes) without sacrificing porosity or compressive properties.

The ability to achieve rapid cure with tunable polymerization profiles is a primary advantage of our polyHIPE system. However, an injectable polyHIPE for use as a bone graft must retain these characteristics when administered in the surgical suite, which includes exposure to an oxygen-rich environment. The utilization of radical mediated

chain-growth polymerization of methacrylate-capped macromers in our scaffold design renders it susceptible to oxygen inhibition. Under oxygen-rich conditions, high levels of initiating and propagating radicals are scavenged and converted to peroxy radicals.[50, 51] These peroxy radicals do not readily reinitiate polymerization of vinyl macromers, terminating further network formation. This often results in reduced cure rates, elevated levels of uncured macromer, and a reduction in mechanical properties.[133] Traditional industrial methods utilized to prevent oxygen inhibition (e.g. purging with inert gases) are not suitable to the proposed application as an injectable graft. Several researchers have reported reduced oxygen inhibition in thiol-ene and thiol-acrylate polymerizations. Thiol–acrylate and thiol-methacrylate polymerization may be initiated via hydrogen abstraction from a thiol functional group or radical addition to the acrylate/methacrylate functional group. Propagation then proceeds via thiol or methacrylic/acrylic radical addition to methacylate/acrylate functional groups.[52, 134-136] Unlike vinyl systems where oxygen scavenges and effectively terminates radicals, the peroxy radicals generated in the presence of oxygen can abstract the thiol hydrogen to generate thiyl radicals that can continue to propagate through addition or chain transfer. Thus, the mixed mode initiation of the thiol-acrylate /methacrylate polymerizations renders them less susceptible to oxygen inhibition. It has been reported that increasing thiol monomer content in diacrylate systems resulted in reduced levels of oxygen inhibition.[52] Furthermore, higher thiol functionality provided a faster polymerization rate and increased viscosity, serving to further reduce diffusion of inhibitory oxygen. We hypothesized that the addition of a thiol-based crosslinker would confer resistance to oxygen inhibition under physiological

environments to our injectable polyHIPE system. Although there are previous reports of thiol-methacrylate and thiol-ene polyHIPE systems, these were not injectable systems and did not characterize the effect of the thiol monomer on oxygen inhibition.[137-139]

In addition to achieving requisite physical properties, success *in vivo* depends on the ability of tissue engineered scaffolds to promote recruitment and attachment of native osteoprogenitor cells. Attachment of cells to extracellular matrix proteins is mediated through a class of heterodimeric surface receptors known as integrins. These linkages play critical roles in activate biomechanical and biochemical signaling pathways responsible for directing cell activity.[140, 141] Unfortunately, synthetic polymeric materials lack these native binding sites required for cell attachment, leading to reduced levels of cell infiltration in unmodified systems. Furthermore, adsorption of serum proteins from media has been shown to be heterogenous and substrate dependent during *in vitro* testing.[142] To combat this lack of native binding, hybrid systems containing natural polymers have been explored as surface modifiers in tissue engineered systems.[143, 144] Specifically, gelatin, a derivative of naturally produced collagen, has been widely utilized to develop scaffolds with improved substrates for cell adhesion and proliferation.[86, 131] An injectable polyHIPE that combined the cell attachment advantages of natural polymers with the physical and mechanical properties of fumarate based polyHIPEs would prove a promising option in bone grafting procedures.

In this study, we explore the use of a tetrafunctional thiol, pentaerythritol tetrakis(3-mercaptoproprionate (tetrathiol), to provide improved resistance to oxygen inhibition to injectable PFDMA polyHIPEs. Rheological properties were monitored to determine the

effect of thiol on crosslinking kinetics by characterizing work and set times. To further probe this relationship, gel fraction was quantified to assess the impact of tetrathiol incorporation on network formation under ambient and inert conditions. To evaluate the potential of our system in orthopaedic applications, the effects of tetrathiol concentration on pore architecture, compressive modulus, and yield strength were assessed. Thiol based scaffolds have previously demonstrated improved degradation rates *in vivo* and could prove a potent method for tuning polyHIPE degradation. To this end, the effect of thiol incorporation on hydrolytic degradation rate was determined by measuring mass loss after accelerated hydrolytic testing. Next, human mesenchymal stem cell (hMSC) activity and scaffold-induced osteogenic differentiation were investigated using established viability, proliferation, and alkaline phosphatase (ALP) assays. Finally, polyHIPE scaffolds were modified with functionalized gelatin to characterize improvements in cell attachment, viability, and spreading in surface modified grafts. This work aims to highlight the strong potential of thiol-methacrylate polyHIPEs to serve as rapid-curing injectable bone grafts that retain desirable properties when applied under physiological conditions.

## 2.2. Materials and Methods

### *2.2.1. Materials*

Polyglycerol polyricinoleate (PGPR 4125) was donated by Palsgaard. Human mesenchymal stem cells were provided by the Texas A&M Health Science Center College of Medicine Institute for Regenerative Medicine at Scott & White. All other chemicals were purchased and used as received from Sigma–Aldrich, unless otherwise noted.

### *2.2.2. PFDMA Synthesis and Purification*

Propylene fumarate dimethacrylate (PFDMA) was synthesized in a two-step process adapted from Timmer et al [145]. Briefly, propylene oxide was added dropwise to a solution of fumaric acid and pyridine in 2-butanone (2.3:1.0:0.033 mol) and refluxed at 75°C for 18 hours. Residual propylene oxide and 2-butanone were removed through a two-step distillation procedure. Residual acidic by-products and water were removed with washing, and the product was dried under vacuum (<0.2 millibar) at ambient temperature for 12 hours. The diester bis(1,2 hydroxypropyl) fumarate product was then end-capped with methacrylate groups using methacryloyl chloride in the presence of triethylamine. The molar ratios of the diester, methacryloyl chloride, and triethylamine were 1:2.1:2.1, respectively. Hydroquinone was added at a molar ratio of 0.008:1 to inhibit crosslinking during synthesis. The reaction was maintained below -10˚C to reduce undesirable side reactions and stirred vigorously overnight under a nitrogen blanket. The macromer was neutralized overnight with 2 M potassium carbonate and residual base removed with an aluminum oxide column (7 $Al_2O_3$:1 TEA). The PFDMA product was then vacuum dried and the structure confirmed using $^1$H NMR (300 MHz, $CdCl_3$), δ 1.33 (dd, 3H, CH3), 1.92 (s, 3H, CH3), 4.20 (m, 2H, -CH2-), 5.30 (m, 1H, -CH-), 5.58 (s, 1H, -C=CH2), 6.10 (s, 1H, -C=CH2), 6.84 (m, 2H, -CH=CH-). The integration ratio of methacrylate protons to fumarate protons in the $^1$H NMR spectra was used to confirm > 90% functionalization prior to polyHIPE fabrication.

### *2.2.3. PolyHIPE Fabrication*

HIPEs were prepared using a FlackTek Speedmixer DAC 150 FVZ-K following a method adapted from Moglia et al.[128] Briefly, PFDMA was mixed with a varied amount of pentaerythritol tetrakis(3-mercaptoproprionate) (0, 5, or 10 mol%) and 200 PPM hydroquinone as inhibitor, **Figure 2.1**. Two mixtures containing either 1 wt% benzoyl peroxide as initiator or 1 wt% trimethylaniline as reducing agent were combined with the organic phase and 10 wt% PGPR prior to emulsification. After homogenous mixing of the organic phase, an aqueous solution of calcium chloride (1 wt%) was added to the organic phase (75% v) in six additions and mixed at 500 rpm for 2.5 min. HIPEs were placed into a double barrel syringe and the two components mixed upon injection using a static mixing head into centrifuge tubes (5 mL syringe with 3 cm straight mixer, Sulzer Mixpac K-System). HIPEs were placed in a 37°C aluminum bead bath to facilitate crosslinking overnight.

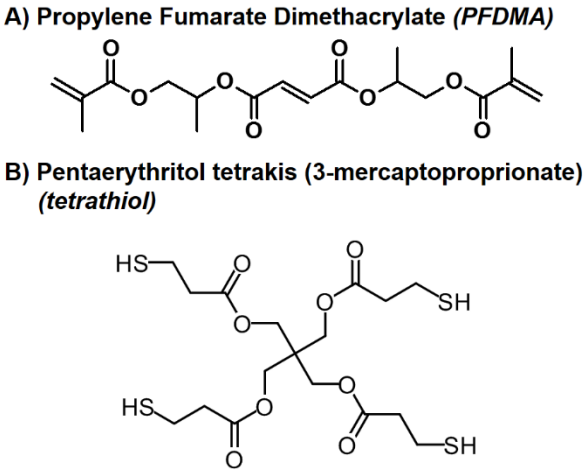


**Figure 2.1.** Molecular structure of propylene fumarate dimethacrylate (PFDMA) (A) and pentaerythritol tetrakis(3-mercaptoproprionate) (tetrathiol) (B). Reprinted from Whitely *et al*.[146]

### *2.2.4. Rheological Analysis*

Work and set times of the polyHIPEs were characterized using an Anton Paar MCR 301 rheometer following a procedure adapted from Foudazi et al.[147] Storage and loss moduli were measured every 15 seconds using a parallel-plate configuration with a 1 mm gap and 0.5% strain. Redox initiated HIPEs were injected through a mixing head onto the plate heated to 37ºC. Work time was determined as the onset of storage modulus increases and set time determined as the tan δ minimum, which corresponds to the yielding of storage modulus. Values were reported as the average of three specimens from three different HIPEs for each composition (n = 9).

### *2.2.5. Gel Fraction and Sol Fraction Composition*

Gel fraction was quantified to assess the impact of tetrathiol incorporation on network formation under ambient and inert conditions. Two distinct polyHIPE specimen

morphologies were utilized to investigate the extent of oxygen inhibition during polymerization. To characterize network formation at the scaffold surface, polyHIPEs were cured into a bead morphology with a high surface-area-to-volume ratio under ambient conditions. Scaffolds were also cured in the same morphology under a nitrogen blanket to confirm inhibition by oxygen (Labconco Controlled Atmosphere Glovebox). To characterize network formation under bulk-cured conditions, polyHIPEs were cured into 15 mL centrifuge tubes and sectioned 1 mm thick from the polyHIPE bulk (Isomet® saw). All specimens were vacuum dried for 48 hours, weighed, and then extracted in dichloromethane (DCM) at a ratio of 1 mL DCM to 10 mg of specimen to facilitate dissolution of uncrosslinked macromer. After extraction on a shaker table for 48 hours, the DCM was decanted and the specimens vacuum dried for 48 hours at ambient temperature. The gel fraction was calculated as the final weight divided by original weight (n = 6). The fraction of mass loss attributed to surfactant was subtracted prior to gel fraction calculation. The extractables of high surface area bead constructs cured under ambient conditions were analyzed with $^{1}$H NMR (300 MHz, $CdCl_3$) after vacuum removal of the DCM from the sol fraction. The integration ratio of the PFDMA methacrylate protons to tetramethylsilane protons in the $^{1}$H NMR spectra was used to identify qualitative differences in residual monomer content present in 0 and 10 mol% thiol-methacrylate polyHIPEs.

*2.2.6. Scaffold Architecture Characterization*

Average polyHIPE pore size was determined using scanning electron microscopy (SEM, Phenom Pro, Nanoscience Instruments). Specimens from three separate polyHIPEs

were vacuum dried for 24 hours to remove water, sectioned into disks, and fractured at the center to produce an unaltered surface for characterization. Each specimen was coated with gold and imaged in a raster pattern yielding five images. Pore size measurements were completed on the first ten pores that crossed the median of each 1000x magnification micrograph. Average pore sizes for each polyHIPE composition were reported (n = 150). A statistical correction was calculated to account for the random fracture plane through spherical voids and pores, $2/\sqrt{3}$.[148] Average diameter values were multiplied by this correction factor to yield a more accurate pore diameter description.

*2.2.7. Compressive Testing*

The effect of thiol concentration on polyHIPE compressive modulus and yield strength was investigated following ASTM D1621-04a. PolyHIPEs were cured in 15 ml centrifuge tubes and sectioned into disks with a 3:1 diameter to height ratio (15 mm diameter, 5 mm thick) using an Isomet® saw. PolyHIPE specimens were compressed using an Instron 3300 at a strain rate of 50 mm/s. The compressive modulus was calculated from the slope of the linear region and the compressive strength was identified, after correcting for zero strain, as the stress at the yield point or 10% strain, whichever point occurred first. Reported compressive moduli and yield strength data were averages of nine specimens for each polyHIPE composition.

*2.2.8. Accelerated Degradation In Vitro*

Accelerated degradation testing was performed on polyHIPE specimens that were sectioned using an Isomet® saw into 1 mm thick sections. Specimens were vacuum dried for 48 hours and dry weights recorded prior to incubation in base solution (0.25 and 0.5M

NaOH) at a ratio of 1 g specimen to 20 mL solution. Specimens were secured with Teflon weights in the solution and placed on a shaker table at 37°C. The solutions were changed every 2-3 days with time points every week for four weeks. At each time point, specimens were washed twice with RO water, incubated for 1 hour with 1 mL RO water to remove any salts and dried under vacuum for 48 hours before weighing (n = 3).

*2.2.9. Culture of Human Mesenchymal Stem Cells*

Bone marrow-derived hMSCs were obtained as passage 1 from the Center for the Preparation and Distribution of Adult Stem Cells at Texas A&M Health Science Center College of Medicine, Institute for Regenerative Medicine at Scott & White through NIH Grant # P40RR017447. Cells were cultured to 80% confluency on tissue-culture polystyrene flasks in standard growth media containing Minimum Essential Media α (MEM α, Life Technologies) supplemented with 16.5% fetal bovine serum (FBS, Atlanta Biologicals) and 1% L-glutamine (Life Technologies) prior to passaging. All experiments were performed with cells at passage 3.

*2.2.10. Cytocompatibility of Leachable Components from PolyHIPEs*

A viability study was performed to assess the cytocompatibility of the extractables from cross-linked polyHIPE networks immediately following scaffold injection and cure. PolyHIPEs containing 0 or 10 mol% tetrathiol were cured into a bead morphology with a high surface-area-to-volume ratio under ambient conditions and incubated in standard growth media at 37°C at a ratio of 0.13 mL HIPE to 1 mL media (surface area ~975 $cm^2$/mL). After 24 hours, the extraction media was collected and sterile filtered. To approximate the extractables from bulk-cured specimens that have roughly 50% of the sol

fraction of the bead specimens, extracts were diluted to 0.5 vol% with media. hMSCs were seeded at a density of 40,000 cells/cm$^2$ in a 96-well plate and allowed to adhere for 24 hours prior to extract exposure. 100 µL of the extract solutions was added to hMSCs and the cells cultured for 24 hours. Viability was assessed utilizing the LIVE/DEAD assay kit (Molecular Probes) according to standard protocols. Briefly, cells were washed with PBS, stained with 2 µM calcein-AM (live) and 2 µM ethidium homodimer-1 (dead) for 30 minutes at 37°C, and washed with PBS for imaging. Imaging (3 images per specimen) was conducted on five specimens (n = 15) with a fluorescence microscope (Nikon Eclipse TE2000-S).

*2.2.11. hMSC Viability on Thiol-Methacrylate PolyHIPEs*

Investigation of hMSC viability and morphology on seeded constructs was performed to assess the effect of tetrathiol addition on cell behavior. PolyHIPEs were fabricated utilizing 0 or 10 mol% tetrathiol and sectioned into 500 µm thick wafers using an Isomet® saw. Specimens were sterilized for 3 hours in 70% ethanol, subjected to a progressive wetting ladder, washed four times with PBS, and incubated overnight in MEM α supplemented with 40 w/v% FBS at 5% $CO_2$, 37°C. hMSCs were seeded at a density of 50,000 cells/cm$^2$ onto the polyHIPE sections. Viability at 24 hours, 72 hours, and 1 week was assessed utilizing the LIVE/DEAD assay kit (Molecular Probes). Cells were washed with PBS, stained with 2 µM calcein-AM (live) and 2 µM ethidium homodimer-1 (dead) for 30 minutes at 37°C, and washed with PBS for imaging. Imaging (3 images per specimen) was conducted on five specimens (n = 15) with a fluorescence microscope (Nikon Eclipse TE2000-S).

*2.2.12. hMSC Proliferation on Thiol-Methacrylate PolyHIPEs*

A Quant-iT™ PicoGreen® dsDNA Assay Kit (Molecular Probes) was utilized to quantify dsDNA to confirm thiol-methacrylate polyHIPEs supported hMSC proliferation. hMSCs were seeded at a density of 50,000 cells/cm$^2$ in standard growth media and allowed to adhere. After 24 hours, growth media or osteogenic media (growth media supplemented with 50 μg/mL ascorbic acid, 10 m*M* β-glycerophosphate, and 10 n*M* dexamethasone) was added and changed every 2 days for 10 additional days. PolyHIPE sections were removed from the culture wells and placed in unused wells for the lysis procedure prior to the PicoGreen assay to ensure only DNA from cells adhered to the scaffolds was measured. The assay was performed according to manufacturer instructions and fluorescence intensity was assessed using a plate reader (Tecan Infinite M200Pro) with excitation/emission wavelengths of 480/520 nm, respectively. Average cell number for day 1, 6, and 11 was determined by converting dsDNA values to individual cell number using 6.9 pg DNA/cell.[149] Specimens were analyzed in triplicate.

*2.2.13. Alkaline Phosphatase Activity of hMSCs on Thiol-Methacrylate PolyHIPEs*

Alkaline phosphatase activity of cells cultured on polyHIPE scaffolds was determined by monitoring the conversion of p-nitrophenyl phosphate (PNPP, Thermo Scientific) to p-nitrophenol. hMSCs were seeded at a density of 50,000 cells/cm$^2$ in standard growth media and allowed to adhere. After 24 hours, growth media or osteogenic media (growth media supplemented with 50 μg/mL ascorbic acid, 10 m*M* β-glycerophosphate, and 10 n*M* dexamethasone) was added and changed every 2 days for 10 additional days following measurement of ALP activity. Scaffold cultures were washed with ALP reaction buffer

(100 mM Tris-HCl, pH 9, containing 100 mM KCl and 1 mM $MgCl^2$) and incubated with pNPP for 30 min. ALP activity was determined as the rate of PNPP conversion to p-nitrophenyl by measuring the absorbance at 405 nm (Tecan Infinite M200Pro) and normalized to cell number obtained from the PicoGreen assay. Specimens were analyzed in triplicate.

*2.2.14. Surface Modification of PolyHIPE Scaffolds*

Methacrylated gelatin was synthesized by adding 2-isocyantoethyl methacrylate (IEMA) to a 2.5% (w/v) gelatin solution in dimethyl sulfoxide. The reaction was allowed to proceed under stirred conditions for 3 h at 40 °C. The fraction of lysine groups was reacted at a 1x ratio with IEMA under the assumption of 11 lysines per protein molecule. After completion, the solution was dialyzed against distilled water for 24 hours at 40 °C to remove impurities and lyophilized. Functionalized gelatin was added as the aqueous phase of the model HIPE (1, 4 butanediol dimethacrylate) at a 2 wt% solution and mixed using standard fabrication methods. The collagen indicator, picrosirius red (PSR), was used to confirm attachment of gelatin to the scaffold surface after polymerization and sterilization. Scaffolds were stained with a 1 mg/mL solution for 30 min at room temperature. After staining, scaffolds were rinsed with deionized water 5× and digitally photographed.

*2.2.15. hMSC Attachment on Gelatin Modified PolyHIPEs*

The impact of polyHIPE surface modification on cellular behavior was determined by characterizing adhesion, spreading, and viability of hMSCs a 24 hours. Gelatin modified scaffolds were prepared and sterilized as described previously. hMSCs were seeded at a

density of 10,000 cells/cm$^2$ onto polyHIPE sections. Viability and spreading was assessed utilizing the LIVE/DEAD assay and imaging protocols outlined previously. Attachment of hMSCs was quantified using ImageJ analysis on viability stained images.

*2.2.16. Pilot Assessment of PolyHIPE Biocompatibility*

*In vivo* deployment procedures and initial biocompatibility of injectable PFDMA HIPEs was assessed in a critical sized rat calvarial defect adapted from Spicer et al. Briefly, an incision was made through outer tissue layers of the scalp and an 8 mm craniotomy made using a dental drilling machine with an 8 mm trephine burr. The resulting defect was cleaned prior to the addition of the HIPE from a double-barrel syringe. HIPE was allowed to cure for 2 minutes, followed by suturing of the periosteum, subcutaneous tissue, and skin. Histological analysis was performed after 4 weeks to characterize preliminary host response. Integration of thiol-methacrylate polyHIPEs with native bone tissue was assessed using a rabbit medial femoral condyle defect with diameter 3.5 mm and depth of 5 mm. Femur specimens with polymerized polyHIPE were harvested, sectioned utilizing a low speed Isomet® saw and imaged utilizing a scanning electron microscope (SEM) (JEOL 6500).

*2.2.17. Statistical Analysis*

The data are displayed as mean ± standard deviation for each composition. A Student's t-test was performed to determine any statistically significant differences between compositions. All tests were carried out at a 95% confidence interval ($p<0.05$).

## 2.3. Results and Discussion

### *2.3.1. Effect of Tetrathiol Concentration on PolyHIPE Fabrication and Architecture*

Given that successful polyHIPE fabrication is dependent on characteristics such as macromer hydrophobicity and viscosity, the effect of the thiol additive on emulsion stability was first assessed. The octanol-water partition coefficient (logP) was used as a means of comparing molecular hydrophobicity. LogP values are a measure of the differential solubility of a compound between two immiscible solvents, typically water and a hydrophobic solvent such as octanol. LogP values range from 0-20 where 0 corresponds to a hydrophilic molecule and 20 a hydrophobic molecule. The tetrathiol has a logP of 1.0 and a viscosity of 0.41 Pa·s compared to PFDMA with a logP of 3.4 and 0.13 Pa·s viscosity. Despite these differences in molecular hydrophobicity and viscosity, all compositions formed stable HIPEs and cured to rigid, interconnected monoliths. Pore size and homogeneity have been used as a relative measure of HIPE stability and strongly influence the monolith compressive properties and cellular behavior. The addition of the tetrathiol had a negligible effect on polyHIPE pore architecture, **Figure 2.2.** Likely, the low concentration of tetrathiol in the organic phase and rapid cure of the PFDMA HIPE limited time for phase separation and resulting effects on polyHIPE architecture. Retention of the desired pore architecture permits investigation of these polyHIPEs as scaffolds with reduced oxygen inhibition.

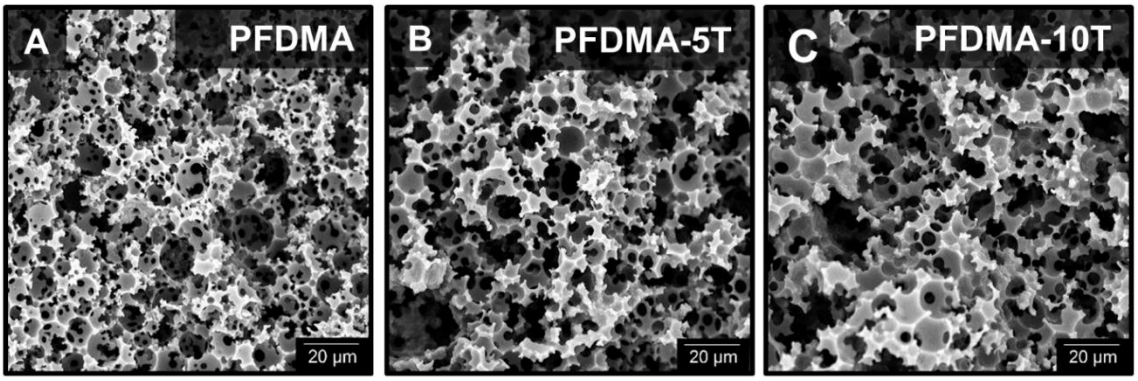


**Figure 2.2.** Representative scanning electron microscopy (SEM) micrographs of PFDMA (A), PFDMA-5T (B), and PFDMA-10T (C) polyHIPE pore architecture. Reprinted from Whitely *et al*.[146]

### *2.3.2. Effect of Tetrathiol Concentration on PolyHIPE Cure Rate*

Developing a material with polymerization kinetics comparable to commonly utilized bone cements is critical to successful translation of our device. In general, the work time of dental cements is defined by ISO 9917 as the time at which a physician can manipulate and inject the graft without altering any material properties. The set time is the point at which the material has reached its gelation point and the network is set. According to ISO 5833, acrylic based cements should have a set time of 10-15 minutes. PolyHIPE cure rates were determined utilizing rheological methods with the onset and yielding of the storage modulus defined as the work and set times, respectively. PFDMA polyHIPE work and set times decreased with the addition of tetrathiol, **Figure 2.3.** The ~1.5 minute work time of PFDMA was reduced to 15 seconds with the addition of either 5 or 10 mol% tetrathiol. Similar trends were observed with the set time of these polyHIPEs. No significant difference in work and set times were observed between thiol concentrations utilizing this method. It was hypothesized that the extent of oxygen consumption needed prior to

initiation provided the increased cure time of the PFDMA polyHIPE control. Increased induction time in the presence of inhibitory oxygen has been well documented in other vinyl mediated systems.[150] It has been reported that the equilibrium dissolved oxygen in acrylate systems is ~$10^{-3}$ M.[51, 151] Decker et al. reported that the dissolved oxygen concentration in these systems must decrease by a factor of 300 to ~4 x $10^{-6}$ M prior to polymerization proceeding.[51] It was hypothesized that the addition of the thiol-based crosslinker permitted a reduced induction period and rapid network formation under ambient conditions due to the mixed mode chain and step growth polymerization mechanism of the thiol-methacrylate HIPEs. In addition to the increase in methacrylate polymerization rate with the addition of the thiol, the delay in methacrylate homopolymerization due to oxygen inhibition is minimized because the peroxy radicals can abstract the thiol hydrogen to generate thiyl radicals that can continue to propagate through addition or chain transfer.[152] Although the presented set times are approximately 10X faster than current bone cement standard values, the cure times can be modulated by decreasing redox initiator concentration, initiator and reducing agent ratios, and chemistries, as shown previously.[128]

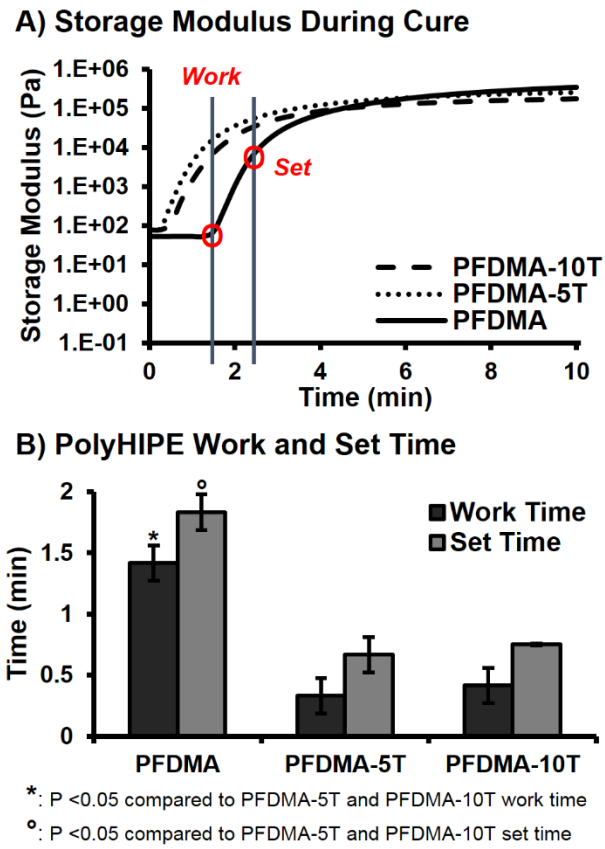


**Figure 2.3.** Storage modulus during polymerization of polyHIPE (A) and work and set times (B) of polyHIPEs cured at 37 °C with 1.0 wt% initiator and reducing agent. Reprinted from Whitely *et al.*[146]

### *2.3.3. Improved Resistance to Oxygen Inhibition in PolyHIPE Scaffolds*

The inhibitory effect of molecular oxygen on the polymerization of multifunctional monomers has been widely acknowledged as a primary limitation in traditional free-radical polymerization.[150, 153, 154] Several methods have been explored to overcome this limitation including the use of elevated concentrations of initiating agents, high-intensity irradiation sources, and fabrication within an inert environment.[155, 156] However, less progress has been made in addressing this limitation in an injectable system intended for

*in situ* polymerization. The primary aim of this work was to fabricate an injectable, polyHIPE bone graft that could provide more rapid and complete network formation in a clinically relevant environment. Specifically, we aimed to better understand the effect of oxygen inhibition on network formation in our polyHIPE system.

A major advantage of the emulsion templating platform is the ability to readily modulate pore architecture and surface area, properties vital to the success of tissue engineered scaffolds.[157] A range of surface areas have been reported from 3-20 $m^2g^{-1}$ for traditional polyHIPEs to greater than 700 $m^2g^{-1}$ for porogen modification scaffolds.[158, 159] Although promising for promoting cell activity, the increased surface area of polyHIPEs provides a challenge over non-porous systems as it allows for increased diffusion of inhibitory oxygen into the HIPE surface. Near-complete network formation at these surfaces is critical to establishing suitable integration with native tissue and providing proper mechanical support. In order to better approximate monomer incorporation at the outer surface of the HIPE, network formation was first characterized in polyHIPEs cured in a high surface area morphology (flat bead) that maximized exposure to ambient oxygen. It was expected that the outer polyHIPE surface would be unable to compensate for the continual diffusion of oxygen into the sample and experience severely reduced polymerization and increased surface tackiness. Gel fraction was reduced to 38% in PFDMA control polyHIPEs cured under ambient conditions, **Figure 2.4A**. It follows that in the absence of inhibitory oxygen, monomer conversion in vinyl systems should increase to levels comparable to those of their oxygen resistant analogues. To this end, network formation was characterized in polyHIPEs cured under an inert nitrogen blanket in the

high surface area morphology. PFDMA polyHIPE gel fraction increased to 60%, confirming the inhibitory effect of oxygen on our system. It is established that incorporation of thiol monomers mitigates the effects of oxygen exposure by acting as chain transfer agents and restoring initiating thiyl radicals. As expected, the addition of 5 and 10 mol% tetrathiol improved network formation to greater than 60% and 70% when cured under ambient conditions. It was hypothesized that the increase in continuous phase viscosity provided by tetrathiol addition further served to improve inhibition resistance by decreasing oxygen diffusion into the scaffold. The effect of monomer viscosity in reducing oxygen inhibition has been studied in other thiol-acrylate systems.[52, 160] Furthermore, network formation in thiol-methacrylate polyHIPEs increased to a lesser extent when cured under inert conditions as compared to PFDMA polyHIPE controls. Differences in network formation between methacrylate and thiol-methacrylate scaffolds cured under nitrogen-purged conditions was attributed to the presence of small amounts of residual oxygen.

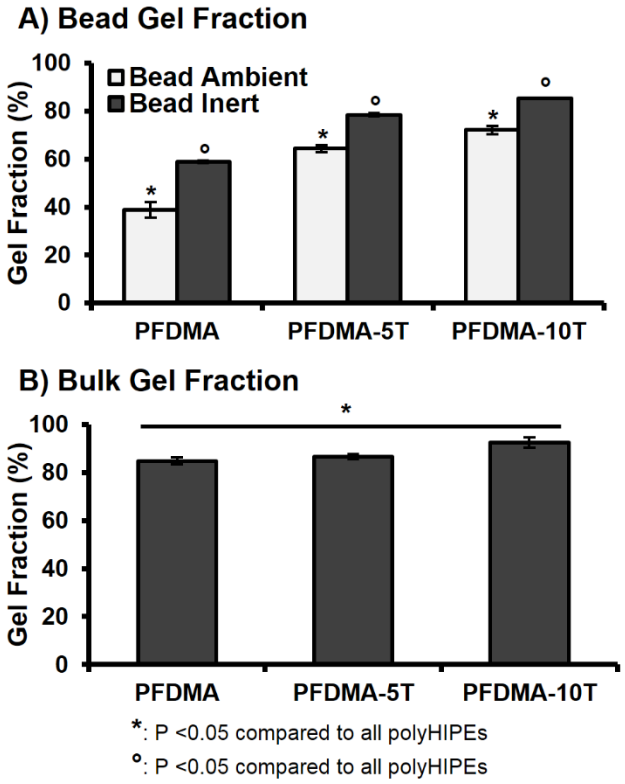


**Figure 2.4.** The effect of increasing tetrathiol concentration on average gel fraction for high surface-area-to-volume ratio polyHIPEs cured under ambient and low oxygen conditions (A) and bulk cured polyHIPEs cured under ambient conditions (B). Reprinted from Whitely *et al.*[146]

Oxygen inhibition has also been modeled in acrylate systems to identify the effect of film thickness on oxygen inhibition.[136] It is accepted that as film thickness increases, inhibitory oxygen levels decrease and allow for polymerization. The subsequent increase in viscosity during cure serves to limit subsequent diffusion of oxygen. Therefore, it was expected that network formation of PFDMA monomers in bulk-cured scaffolds would be comparable to thiol-methacrylate systems. Gel fraction values were 85% for PFDMA controls, 87% for 5 mol% tetrathiol, and 92% for 10 mol% tetrathiol, **Figure 2.4B**.

Observed increases in gel fraction for thiol-methacrylate polyHIPEs under these conditions was attributed to the presence of dissolved oxygen prior to cure. Previous work has demonstrated injectable, fumarate based systems with sol fraction values greater than 10% to be biocompatible and support new bone formation *in vitro* and *in vivo*.[161-163] Furthermore, commercially available bone cements have been shown to exhibit site specific network formation within the implant site.[164] Our ability to improve network formation in the presence of oxygen, combined with the success of similar fumarate systems, illustrates the strong clinical potential of these polyHIPE bone grafts.

*2.3.4. Improved Storage Stability with Hydroquinone Additive*

We have previously demonstrated that redox initiated polyHIPEs have the ability to be stored for extended periods and serve as an off-the-shelf graft. Although thiol-methacrylate polyHIPEs demonstrated improved resistance to oxygen inhibition, an increase in emulsion viscosity that precluded proper injection and space filling was observed after only one week of storage. It has been reported that thiol monomers may act as a primary reducing agent and yield high monomer conversion rates in redox initiated thiol-ene systems.[165] It was hypothesized that the loss of storage stability in our system resulted from the uninhibited reaction of benzoyl peroxide with the tetrathiol monomer during fabrication and storage. This allowed marginal levels of initiating radicals to form prior to mixing, facilitate early crosslinking, and increase emulsion viscosity. This high reactivity of thiol-ene systems often prompts the need for additional stabilizing agents to prevent undesired polymerization.[134, 166] To this end, hydroquinone was added as a stabilizing agent to the HIPE to scavenge propagating radicals and prevent early

polymerization, **Figure 2.5A**. Quinone based inhibitors have been utilized to control the induction period and polymerization rate of thiol-ene polymerizations initiated with benzoyl peroxide.[165] Inhibitor concentration of 200 PPM was selected as the lowest concentration required to prevent early polymerization while retaining a reduced activation profile to allow rapid cure during redox initiation. Storage time of stabilized polyHIPEs with 10 mol% tetrathiol was monitored for 30 days to ensure an increase in storage time. Cure rate and gel fraction of stabilzed polyHIPEs was characterized to ensure the addition of inhibitor did not negatively impact key scaffold properties. Although a minimal decrease in cure rate and gel fraction was observed in stabilized polyHIPEs as compared to non-stabilized controls, the values still provide a marked increase over PFDMA only and support significant resistance to oxygen inhibition, **Figure 2.5**.

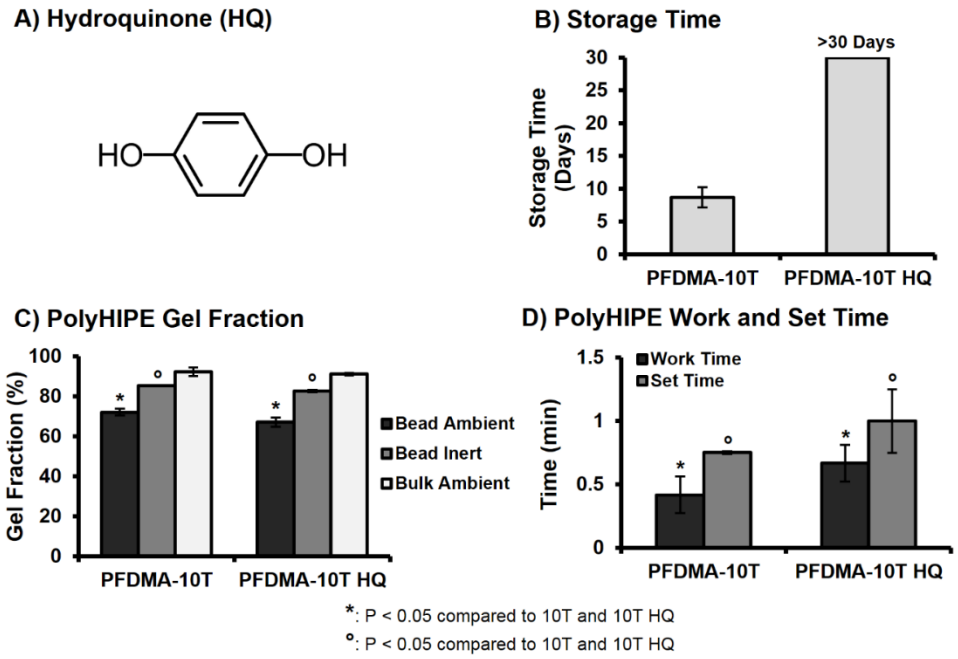


**Figure 2.5.** The effect of hydroquinone inhibitor (A) on average storage time (B), work and set time (C), and gel fraction (D) of thiol-methacrylate polyHIPEs. Reprinted from Whitely *et al*.[146]

### *2.3.5. Retention of Compressive Properties*

PFDMA/tetrathiol polyHIPE compressive modulus and yield strength were assessed to ensure that these polyHIPEs retained appropriate compressive mechanical properties for use as bone grafting materials. A significant decrease in compressive modulus and yield strength was observed with an increase in tetrathiol concentration, **Figure 2.6.** PFDMA polyHIPEs fabricated with greater than 10 mol% tetrathiol exhibited decreases in compressive properties greater than 40% as compared to PFDMA controls and were not further characterized. PFDMA polyHIPEs with 10 mol% tetrathiol resulted in an average compressive modulus of 15 MPa and strength of 0.7 MPa. It was hypothesized that the observed decrease in compressive properties was due to a reduction in crosslink

density. Increasing the number of thiol functional groups resulted in an increase in chain transfer during polymerization with a resulting reduction in chain length and the number of crosslinks attached to each kinetic chain. A similar decrease in compressive modulus with increasing amount of trithiol was observed by Rydholm et al. in poly(ethylene glycol)-based hydrogels.[152]

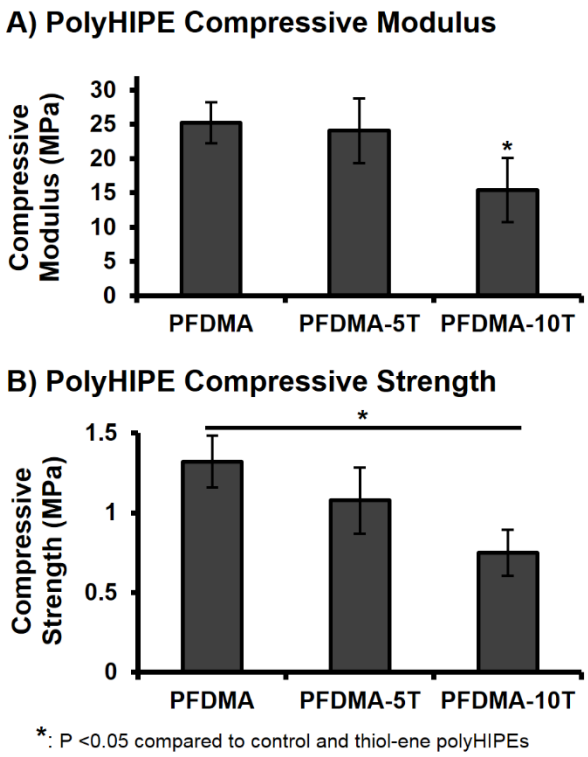


**Figure 2.6.** The effect of increasing tetrathiol concentration on polyHIPE compressive modulus (A) and yield strength (B). Reprinted from Whitely *et al*.[146]

Although there was a reduction in compressive modulus and yield strength, the values were still within the range of typical bone grafting materials. The ability to promote new bone formation within porous and biodegradable systems has been reported with scaffold

compressive moduli ranging from 2-100 MPa.[167-170] Introduction of porosity into these systems is often achieved through particulate leaching or gas foaming, techniques that may result in reduced compressive properties as porosity is increased.[171-174] In contrast, emulsion templating yields a uniform and spherical pore architecture that eliminates the potential for stress concentrators. As a result, PFDMA and thiol-methacrylate polyHIPEs exhibit improved mechanical properties over similar systems of >70% porosity, and retain compressive properties within a range demonstrated suitable *in vivo*.[171, 172] Recent work has focused on incorporating additional methacrylate-functionalized monomers into the HIPE organic phase to further modulate viscosity for cell encapsulation. PolyHIPEs fabricated from these monomers alone have increased crosslink density and therefore increased compressive properties. As a result, it is probable that modulating the molar ratio of PFDMA:methacrylated-monomer will result in an increase in compressive properties relative to standard PFDMA polyHIPEs.

*2.3.6. Tunable Degradation Profiles*

An additional goal of fabricating thiol-methacrylate polyHIPEs was to generate scaffolds with a tunable degradation profile for future matching with *in vivo* neotissue formation. Thiol-methacrylate scaffolds with tunable degradation profiles have previously shown promise for use as tissue engineered scaffolds. Accelerated degradation scouting studies were conducted at two sodium hydroxide concentrations (0.25 and 0.5 M NaOH) to determine the effect of tetrathiol on PFDMA polyHIPE degradation. Values reported reflect mass loss after accounting for the theoretical mass of the surfactant, PGPR. An increase in mass loss was observed with an increase in tetrathiol concentration when

assessed in basic, accelerated conditions, **Figure 2.7**. In 0.5 M NaOH conditions, all thiol-methacrylate polyHIPEs exhibited complete loss of integrity by 3 weeks whereas the PFDMA polyHIPE control maintained ~35% mass loss after the initial mass loss at 1 week. The initial PFDMA mass loss at one week was attributed to the removal of unreacted macromer or the formation of rapidly degrading microgels, which was further supported with the lower gel fraction of PFDMA control polyHIPEs.[175] This increase in hydrolytic degradation rate of thiol-methacrylate polyHIPEs was attributed to the incorporation of β-thioesters and reduction in crosslink density due to increased chain transfer.[176] Schoenmaker et al. demonstrated an increase in atomic charge on the carbon atom of an ester as the distance from the sulfide decreased rendering it more susceptible to hydrolytic attack. It is believed that the increased number of hydrolytically labile ester linkages present in the fumarate backbone of PFDMA would allow for increased degradation over similar methacrylate monomers without requiring increased thiol content. Although an increase in degradation rate was observed *in vitro*, the *in vivo* degradation rate of these specific polyHIPE formulations is unknown and would need to be explored in an animal model. Degradation and cytocompatibility profiles of similar fumarate based systems have been previously reported in *in vitro* and *in vivo* models.[177-179]

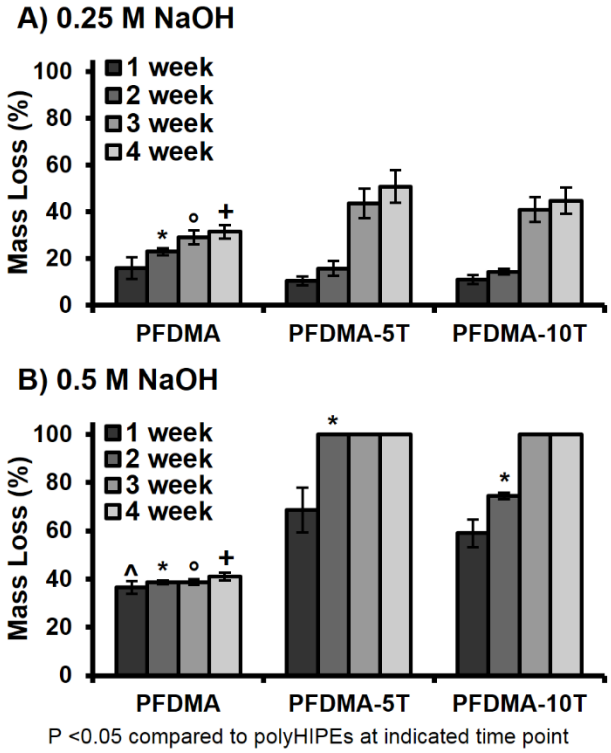


**Figure 2.7.** The effect of increasing tetrathiol concentration on polyHIPE degradation up to 4 weeks in 0.25 M NaOH (A) and 0.5 M NaOH (B). Reprinted from Whitely *et al.*[146]

### *2.3.7. Osteogenic Activity Supported on Thiol-Methacrylate PolyHIPEs*

A primary aim in bone tissue engineering is the development of scaffolds that allow for the recruitment and retention of stem cell populations at the site of injury. Therefore, a main goal of this work was to create a highly porous, oxygen resistant bone graft that would support desired cellular activity through verification of viability, proliferation and osteogenic activity of hMSCs. Studies with poly(propylene fumarate)-based biomaterial scaffolds with similar chemistries demonstrated in vitro cytocompatibility and in vivo biocompatibility illustrating the potential of PFDMA based systems.[39, 167, 180] Furthermore, our lab previously demonstrated PFDMA polyHIPEs are capable of supporting hMSC

viability up to 2 weeks.[128] Given the proposed application of polyHIPEs to be injected and cured in situ, an extraction study was performed on cross-linked PFDMA control and 10 mol% thiol-methacrylate scaffolds to provide an initial assessment of the cytocompatibility of the injectable polyHIPE immediately following cure. Although acute viability of hMSCs exposed to undiluted extraction media of polyHIPE bead specimens was poor (<30%), a significant improvement in acute viability and morphology was observed for the thiol-methacrylate polyHIPEs at 0.5 vol% over the PFDMA control. Viability increased to greater than 94%, with no morphological differences observed between hMSCs cultured with the thiol-methacrylate extract compared to standard growth media, **Figure 2.8**. The bead morphology was used to provide high surface-area-to-volume ratios that would maximize the effect of oxygen inhibition and sol fraction. The 2X dilution of the extraction solution was used to estimate extractable concentrations of bulk polymerized specimens (roughly 50% sol fraction of bead specimens, Figure 2.4), which are expected to be more similar to bone grafting applications. It was hypothesized that the improvement in network formation in thiol-methacrylate systems reduced leachable monomer content present in the extraction media and resulted in improved viability over the PFDMA control. **Figure 2.9,** illustrates a decrease in PFDMA macromer content present in extraction media as determined by $^{1}$H NMR.

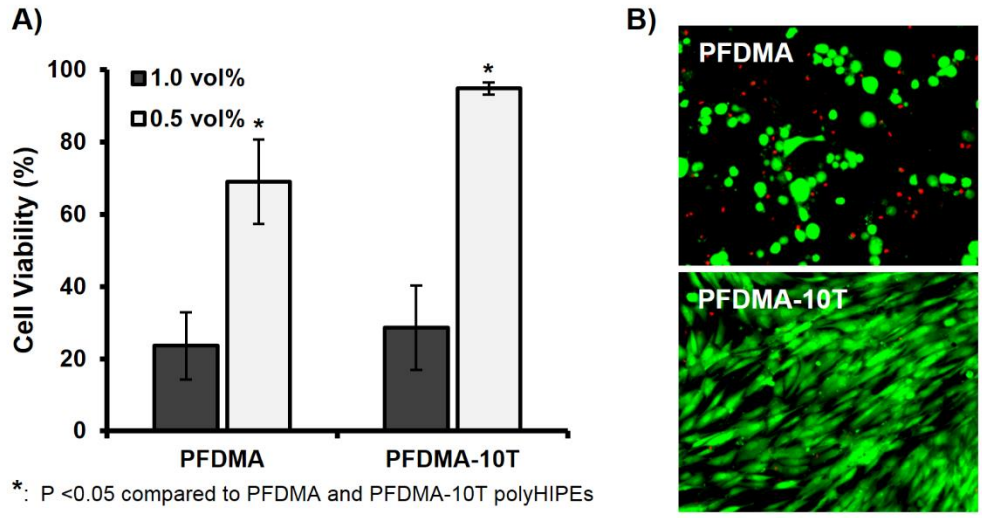


**Figure 2.8.** hMSC viability after 24 h incubation with two concentrations of PFDMA and PFDMA-10T extracts (1.0 and 0.5 vol%) (A). Micrographs illustrating live (green) and dead (red) cells cultured with respective polyHIPE extracts at 0.5 vol% (B). Reprinted from Whitely *et al.*[146]

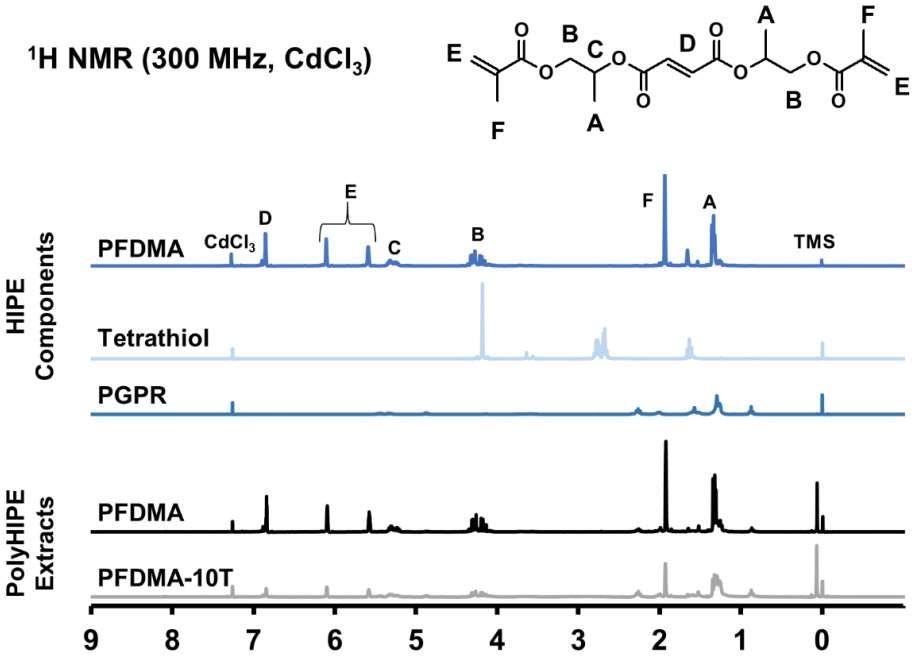


**Figure 2.9.** NMR spectrum of PFDMA and PFDMA-10T polyHIPE extracts. Reprinted from Whitely *et al.*[146]

After confirming an improvement in acute cytocompatibility with tetrathiol incorporation, hMSCs were seeded directly onto cleaned PFDMA control and 10 mol% thiol-methacrylate polyHIPEs up to one week to further characterize cell response. Thiol-methacrylate polyHIPE scaffolds supported hMSC viability of greater than 80%, while PFDMA controls exhibited viability greater than 90% **Figure 2.10**. Minor differences in viability between scaffold compositions was attributed to differences in initial cell attachment as a result of altered surface chemistry and protein adsorption. In addition, a 2 and 3 fold increase in cell number was observed at 11 days on PFDMA controls and thiol-methacrylate polyHIPEs respectively, **Figure 2.11**. The ability of thiol-methacrylate polyHIPEs to support long-term proliferation permits further investigation into osteogenic activity of seeded hMSCs. Notably, the specimens were sterilized with ethanol washes prior to cell seeding that may remove extractables and not fully replicate the injected form, which is a limitation of the current study. In future studies, each of the components will be sterilized prior to HIPE formation and sterility maintained prior to injection. This method will permit cytocompatibility and other biocompatibility assessments immediately following injection and cure without additional processing. It is expected that possible leachables will likely to be removed by the native vasculature, as postulated previously for other fumarate systems.[161]

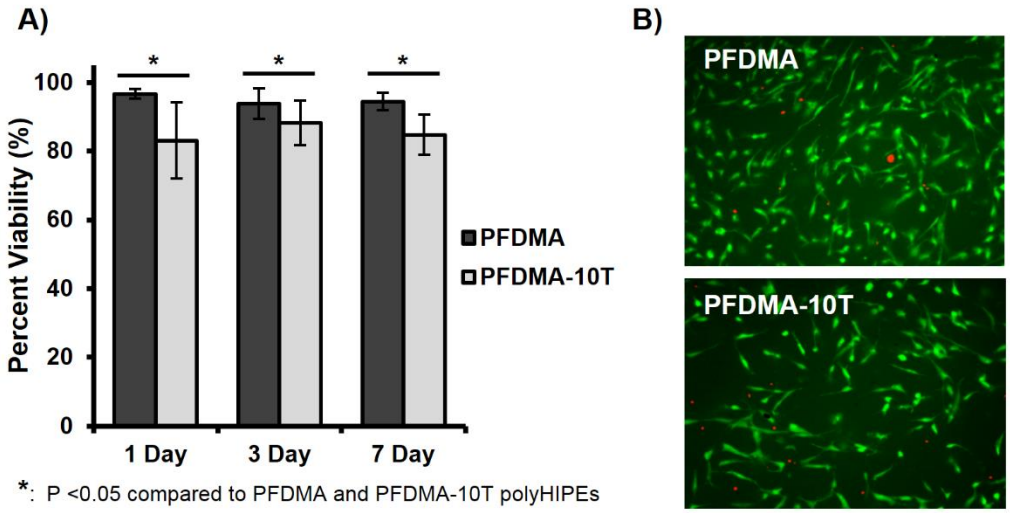


**Figure 2.10.** hMSC viability on PFDMA and PFDMA-10T polyHIPEs at 1, 3, and 7 days (A). Micrographs illustrating live (green) and dead (red) cells on the respective polyHIPE sections at 7 days (B). Reprinted from Whitely *et al*.[146]

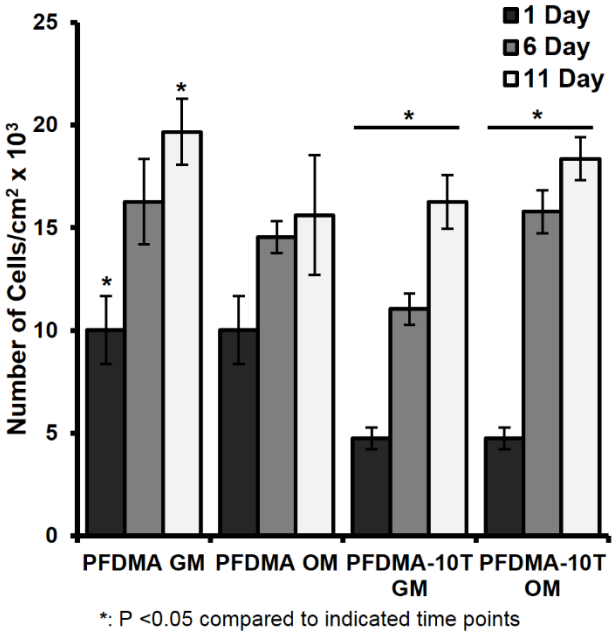


**Figure 2.11.** Proliferation of hMSCs seeded on PFDMA and PFDMA-10T polyHIPEs at 1, 6, and 11 days as determined by DNA quantification. hMSCs were cultured in growth media (GM) and osteogenic media (OM) with an initial cell seeding density was 50,000 cells/cm$^2$. Reprinted from Whitely *et al*.[146]

The ability to direct bone-marrow derived cells down a discrete lineage is a potent tool for improving the regenerative capacity of our tissue engineered graft. We previously demonstrated the ability of polyHIPE scaffolds to serve as a delivery vehicle for a multitude of osteoinductive agents and support osteogenic activity of seeded hMSCs as confirmed by early and late stage gene expression.[129] Furthermore, unmodified PFDMA scaffolds also reported osteogenic differentiation under standard culture conditions demonstrating an inherent osteoinductive character of these grafts. In this study, ALP enzyme activity was assessed as an early marker of osteoblastic differentiation of seeded hMSCs to confirm that thiol-methacrylate polyHIPEs retained this ability to support osteogenic activity. ALP activity increased (2-3 fold) for all scaffold compositions at 11 days for scaffolds cultured in both growth and osteogenic media, **Figure 2.12**. It was noted that the rate of proliferation decreased while the rate of increase in ALP activity increased for both scaffold compositions from day 6 to day 11, when hMSCs were cultured in ostegenic media. No significant differences were observed between PFDMA control and thiol-methacrylate polyHIPEs. These observations support established activity profiles for MSC differentiation and illustrate the retained ability of these grafts to support osteogenic activity.

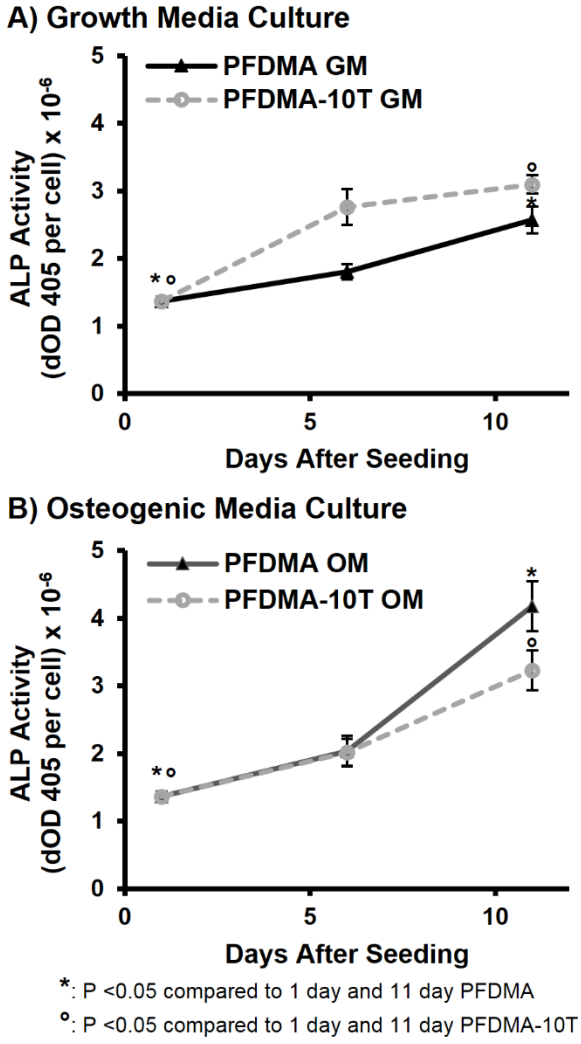


**Figure 2.12.** Alkaline phosphatase activity of hMSCs seeded on PFDMA and PFDMA-10T polyHIPEs at 1, 6, and 11 days. PolyHIPEs were cultured in growth media (GM) (A) and osteogenic media (OM) (B). Reprinted from Whitely *et al.*[146]

Although initial activity of MSCs seeded on our polyHIPE graft provide a clear promise for success in vitro, a future goal of this project is the development of an injectable polyHIPE system with the potential to support encapsulation and in vivo delivery of these cells to the injury site. The addition of tetrathiol into our injectable polyHIPE may provide

added benefit in this work to adapt our system as a rigid cell carrier. Roberts et al. demonstrated that thiol-ene based polymerization mechanisms can have long-term effects on the quality of engineered cartilage in thiol-ene systems over acrylate based PEG hydrogel scaffolds.[181] Furthermore, the role of thiol-ene chemistries in reducing intracellular ROS damage was noted, a characteristic of thiol-methacrylate polyHIPEs that would further support viability and retention of encapsulated cells.

*2.3.8. PolyHIPE Surface Modification*

In this work, methacrylated gelatin was utilized to modify polyHIPE pore surfaces fabricated with the macromer 1,4 butanediol dimethacrylate. The collagen denaturation process utilized to form gelatin exposes RGD binding sites that are strong promoters of cell attachment.[182] Increased intensity of Picrosirius Red staining confirmed gelatin modification of polyHIPE pore surfaces post sectioning and sterilization procedures, **Figure 2.13**. It is hypothesized that the hydrophobicity of gelatin relative to macromer resulted in relocation of the protein closest to the aqueous phase at the pore wall. A corollary increase in attachment, viability, and spreading of hMSCs was observed on gelatin modified constructs as compared to untreated polyHIPEs. Viability on modified scaffolds was greater than 90% with a 50% increase in cell attachment. A significant increase in cell spreading was also observed. This work holds significant promise for future polyHIPE surface modification work as this approach can be utilized to incorporate targeted proteins capable of guiding cell activity. Specifically, a class of engineered, streptococcal collagen-like proteins are currently being explored due to their ability to present specific and targeted receptor binding motifs.[183] Integrin mediated signaling plays

a prominent role in the regulation of hMSC differentiation and promotion of mineralization through both biomechanical and biochemical pathways.[184, 185] The ability to not only control cell attachment but facilitate activation of targeted signaling pathways has the potential to significantly improve osteogenesis.

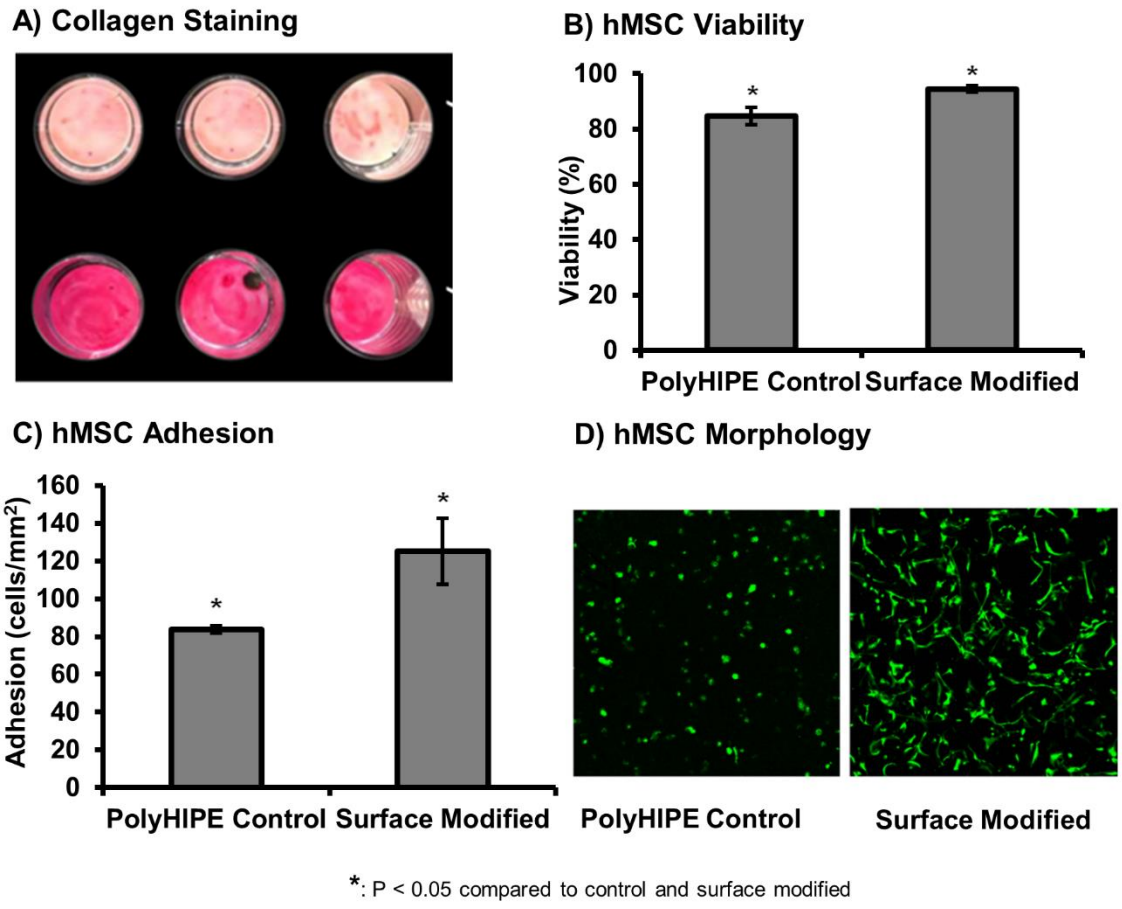


**Figure 2.13.** The effect of gelatin surface modification on collagen staining (A), attached hMSC viability (B), hMSC adhesion (C), and hMSC morphology and spreading (D) of polyHIPE scaffolds.

### *2.3.9. Pilot Assessment of PolyHIPE Biocompatibility*

Pilot studies were performed to demonstrate the ability to deploy injectable HIPEs *in vivo* and characterize biocompatibility. PolyHIPE scaffolds injected into a critical sized rat calvarial defect were evaluated for host response at 4 weeks and compared to an empty defect control, **Figure 2.14**. PolyHIPE grafts supported cell attachment and migration demonstrated by moderate lymphocytic/plasmacytic infiltrate. Ordinal scoring of negative control and polyHIPE (n=6 evaluated tissue sections) indicated no significant differences in the biologic response, with the exception of lymphocyte infiltrate. A rat femoral defect model was utilized to characterize polyHIPE integration with native tissue prior to investigation in load bearing models, **Figure 2.15.** Scanning electon microscopy of filled defects demonstrates excellent, microscale integration with the native bone tissue. Success of this procedure allows for more in depth investigation of scaffold integration through mechanical, push out testing. Overall, these studies represent an important milestone in the development of an injectable bone graft.

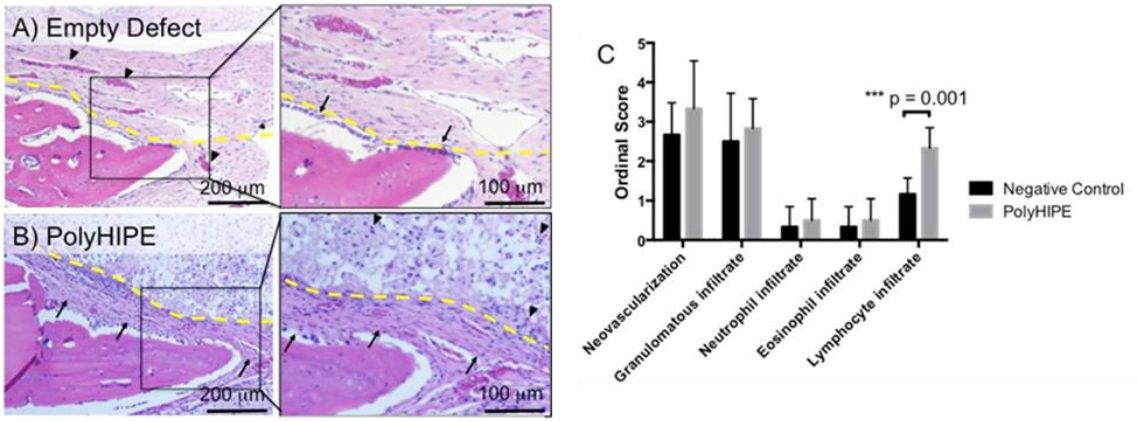


**Figure 2.14.** Biocompatibility of polyHIPE in rat calvarial defect model. A: Negative control defects contain neovascularization (arrowheads), spindle shaped fibroblasts, and collagenous matrix. B: The polyHIPE treated defect contains similar fibrous tissue (arrowheads). C: Ordinal scoring of negative control and polyHIPE (n = 6 tissue sections) indicated no significant differences in the biologic response, except for lymphocyte infiltrate, which was increased in polyHIPEs.

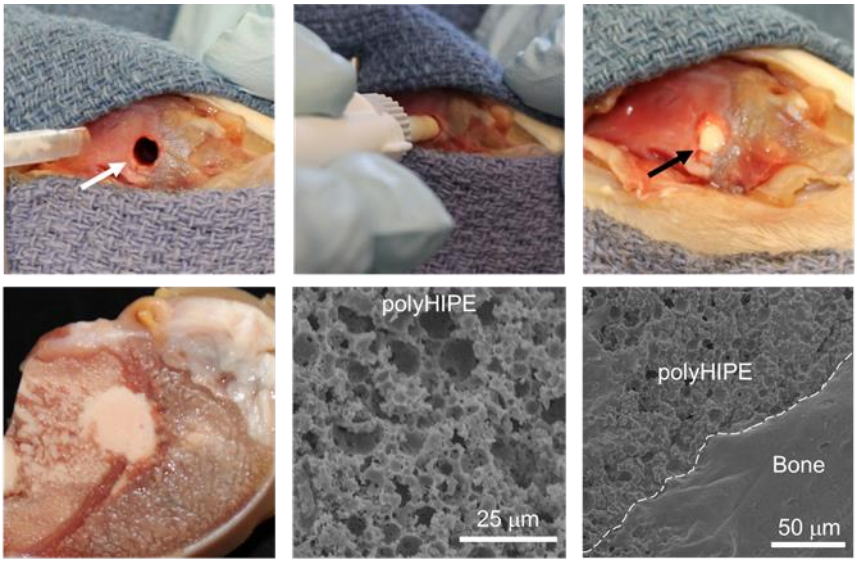


**Figure 2.15.** Rabbit medial femoral condyle defect with diameter 3.5 mm and depth of 5 mm (white arrow) (A). PolyHIPE injected into the defect (B). PolyHIPE interdigitates with the bone, and solidifies (black arrow) (C). Harvested and sectioned image of the filled defect (D), and representative SEM images of the injected polyHIPE (E) and bone/graft interface (F).

## 2.4. Conclusions

This study demonstrates the potential of thiol-methacrylate polyHIPEs to serve as an injectable bone graft with improved resistance to oxygen inhibition. Incorporation of tetrathiol monomer provided more rapid and complete network formation in the presence of oxygen with minimal impact on compressive modulus, yield strength, and pore architecture. The introduction of β-thioesters also served to increase the rate of hydrolytic degradation of the polyHIPE, providing a potent tool for tuning desired degradation profiles. Finally, thiol-methacrylate polyHIPEs demonstrated strong potential as a tissue engineered scaffold by supporting extended viability and proliferation of hMSCs and retaining the osteoconductive character previously observed in our PFDMA system. Overall, the investigation of thiol-methacrylate based grafts improves the translational potential of polyHIPEs by providing a material with improved function in clinically relevant environments and demonstrating the potential to influence cellular activity.

# CHAPTER III

# IMPROVED IN SITU SEEDING OF 3D PRINTED BONE GRAFTS USING CELL-RELEASING HYDROGELS

## 3.1. Introduction

Despite the high regenerative potential of bone, treatment of large defects and nonunions remains a significant challenge and often requires surgical intervention. Autologous grafting serves as the current standard of care due to its high regenerative capacity. However, this treatment is unavailable in a large number of patients due to anatomical limitations associated with harvesting.[186] Patients eligible for autologous grafting face elevated risk of donor site morbidity, pain, and infection. Tissue engineering aims to provide a bone replacement that combines the regenerative potential of autologous grafts with the availability and tunability of synthetic materials. Tissue engineered bone grafts are designed to be a porous scaffold that matches defect geometry, degrades at a rate complementary to new tissue formation, and exhibits requisite mechanical properties to withstand physiological loading.[187, 188] It is often challenging to achieve this combination of properties using traditional fabrication techniques. For example, highly porous constructs that facilitate nutrient and waste transport often struggle achieving desired mechanical properties.[171, 172] Expansion of 3D printing technologies into tissue engineering has provided researchers new tools to independently control and optimize these properties. We recently developed a multi-modal printing system to generate tissue engineered scaffolds that mimics the native structure of bone.[189, 190] In this system,

fumarate-based emulsion inks with hierarchical porosity were reinforced with a poly(ε-caprolactone) or poly(lactic acid) shell to achieve simultaneous improvements in permeability and compressive properties.

In addition to the design of scaffold properties, success as a tissue engineered bone graft depends on the delivery or recruitment of mesenchymal stem cells (MSC). These multipotent progenitor cells aid regeneration through a variety of mechanisms including serving as new centers of bone formation and secretion of trophic factors that modulate inflammation, stimulate angiogenesis, and limit fibrosis.[65, 191-193] Despite the therapeutic advantages of MSCs, traditional cell delivery (e.g. direct injection of stem cells via syringe or catheter) are associated with limited cell engraftment, often retaining less than 5% of injected cells.[81, 82, 194] Furthermore, the hostile environment of injured or diseased tissue can reduce retention of transplanted cells by depriving them of nutrients or subjecting them to early clearance by surveying inflammatory cells.

To overcome this limitation, researchers have investigated and reviewed numerous hydrogel carriers to improve retention and viability of transplanted cells.[83, 84, 195, 196] Encapsulation within an external matrix improves retention by acting as a mechanical barrier to cell wash out and providing an improved substrate for tissue engraftment. Multiple natural and synthetic hydrogel platforms have been investigated for cell encapsulation based on modfied gelatin, fibrin, and poly(ethylene glycol)-based systems.[197-202] Although these have improved cell retention, use of hydrogel scaffolds alone are not ideal for bone grafting due to their poor compressive properties. Multiple groups have reported on the benefits of using mechanically robust scaffolds coupled with

microsphere mediated cell delivery to improve both cell retention and mechanical stability. Alginate based microspheres have been utilized as cell delivery vehicles in both calcium phosphate and polyurethane scaffolds.[93, 94] Although these systems illustrate the potential of combination delivery methods, these protocols often require significant processing prior to use that add significant cost and regulatory hurdles. In contrast, we propose to use an *in situ* curing hydrogel as a cell carrier to seed the bone graft with MSCs at the time of surgery, **Figure 3.1**. Combination with advanced 3D manufacturing technologies has the potential to generate a graft with patient specific geometries and improved retention of stem cells.

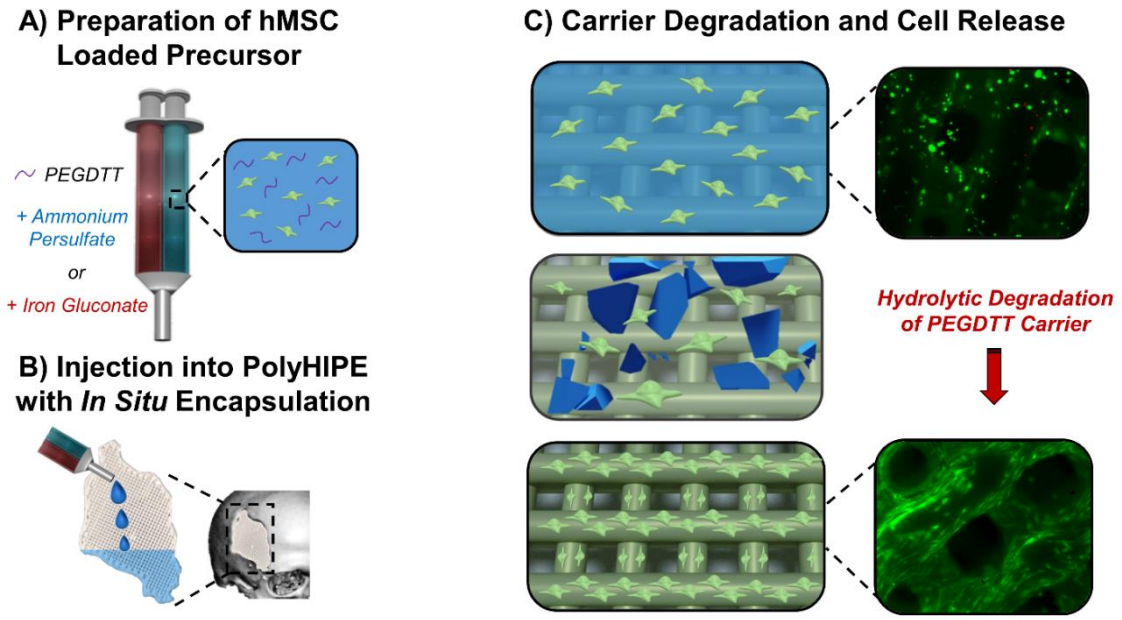


**Figure 3.1** Schematic illustrating hMSCs loading in hydrogel precursor solutions (A), injection and encapsulation in 3D printed polyHIPE scaffold (B), and protection during early stages of implantation (C).

In this study, 3D printed polyHIPE scaffolds were seeded with MSCs using a cell-releasing hydrogel carrier that cures *in situ* using redox initiation. The hydrolytically degradable macromer, poly(ethylene glycol)-dithiothreitol, was investigated as a cell carrier and the effect of the oxidant-to-reductant ratio on network formation time, sol-gel fraction, and swelling ratio was investigated to identify candidate cell carriers. The viability and release profiles of MSCs encapsulated in these *in situ* cured hydrogels was then characterized. To confirm the benefits of hydrogel delivery in 3D printed polyHIPEs, MSC-loaded macromer solutions were injected into multi-layered constructs and cell distribution compared to a traditional suspension seeding method. Mesenchymal stem cell activity on 3D printed polyHIPEs was monitored using established alkaline phosphatase (ALP) and mineralization assays to ensure delivered cells retained the ability to undergo osteoblastic differentiation. We previously reported that unmodified scaffolds based on propylene fumarate dimethacrylate (PFDMA) promoted osteoblastic differentiation under standard culture conditions, demonstrating the inherent osteoinductive character of these grafts.[129] In the current study, we aimed better understand the mechanism behind this osteoinductive character by isolating the effects of scaffold chemistry and surface area on osteoblastic differentiation. Collectively, this work aims to highlight the potential of cell-laden 3D printed scaffolds to serve as rigid cell carriers and improve the regenerative capacity of tissue engineered bone grafts.

## 3.2. Materials and Methods

### *3.2.1. Materials*

Polyglycerol polyricinoleate (PGPR 4125) was donated by Palsgaard. Human mesenchymal stem cells were provided by the Texas A&M Health Science Center College of Medicine Institute for Regenerative Medicine at Scott & White. All other chemicals were purchased and used as received from Sigma–Aldrich, unless otherwise noted.

### *3.2.2. hMSC Culture*

Bone marrow-derived hMSCs were obtained as passage 1 from the Center for the Preparation and Distribution of Adult Stem Cells at Texas A&M Health Science Center College of Medicine, Institute for Regenerative Medicine at Scott & White through NIH Grant # P40RR017447. Cells were cultured to 80% confluency on tissue-culture polystyrene flasks in standard growth media containing Minimum Essential Media α (MEM α, Life Technologies) supplemented with 16.5% fetal bovine serum (FBS, Atlanta Biologicals) and 1% L-glutamine (Life Technologies) prior to passaging. All experiments were performed with cells at passage 3.

### *3.2.3. PEGDTT Synthesis*

Poly(ethylene glycol)-dithiothreitol (PEGDTT) was synthesized by adding a solution of d,l-dithiothreitol (DTT), TEA, and DCM dropwise to a solution of PEGDA 2kDa in DCM. The molar ratios of DTT, PEGDA and TEA were 2:3:0.9. After the addition of the DTT and TEA solution in DCM, the reaction was stirred for 24 hours at room temperature. The resulting solution was then precipitated in cold diethyl ether, washed, filtered, and

dried under ambient conditions for 24 hours. The resulting macromer was placed under vacuum to remove excess solvent until the weight was stabilized.

### *3.2.4. Fabrication of Redox Initiated hMSC-releasing Hydrogels*

Hydrogel solutions were prepared by dissolving PEGDTT (10 wt%) in PBS containing either ammonium persulfate as oxidant or iron gluconate as reductant. Precursor solutions were then loaded into a double barrel syringe and injected through a mixing head to facilitate crosslinking. In specified studies, precursor solutions were used to resuspend hMSCs at a density of 1 million cells/mL prior to loading. Cell-laden hydrogels were injected either into neat hydrogel constructs (5 mm diameter x 1 mm height) or used to fill pre-fabricated polyHIPE prints and allowed to cure for 5 minutes. After the specified time, cell-laden constructs were moved to culture media and incubated.

### *3.2.5. Rheological Characterization*

Work and set times of the polyHIPEs were characterized using an Anton Paar MCR 301 rheometer following adapted procedures. Storage, loss, and complex moduli were measured every 3 s using a parallel-plate configuration with a 1 mm gap and 0.5% strain. Redox initiated hydrogels were injected through a mixing head onto the plate heated to 37 °C. Gelation onset was determined as the crossing of loss and storage modulus. Complete network formation was determined as the fourth point after which there was a less than 1% change in complex viscosity. Values were reported as the average of three specimens.

### *3.2.6. Characterization of Network Formation*

To characterize sol-gel fraction of redox initiated hydrogels, precursor solutions were injected into cylindrical tubes and allowed to cure for 1h. Specimens were then sectioned

(8 mm diameter, 2 mm thick) and vacuum-dried for 24 h. Dry polymer mass was obtained and placed in dichloromethane (DCM) at a ratio of 1 mL of DCM to 10 mg of specimen to facilitate dissolution of un-cross-linked macromer. After extraction for 24 h, the DCM was decanted and the specimens vacuum-dried for 24 h at ambient temperature. The gel fraction was calculated as the final weight divided by original weight. Similarly, swelling ratio was determined from bulk cured samples. Specimens were swelled in RO water to reach equilibrium swelling mass ($W_s$). Then, specimens were dried under vacuum for 24 hours and weighed to assess dry (polymer) mass ($W_d$). The equilibrium volumetric swelling ratio, Q, was calculated from the equilibrium mass swelling ratio: $W_s/W_d$.

*3.2.7. Preparation of Emulsion Inks and 3D Printed PolyHIPEs*

Propylene fumarate dimethacrylate (PFDMA) was synthesized in a two-step process detailed previously. Briefly, propylene oxide was added dropwise to a solution of fumaric acid and pyridine in 2-butanone and refluxed at 75°C to yield the diester, bis(1,2 hydroxypropyl). Following purification, the diester was end-capped with methacrylate groups using methacryloyl chloride in the presence of trimethylamine and purified to yield the final product. To prepare emulsion inks, propylene fumarate dimethacrylate (PFDMA) was combined with 10 wt% surfactant (polyglycerol polyricinoleate), 1 wt% initiator (phenylbis (2,4, 6-trimethylbenzoyl)- phosphine oxide)(BAPO), and mixed in a FlacTek Speedmixer. An aqueous solution of calcium chloride (1 wt%) was then added to the organic phase (w:o 75:25) and mixed. Emulsion inks were extruded layer-by-layer through respective syringes and motor actuated plungers. The emulsions inks rapidly cured after deposition by UV exposure.

### *3.2.8. hMSC Viability during Preparation, Encapsulation and Degradation*

Investigation of hMSC viability and morphology was performed to ensure redox initiated PEGDTT hydrogels were cytocompatible during precursor preparation, encapsulation and carrier degradation stages. Viability was assessed utilizing the LIVE/DEAD assay kit (Molecular Probes) after specified exposure conditions. Briefly, cells were washed with PBS, stained with 2 µM calcein-AM (live) and 2 µM ethidium homodimer-1 (dead) for 30 minutes at 37°C, and washed with PBS for imaging. Imaging (3 images per specimen) was conducted on four specimens (n = 12) with a fluorescence microscope (Nikon Eclipse TE2000-S).

### *3.2.9. Distribution of hMSCs in 3D Printed PolyHIPE Scaffolds*

A Quant-iT™ PicoGreen® dsDNA Assay Kit (Molecular Probes) was utilized to quantify cell distribution throughout multi-layer polyHIPE scaffolds. hMSC-PEGDTT precursor solutions were prepared and injected 3mm tall polyHIPE prints, allowed to cure for 5 minutes, and placed in standard growth media. Cell density was characterized at 1 and 7 days post release at depths of 1, 2, and 3mm to confirm improved distribution of hMSCs throughout the bulk of the scaffold. At selected time points, polyHIPEs were removed from the culture wells and placed in unused wells for thermal shock lysis procedure to ensure only DNA from cells adhered to the scaffolds was measured. The assay was performed according to manufacturer instructions and fluorescence intensity was assessed using a plate reader (Tecan Infinite M200Pro) with excitation/emission wavelengths of 480/520 nm, respectively. Average cell number was determined by

converting dsDNA values to individual cell number using 6.9 pg DNA/cell. Specimens were analyzed in triplicate.

### *3.2.10. Alkaline Phosphatase Activity of hMSCs Released into 3D Printed PolyHIPE Scaffolds*

Alkaline phosphatase activity of cells encapsulated and released into 3D printed polyHIPE scaffolds was determined by monitoring the conversion of p-nitrophenyl phosphate (PNPP, Thermo Scientific) to p-nitrophenol. After 24 hours post encapsulation, growth media or osteogenic media (growth media supplemented with 50 μg/mL ascorbic acid, 10 m*M* β-glycerophosphate, and 10 n*M* dexamethasone) was added and changed every 2 days for 21 additional days following measurement of ALP activity. Scaffold cultures were lysed using thermal shock treatment and incubated with pNPP for 30 min. ALP activity was determined as the rate of PNPP conversion to p-nitrophenyl by measuring the absorbance at 405 nm (Tecan Infinite M200Pro) and normalized to cell number obtained from the PicoGreen assay. Specimens were analyzed in triplicate.

### *3.2.11. Mineralization Activity of hMSCs Released into 3D Printed PolyHIPE Scaffolds*

Alizarin red staining was performed to detect calcium phosphate mineral deposition of hMSCs encapsulated and released into 3D printed polyHIPE scaffolds. After 24 hours post encapsulation, growth media or osteogenic media (growth media supplemented with 50 μg/mL ascorbic acid, 10 m*M* β-glycerophosphate, and 10 n*M* dexamethasone) was added and changed every 2 days for 28 additional days following staining of mineralized nodules. hMSCs were fixed in 3.7% glutaraldehyde and incubated for 5 minutes in 2% Alizarin Red S. Scaffolds were then washed with PBS to remove excess stain and

photographed under optical microscopy. A semi-quantitate procedure was then performed by destaining scaffolds in 10% acetic acid solution and monitoring absorbance at 405 nm. Specimens were analyzed in triplicate.

*3.2.12. Mechanism of PolyHIPE Osteoinductivity*

To investigate the underlying mechanism of polyHIPE osteoinductivity, ALP activity of seeded hMSCs was monitored on three differing substrates, PFDMA polyHIPEs, PFDMA films, and poly(lactic acid) (PLA) films. Briefly, poly(lactic acid) filament was heated to 200°C, extruded into films, and allowed to cool under ambient temperatures. PFDMA films were fabricated by mixing the pre-polymer with 1 wt% BAPO, adding dropwise into round molds and UV cured. Finally, PFDMA polyHIPE scaffolds were fabricated as described previously with the exception of utilizing a 100% infill density. Scaffolds were sterilized using ethylene oxide sterilization prior to cell culture.

*3.2.13. Statistical Analysis*

The data are displayed as mean ± standard deviation for each composition. An analysis of variance (ANOVA) comparison was used for multiple composition comparisons with a Tukey's multiple comparison to analyze the significance of the data. A Student's t-test was performed to determine any statistically significant differences if only two compositions were present. All tests were carried out at a 95% confidence interval ($p<0.05$).

## 3.3. Results and Discussion

### *3.3.1. Rheological Characterization of Redox Initiated PEGDTT Hydrogels*

Photopolymerization of acrylated poly(ethylene glycol) is a widely studied delivery platform that allows cell encapsulation in mild conditions with high cell survival.[88, 203, 204] Despite these advantages, reliance on an external UV source to initiate polymerization often results in depth dependent properties that can limit translation of these systems.[153] Increased depths and irregular geometries of bone injuries make sufficient filling and curing within these defects difficult with photopolymerization alone. In contrast, this study aimed to develop and characterize an *in situ* curing hydrogel based on redox initiation of the biodegradable macromer, poly(ethylene glycol)-dithiothreitol. An *in situ* curing cell carrier would allow for facile incorporation of marrow derived cells in the surgical setting and improve spatial distribution of cells within a tissue engineered scaffold. To assess the feasibility of the proposed carrier, polymerization times were characterized as a function of initiator concentration to ensure encapsulation occurred in a relevant time scale. [132] First, onset of gelation was determined by monitoring the rheological transition between the liquid and gelled state to ensure appropriate time for injection and filling of the scaffold was allowed, **Figure 3.2A**. Next, complete network formation was determined by identifying the plateau of complex viscosity to ensure uniform property formation and retention of cells at the defect site, **Figure 3.2B**. Multiple researchers have reported use of the water-soluble initiator, ammonium persulfate (APS) in cell encapsulation platforms.[90, 205] Temeneoff *et al.* demonstrated rapid encapsulation of rat marrow stromal cells in a thermal initiated, oligo(poly(ethylene glycol) fumarate) hydrogel with gelation onset

occurring in less than 5 minutes at an initiator concentration of 25 mM. Traditional redox carriers such as these often utilize N, N, N, N-tetramethylethylendiamine (TMED) to accelerate radical formation. As an alternative, ferrous based reducing agents facilitate radical formation at an elevated rate, introducing the potential to retain rapid polymerization rates with reduced initiator concentrations.[206, 207] In this study, ammonium persulfate was added at concentrations of 1.25, 2.5, 5, 10 and 25 mM with equal molar iron gluconate dihydrate added as reducing agent. As expected, increasing initiator concentration resulted in more rapid gelation onset ranging from approximately 10 minutes to less than 10 seconds. Uniquely, the use of a ferrous reducing agent allowed for gelation to occur at rates comparable to other APS systems with the benefit of a 10-fold reduction in required concentration. Furthermore, complete network formation time was could be tuned from approximately 15 minutes to less than 5 minutes. To further develop tools that could be utilized to modulate cure rate independent of initiator concentration, the effect of initator:reductant ratio on cure rate was explored by adding iron gluconate dihydrate concentration at relative molar concentrations of 1:0.5, 1:1, 1:2 (ammonium persulfate:iron gluconate dihydrate). Thoughtful selection of iron based reducing agent concentration is required as excessive concentrations of ferrous ions are known to inhibit polymerization through oxidation of propagating radicals. In this work, no inhibitory effects of increasing iron gluconate concentration was observed and it is hypothesized that a more rapid production of the APS-iron gluconate complex led to a tunable range of cure rates with a single initiator concentration. A minimum of 2-fold range in polymerization times were observed with increasing ratio of reductant to initiator. Studies investigating

enzyme-mediated reodox initiation of hydrogel cell carriers have also demonstrated no inhibitory effects in similar ranges of ferrous ion concentration.[208] However, the potential impact on final double bond conversion has been noted, and as such, it is critical to ensure requisite network formation in this system.

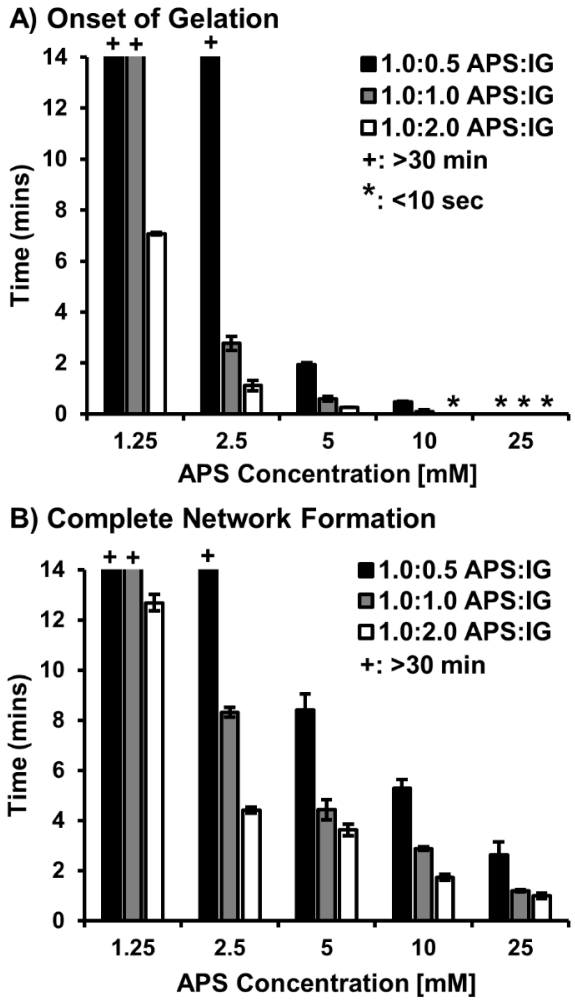


**Figure 3.2.** Effect of initiator concentration and reducing agent ratio on gelation onset (A) and complete network formation (B) of hydrogel carrier. The + represents a gelation and network formation time of greater than 30 minutes. The * represents a gelation onset time of less than 10 seconds. All data represents average ± standard deviation for n = 3.

### *3.3.2. Network Formation of Redox Initiated PEGDTT Hydrogels*

Complete and consistent network formation is critical to controlling carrier properties and degradation profiles.[209, 210] To this end, sol-gel fraction and swelling ratio were characterized to assess the effect of oxidant and reductant concentration on hydrogel network formation, **Table 3.1** Sol-gel fraction increased with elevated initiator, ranging from greater than ~95% for 25 mM concentrations, to ~70% for 1.25 mM concentrations. For comparison, photopolymerized PEGDTT hydrogels were cured with 5mM concentration of irgacure 2959 and exhibited a sol-gel fraction of 98%. Differences in sol-gel fraction for redox systems versus UV systems is attributed to dissociation of the photoinitiatior resulting in a pair of free radicals, versus only a single free radical site being generated with the formation of each redox complex site.[207] Furthermore, due to double barrel mixing, initiator concentration is diluted in half upon mixing of the two phases. Therefore, when matched by radical generation, sol-gel fractions were more closely aligned at greater than 95%. Hydrogel swelling ratios further confirmed efficient network formation with a less than 15% change in swelling for all compositions when compared to photoinitiated control. After completing physical characterization of the hydrogel carrier, selection criteria were implemented to identify potential carriers to investigate in cytocompatibility studies. Initiator concentrations of 2.5 mM or greater had complete network formation times of less than 10 minutes, sol-gel fraction greater than 80%, and less than 10% change swelling. As such, these compositions moved forward in the testing.

**Table 3.1.** Effect of initiator and reducing agent concentration on hydrogel compressive modulus, swelling rato, and gel fraction.

| [APS] | APS:IG (molar ratio) | Gel Fraction | Swelling Ratio |
|---|---|---|---|
| **1.25 mM** | 1:0.5 | -- | -- |
| | 1:1 | -- | -- |
| | 1:2 | 66 ± 6 | 18.2 ± 2 |
| **2.5 mM** | 1:0.5 | -- | -- |
| | 1:1 | 78 ± 4 | 18.9 ± 4 |
| | 1:2 | 81 ± 6 | 17.6 ± 6 |
| **5 mM** | 1:0.5 | 81 ± 2 | 18.4 ± 2 |
| | 1:1 | 88 ± 2 | 17.2 ± 3 |
| | 1:2 | 90 ± 2 | 17.2 ± 4 |
| **10 mM** | 1:0.5 | 85 ± 2 | 17.1 ± 3 |
| | 1:1 | 88 ± 7 | 17.1 ± 1 |
| | 1:2 | 88 ± 4 | 17.5 ± 1 |
| **25 mM** | 1:0.5 | 91 ± 2 | 16.9 ± 3 |
| | 1:1 | 95 ± 2 | 16.8 ± 3 |
| | 1:2 | 95 ± 2 | 16.8 ± 2 |
| **Irgacure 2959** | | | |
| **5 mM** | -- | 98 ± 1 | 16.4 ± 1 |

### *3.3.3. Effect of Redox Initiation on Stem Cell-Loaded Hydrogel Viability*

*In situ* delivery of marrow derived cells within a biodegradable carrier has the potential to improve translation by eliminating timely pre-culture and reducing external equipment required for the surgical procedure. However, these benefits must be achieved without compromising cytocompatibility observed in photoinitiated systems.[211, 212] As PEGDTT has been demonstrated cytocompatible in previous cell encapsulation studies, the only anticipated source of potential cytotoxicity was due to the redox initators.[91, 213] Cell

delivery in this *in situ* system occurs through mixing of two distinct hydrogel suspensions containing the cell payload and either the initiator or reducing agent. As a result, it was critical to identify the exposure limits of these agents to ensure a formulation was selected that optimizes cell survival during encapsulation. Previously, it has been reported that extended exposure to elevated concentrations of redox initiators can result in poor cytocompatibility resulting from significant changes to pH.[214] However, cell carrier studies that utilize redox initiator concentrations at the maximum end of our experimental design demonstrate minimal pH change in buffered environments, with a return to neutral conditions after mixing.[90, 198] These studies also confirmed cells encapsulated in redox carriers supported markers of osteoblast and chondrocyte differentiation. hMSC viability was first assessed following ten minute exposure to initiator or reducing agent, mimicking anticipated conditions during early stages of carrier polymerization. As shown in **Figure 3.3A**, all concentrations of APS and iron gluconate supported viability greater than 95%. Next, to ensure encapsulated cells did not experience long term effect due to precursor exposure, cells were cultured for an additional 24h at a 10-fold dilution to mimic hydrogel swelling and dilution of excess initiator following cure, **Figure 3.3B**. All APS concentrations lower than 25 mM supported high viability of greater than 95%. The slight reduction in viability, ~70%, for the 25 mM APS is attributed to the reduction in media pH resulting from initiator addition. After confirming hMSCs would survive exposure to initiating agents, the effect of initiator mixing, radical formation, and resultant encapsulation on viability was assessed, **Figure 3.3C**. Two critical observations were made during the encapsulation procedure. First, as was seen in single the initiator studies,

all compositions below 25 mM experienced excellent viability and retained high cell densities. Second, a cell-dependent effect was observed on the lowest, 2.5 mM concentration, resulting in a slower cure rate than was observed during rheological characterization. The radical scavenging effect of cell encapsulation is believed to have caused this composition to cure slower than desired for an *in situ* encapsulation procedure. As a result, the 10 mM formulation was selected for subsequent cell release and osteogenic activity studies.

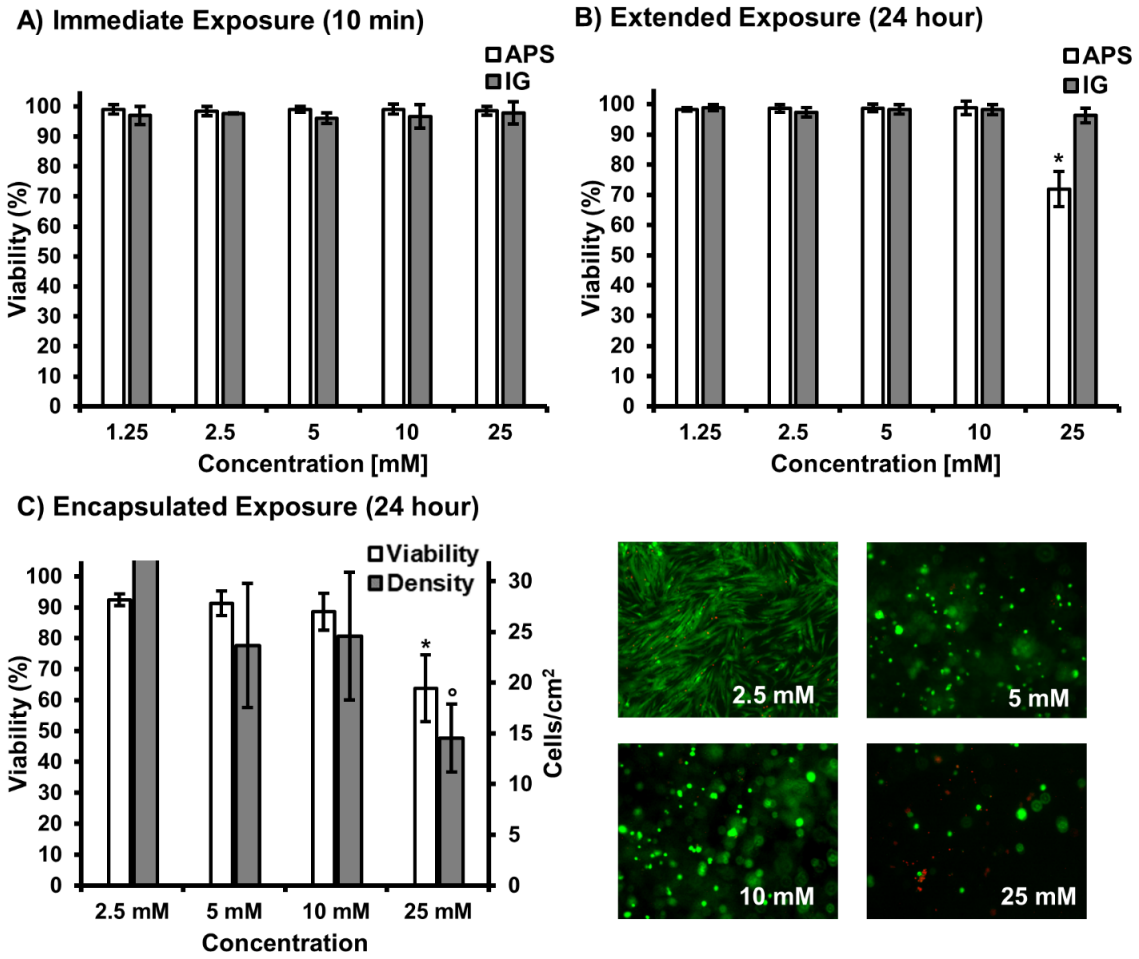


**Figure 3.3.** Percent hMSC viability following 10 min exposure to redox agents, ammonium persulfate and iron gluconate (A); 24h additional culture (B). Percent hMSC viability and cell density following carrier encapsulation with micrographs illustrating live (green) and dead (red) cells in respective hydrogel formulations (C). All data represents average ± standard deviation for n = 12. The * and ° represent significant difference ($p<0.05$) for 25 mM concentration compared to other concentrations.

### *3.3.4. Improved Stem Cell Loading of 3D Printed PolyHIPE Scaffolds*

The primary aim of this work was to develop a transient, hydrogel carrier that could improve cell retention during early stages of delivery, then undergo biodegradation and provide targeted stem cell release into 3D printed polyHIPE scaffolds under more

hospitable conditions. Degradable hydrogels formed by the Michael-type addition reaction of dithiothreitol and poly(ethylene glycol) diacrylate have been successfully explored for cell encapsulation and delivery applications.[91, 213, 215] Biodegradation is achieved by introducing hydrolytically labile DTT linkages into the macromer backbone. Resultant thioether linkages change the atomic charge of adjacent acrylate ester bonds, increasing susceptibility to nucleophilic attack and hydrolytic degradation.[216] Simulated degradation profiles for the selected hydrogel composition demonstrated complete hydrolytic degradation after 7 days in buffered saline conditions. Cell-loaded PEGDTT hydrogels were cultured for 2 weeks to assess hMSC loaded carrier degradation and viability of released cells. As high encapsulation viability was observed in PEG based systems under this target degradation time frame, any viability effects would arise from exposure to carrier degradation products.[87] Partial release of the hMSC loaded carrier was observed after 4 days in culture, with significant cell numbers remaining entrapped in the hydrogel network (data not shown). After 7 days, hMSCs were completely released from the hydrogel carrier and successfully adhered to tissue culture polystyrene substrate and polyHIPE substrates, **Figure 3.4A**. Viability was monitored for an additional 7 days to ensure cells remained viable and persisted on the target substrate, **Figure 3.4B**. hMSCs released onto 3D printed polyHIPE scaffolds demonstrated viability of greater than 90% with morphology matching that of a direct-seeded polyHIPE scaffold, indicating no effects of degradation products on cell survival.[189] In this study, a single hydrogel degradation profile was studied; however, use of the PEGDTT platform allows for facile tuning of degradation through modulation of the number of DTT linkages.[213] Modulation of carrier

degradation profile has been shown to play a major role in cell retention. Qui *et al.* demonstrated that a range of carrier degradation profiles could be engineered utilizing the PEGDTT macromer and that increasing carrier degradation rate resulted in a greater than 2-fold increase in cell retention in a tendon tissue explant model.[91]

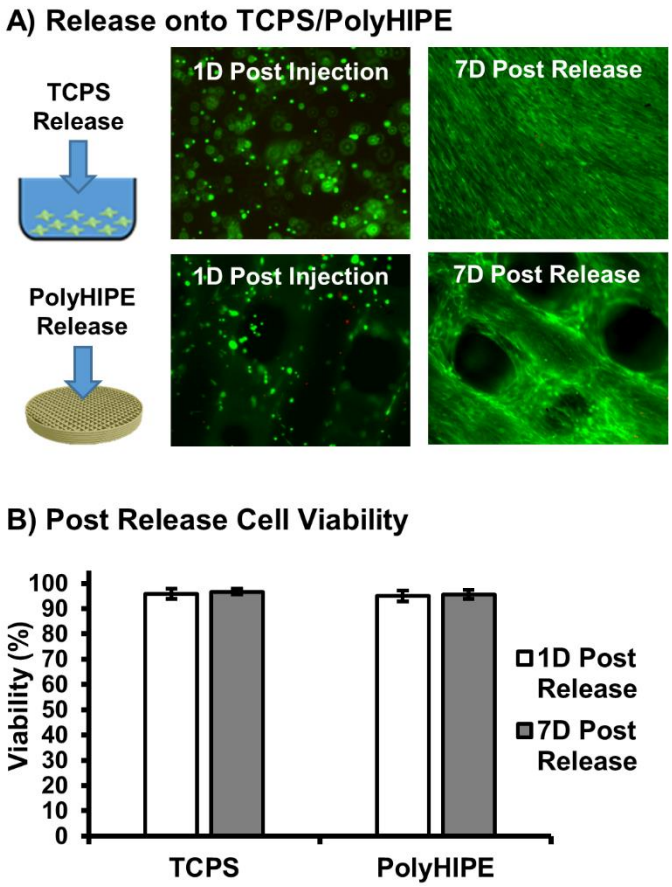


**Figure 3.4.** Micrographs illustrating live (green) and dead (red) cells 1 day post encapsulation and 7 days post release onto TCPS and polyHIPE substrates (A). Percent hMSC viability 1 day and 7 days following release and attachment onto TCPS and polyHIPE substrates (B). All data represents average ± standard deviation for n = 12.

A major hurdle to achieving the full potential of stem cell therapies is retaining cells at the target site after transplantation. Direct injection often results in rapid dispersal of cells away from the injury site, resulting in subtherapeutic retention levels.[81, 217] Rapid curing hydrogels act as a physical barrier to cell dispersal and 3D substrate to improve cell engraftment. A primary hypothesis of this work was that an *in situ* curing hydrogel carrier would improve spatial distribution and retention of hMSCs in our 3D printed polyHIPE grafts. To this end, cell density was monitored after encapsulation and release onto multilayered polyHIPE scaffolds and compared to a standard suspension seeding method, **Figure 3.5**. Cell distribution was quantified at 1 mm depths with a total construct size of 3 mm. In contrast to standard suspension seeding, encapsulation loading resulted in uniform cell distribution across the three scaffold layers. Suspension seeding demonstrated irregular distribution with a significantly reduced number of cells observed on the top two layers and high settling at the bottom most layer. Furthermore, a 3-fold increase in cell density was observed on the top two layers while retaining a 2-fold increase over the bottom layer. This improved control over seeding density across scaffold depth is a significant advantage over standard seeding techniques as seeding density has been shown to influence osteoblastic differentiation of transplanted marrow stromal cells on poly(propylene fumarate) scaffolds.[218] Kim *et al.* investigated the role of cell-cell paracrine signaling distance, demonstrating that controlling cell seeding density resulted in elevated osteoblastic gene expression of marrow derived cells. It is believed that *in vivo* application of this system will result in greater improvements in cell retention as rapid wash out effects are often observed during the early stages following surgery.[219] Current

studies are investigating improved loading of printed constructs with sizes greater than 2 cm in the aim of developing a platform to explore healing in critical sized defects of more clinically relevant large animal models.[79, 220, 221]

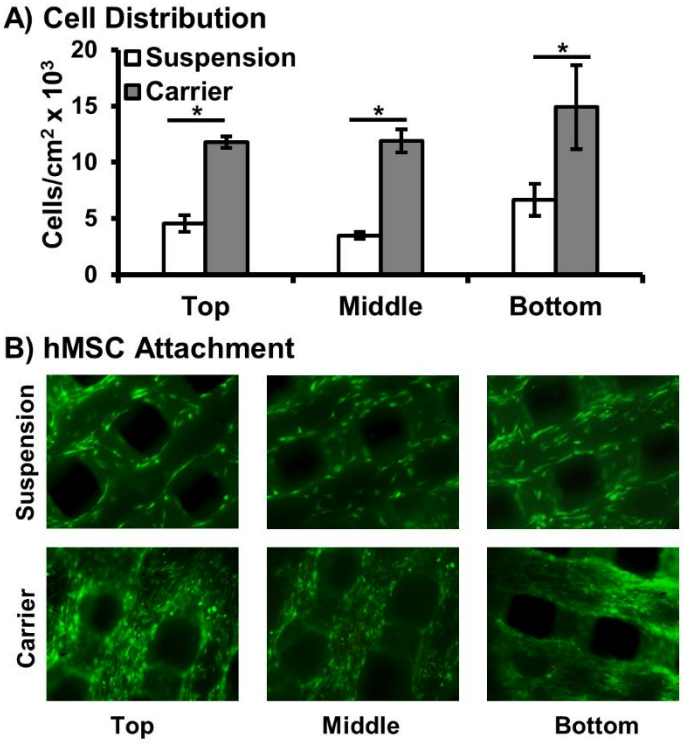


**Figure 3.5.** Distribution of hMSCs using carrier seeding onto multilayer polyHIPE scaffolds determined by dsDNA quantification and compared to suspension seeding control (A). Representative micrographs of top, middle and bottom layers of scaffold (B). All data represents average ± standard deviation for n = 3. The * represents significant difference ($p<0.05$) between suspension and carrier seeding at specified layer.

### *3.3.5. Osteoblastic Activity of hMSCs Released into 3D Printed PolyHIPE Scaffolds*

To fully assess the potential of this *in situ* cell carrier to improve the regenerative capacity of our 3D printed bone graft, it was essential to confirm encapsulated stem cells

retained their potency and ability to undergo osteoblastic differentiation post release. To this end, alkaline phosphatase activity was investigated as an early marker of differentiation at 7 and 14 days post release onto tissue culture polystyrene and polyHIPE substrates, **Figure 3.6**. ALP activity of hMSCs released onto TCPS increased ~3-fold when cultured in osteogenic conditions compared to control cells cultured in standard growth conditions. A 7-fold increase in ALP activity was observed at 7D post release on polyHIPE substrates, with no statistical effect of culture in osteogenic media observed. This peak was followed by a 5-fold increase in activity at 14D for polyHIPE substrates in osteogenic conditions. These expression profiles support conclusion of osteoblastic differentiation as observed in other systems investigating MSC differentiation.[222, 223] It is noted that encapsulated cells also retained proliferative potential as demonstrated by an increase in cell density during the two week period post release. Next, mineralization was characterized as a late stage marker of differentiation. Alizarin red staining indicated encapsulated hMSCs retained the ability to facilitate mineralization 4 weeks following release onto TCPS substrates, **Figure 3.7A**. Calcium deposition was further characterized as a function of TCPS or polyHIPE substrate, **Figure 3.7B-C**. A synergistic effect was observed for hMSCs cultured on polyHIPE scaffolds in osteogenic conditions as a 5-fold increase in calcium deposition was observed over hMSCs cultured on TCPS in same conditions. Overall, these profiles support retention of stem cell potency after encapsulation and promotion of osteoblastic activity after release onto 3D printed polyHIPEs, demonstrating the strong potential of stem cell seeded polyHIPE grafts.

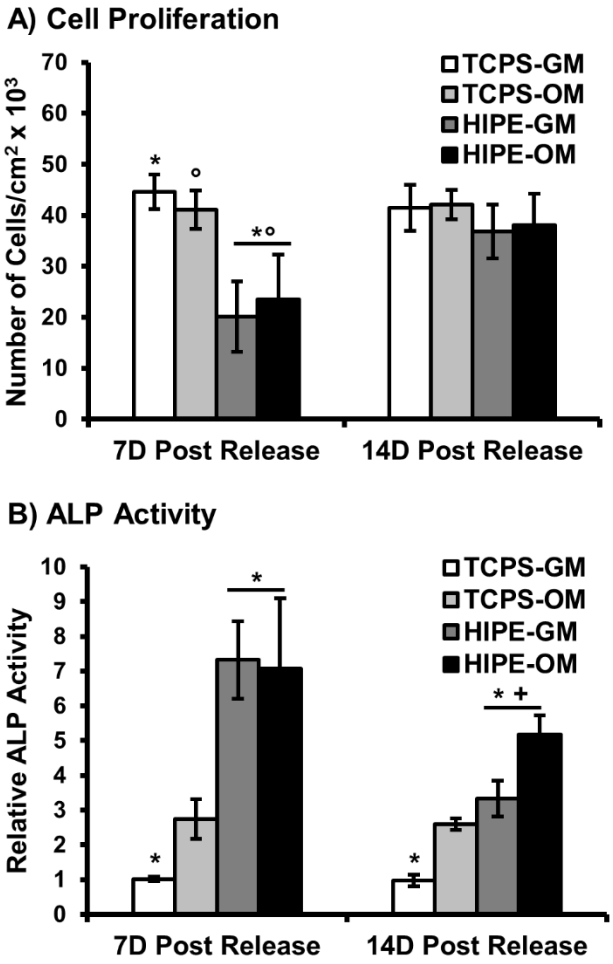


**Figure 3.6.** Adhesion of hMSCs released onto TCPS and polyHIPE substrates determined by dsDNA quantification (A). Alkaline phosphatase activity of hMSCs 7D and 14D post carrier release. Cells were cultured in growth media (GM) and osteogenic media (OM) as positive control. All data represents average ± standard deviation for n = 3. The * and ° represent significant difference ($p<0.05$) for TCPS substrates compared to polyHIPEs at indicated time points. The + represents significant difference ($p<0.05$) for ALP activity on polyHIPE substrates at 14D.

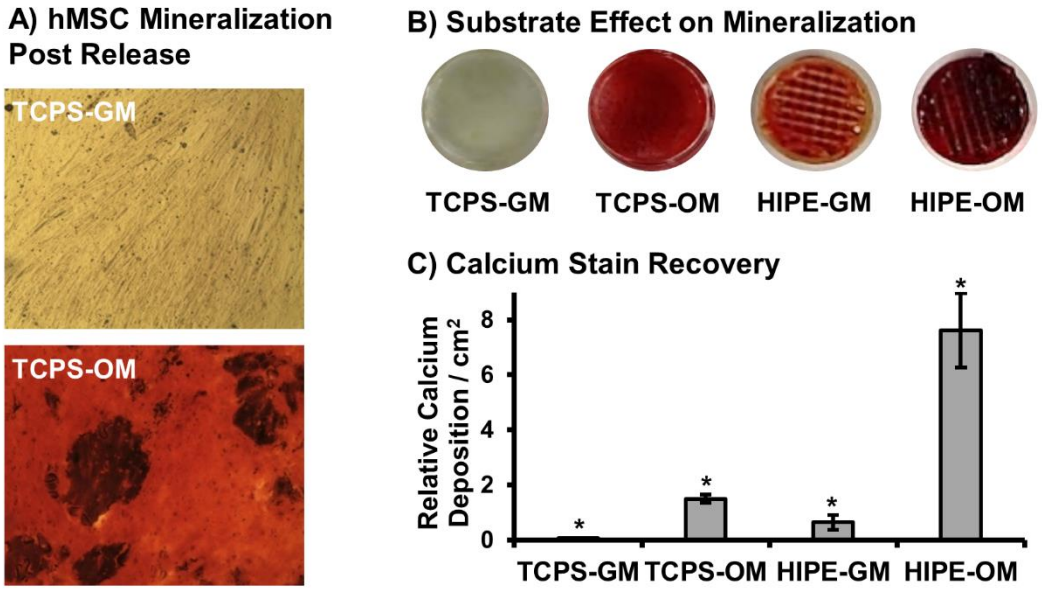


**Figure 3.7.** Alizarin red staining of hMSC cultures 4 weeks following carrier release. hMSC mineralization post release onto TCPS substrates in growth vs osteogenic media (A). Effect of release substrate (TCPS vs polyHIPE) and media conditions (growth vs osteogenic) on hMSC mineralization (B). Semi-quantitative analysis of mineralization determined by alizarin red stain recovery (C). All data represents average ± standard deviation for n = 4. The * represents significant difference ($p<0.05$) between all compositions.

We previously demonstrated the ability of fumarate-based polyHIPEs to promote osteoblastic activity in the absence of dexamethasone supplements through increased deposition of media derived calcium ions onto the polyHIPE surface.[129] In addition to confirming osteogenic potential, this study aimed to elucidate a potential mechanism behind this increased calcium deposition and assess its impact on osteoblastic differentiation. Extracellular calcium is known to play a key role in bone regeneration via direct activation of Ca-sensing receptors that result in increased osteoblast proliferation, expression of osteoinductive factors, and matrix mineralization.[224-226] To this end, three

substrates were tested (PFDMA polyHIPE, PFDMA film and PLA film) to isolate and explore the effects of surface area and scaffold chemistry on calcium deposition, **Figure 3.8**. Alizarin red staining was performed on neat, cell-free scaffolds that had been soaked in growth media for 2 weeks for a qualitative assessment of calcium deposition. Fumarate-based chemistries have been shown to support surface mineralization when soaked in concentrated solutions of simulated body fluid.[227] In this study, calcium concentrations were limited to those present in basal media, ~1.6 mM, plus calcium found in the fetal bovine serum supplement. Despite a buffered environment conducive to mineral deposition, minimal calcium was observed on neat PFDMA and PLA films. In contrast, PFDMA polyHIPEs displayed significant levels of staining. Surface roughening has been used previously in titanium implants to provide an improved substrate for apatite precipitation.[228, 229] Specifically, Chen *et al.* identified surface grooves approximately 3 microns wide to be ideal for surface mineralization.[228] It is hypothesized that the increased surface area of polyHIPE scaffolds over neat films, combined with a pore size on the scale of several microns had a similar effect, providing an ideal substrate for surface deposition. Initial investigation of hMSC activity supports this hypothesis as polyHIPE scaffolds promoted increased levels of ALP activity in standard growth media. Elevated activity was observed when cultured in osteogenic conditions as the substrate most likely provided an ideal surface for nucleation and mineral growth.

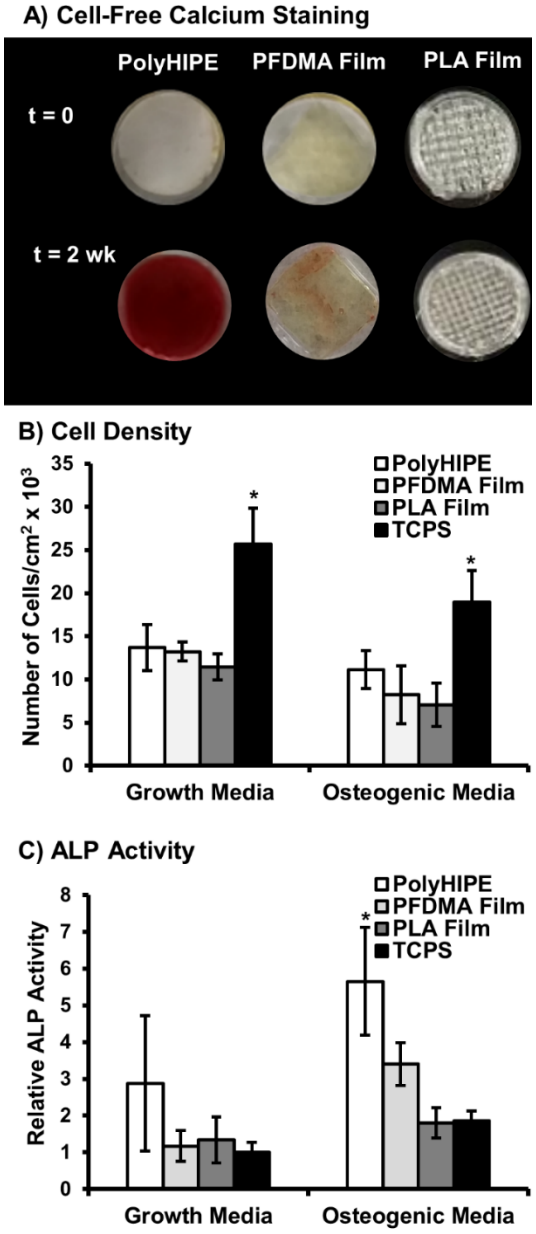


**Figure 3.8.** Effect of scaffold chemistry (PFDMA vs PLA films) and scaffold porosity (PFDMA polyHIPE vs PFDMA film) on calcium deposition in cell free conditions (A). Quantification of hMSC adhesion on varied substrate determined by dsDNA quantification (B). Effect of substrate on hMSC alkaline phosphatase activity after 14 days (C). Cells were cultured in growth media (GM) and osteogenic media (OM) as positive control. All data represents average ± standard deviation for n = 4. The * represents significant difference ($p<0.05$) for indicated composition compared to all others in respective media.

## 3.4. Conclusions

This study demonstrates the ability of biodegradable poly(ethylene glycol)-dithiothreitol hydrogels to serve as injectable stem cell carriers and improve *in situ* seeding of 3D printed polyHIPE grafts. Oxidant and reductant concentration were modulated to achieve desired cure rates while maintaining high cell viability during cure and after release. This redox-based initator system demonstrated the ability to encapsulate stem cells without relying on external stimuli (e.g. UV) that can be attenuated in large constructs or tissues. As expected, the cell carrier improved cell distribution in 3D printed polyHIPE scaffolds over standard suspension cell seeding. Finally, these polyHIPEs demonstrated strong potential as tissue engineered scaffolds by supporting long term viability and osteoblastic differentiation of carrier-delivered hMSCs. Overall, this approach has strong potential to improve bone regeneration with broader applications in stem cell delivery for regenerative medicine.

# CHAPTER IV

# TUNABLE RELEASE OF BMP-2 FROM POROUS POLYHIPE MICROSPHERES

## 4.1. Introduction

Limitations of current treatments for large bone defects and non unions has resulted in significant efforts to develop novel grafting materials with improved regenerative potential.[230, 231] A promising approach has been the incorporation of bone morphogenetic proteins (BMPs) into biomaterial scaffolds. BMPs are a family of potent osteogenic factors active in bone tissue formation during embryonic development and skeletal repair.[232, 233] Of the numerous members of the BMP family that have demonstrated efficacy in bone regeneration, BMP-2 has been the most extensively studied due to its putative role in osteoblastic differentiation, angiogenesis, chemoattraction, and cell signaling during fracture healing.[101-104, 234, 235] As a result, numerous platforms have been investigated as carriers for this potent osteoinductive factor.[1, 236-240]

Recently, delivery of recombinant expressed BMP-2 (rhBMP-2) in a collagen sponge was approved for commercial use by the FDA for treatment of specific spine, tibia, and craniofacial defects.[107, 108] Since its release, this graft has demonstrated strong clinical efficacy and become a leader in the bone grafting market. Despite its regenerative potential, there were several safety concerns including inflammation, ectopic bone formation and neurological deficits.[111] The bolus release of rhBMP-2 from the collagen sponge is rapidly cleared away from the injury and this necessitates the use of supraphysiological dosages to ensure therapeutic levels.[241, 242] Although this bolus release

of growth factor has demonstrated improved bone formation, it also leads to undesirable off-target complications.

The dynamic role that BMP-2 plays during various stages of the healing process suggests that a more local and sustained approach may be beneficial. It has been reported that there is an innate upregulation of ectopically osteoinductive BMP expression for several weeks following injury.[11, 243] Sustained BMP levels over this period provides a robust osteogenic effect, allowing appropriate time for osteoprogenitor cell recruitment, retention, and differentiation.[99, 103, 244] As such, numerous systems have been investigated to provide more physiologically relevant growth factor delivery profiles including hydrogels carriers, ceramic materials, and synthetic polymer scaffolds.[245, 246] Although the mild processing conditions of hydrogels make them attractive carriers for growth factors, typical mesh sizes often result in burst release profiles with limited controls of kinetics without the addition of an affinity-based functionality (e.g. heparin).[247-249] Surface-modified ceramics that improve regeneration may experience reduced loading efficiencies during fabrication that raise scale-up concerns.[1, 250, 251] As a result, encapsulation of BMPs into polymeric microspheres has emerged as one of the most promising methods to provide local and controlled delivery of these factors.

The most widely studied of these systems is the fabrication of poly(lactic-co-glycolic acid) (PLGA) microspheres using emulsification-evaporation or porogen-leaching methods.[239, 240, 252-256 257] These established techniques yield biodegradable particles with a range of porosities and sizes. Delivery of rhBMP-2 in these vehicles has been shown to significantly extend delivery profiles and improve bone regeneration in numerous in vivo

models. Kempen *et al.* reported a marked increase in ectopic and orthotopic bone formation with sustained rhBMP-2 release from a composite PLGA microsphere/poly(propylene fumarate) scaffold.[258] Furthermore, Brown *et al.* demonstrated that microsphere mediated release could be used to enhance pharmacokinetic profiles in an injectable polyurethane scaffold and improve regeneration over current BMP-2 soaked scaffolds.[259] Despite the strong potential of this traditional microsphere fabrication method, the requisite use of toxic solvents during fabrication poses significant challenges to bioactivity retention and commercialization. In addition to loss of therapeutic activity, protein denaturation resulting from unsatisfactory processing has been shown to introduce immunogenicity and toxicity concerns.[260] Post fabrication loading of growth factors has been explored to minimize processing effects, but often results in reduced loading efficiency and elevated costs.[246, 261] As a result, fabrication strategies that eliminate harsh processing conditions and allow for more efficient loading of costly therapeutics could offer several translational benefits for microsphere delivery of growth factors.

We recently reported a method for solvent-free fabrication of porous microspheres using the principles of emulsion templating and fluid dynamics.[262] This new methodology provides in-line loading of therapeutics and independent control over particle size and pore architecture, properties known to strongly influence release kinetics of encapsulated growth factors.[117, 252, 263] Furthermore, the same macromer chemistry can be used for both the microsphere and the porous bone graft, which is expected to improve microsphere-scaffold integration and mechanical integrity. Incorporation of microsphere delivery

systems with unmatched chemistries and porosities (e.g. hydrogel microspheres in PLGA graft) has been shown to significantly reduce mechanical properties.[264, 265] As such, this novel fabrication technique provides significant advantages over traditional microsphere methods and has the potential to minimize commercialization and safety concerns.

The focus of the current study was to establish fundamental relationships between microsphere properties and the resulting protein release kinetics. First, loading efficiencies and release kinetics were investigated as a function of microsphere diameter and pore architecture using a model protein. Bioactivity retention of encapsulated rhBMP-2 was then confirmed by monitoring luciferase activity in a BMP-responsive osteoblast reporter cell line. Next, the ability of rhBMP-2 loaded polyHIPEs to induce osteoblastic differentiation of human mesenchymal stem cells (hMSCs) was assessed using alkaline phosphatase (ALP) and mineralization assays. Finally, the effects of microsphere incorporation on composite scaffold architecture, compressive modulus, and yield strength were assessed to ensure no deleterious effects were observed. Collectively, this work aims to highlight the potential of polyHIPE microspheres to serve as a tunable, sustained release system and improve the regenerative capacity of polyHIPE bone grafts.

## 4.2. Materials and Methods

### *4.2.1. Materials*

Polyglycerol polyricinoleate (PGPR 4125) was donated by Paalsgard. All other chemicals were purchased and used as received from Sigma Aldrich unless otherwise noted. Ethylene glycol dimethacrylate (EGDMA) was filtered through an aluminum oxide column to remove the inhibitor monomethyl ether hydroquinone.

*4.2.2. Fabrication of BSA-FITC Loaded Microspheres*

Microspheres were fabricated via a fluidics double emulsion technique (w/o/w) adapted from Moglia et al., **Figure 4.1**.[262] Briefly, primary high internal phase emulsions (HIPEs) were fabricated by combining the photocurable macromer EGDMA with PGPR surfactant (10 or 30 wt%) and 2 wt% of the organically soluble photoinitiatior, 2,2-Dimethoxy-2-phenylacetophenone (DMPA). Once mixed, an aqueous solution containing calcium chloride (1 wt%) and the model protein (200 ug/mL), bovine serum albumin – fluorescein isothiocyanate conjugate (BSA-FITC), was added to the organic phase (75% v) and emulsified using a FlackTek Speedmixer DAC 150 FVZ-K. This primary HIPE was then injected dropwise (KD Scientific-100 Infusion Pump) into a continuously flowing external aqueous phase containing 3 wt% poly(vinyl alcohol) (PVA) aqueous solution and passed through UV excitation (UVP High Performance Transilluminator 365 nm) to initiate radical crosslinking. Needle gauge, tubing diameter, aqueous flow rate, and surfactant concentration were varied to modulate particle and pore size using previously established relationships as outlined in **Table 4.1**. Collected microspheres were dried *in vacuo* for a minimum of 24 hours prior to characterization. Four model compositions were fabricated containing a particle diameter of ~900 or ~300 microns with a pore diameter of ~45 or ~15 microns.

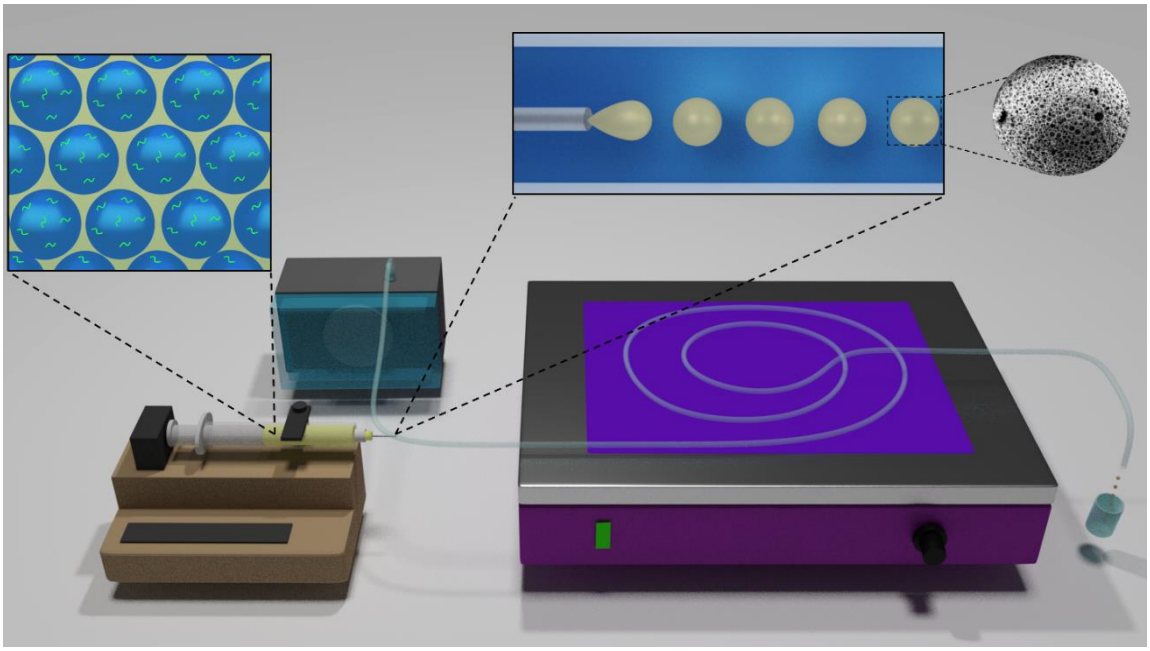

**Figure 4.1.** Schematic of microsphere fabrication. HIPE is injected through a needle parallel to the flow of 3 wt% PVA solution and polymerized via UV irradiation. Polymerized particles are collected and filtered prior to use.

**Table 4.1.** Summary table of fabrication parameters including tubing diameter, needle size, flow rate, and surfactant compositions for model compositions.

| Composition | Tubing ID | Needle Size | External Flow Rate | HIPE Injection | PGPR |
|---|---|---|---|---|---|
| Part L-Pore S | 1.6 mm | 27 Ga | 1.2 ml/min | 0.2 ml/hr | 30 wt% |
| Part L-Pore L | 1.6 mm | 27 Ga | 1.2 ml/min | 0.2 ml/hr | 10 wt% |
| Part S-Pore S | 0.8 mm | 30 Ga | 6.0 ml/min | 1.0 ml/hr | 30 wt% |
| Part S-Pore L | 0.8 mm | 30 Ga | 6.0 ml/min | 1.0 ml/hr | 10 wt% |

*4.2.3. SEM Analysis*

Average particle and pore diameter of varying compositions was determined using SEM (JOEL 6500) image analysis. A minimum of twenty-five particles, distributed over three fabrication batches, were coated with gold, imaged, and particle diameter measured.

Pore size measurements were completed on these particles using the first ten pores that crossed the median of each representative micrograph. Average particle (n = 25) and pore sizes (n = 100) for each polyHIPE microsphere composition are reported.

### *4.2.4. Loading Efficiency Model Protein*

Loading efficiency of each composition was determined using an accelerated release protocol. Prior to incubation, microspheres were crushed to increase surface area and minimize barriers to diffusion. Specimens were then placed in 2 mL centrifuge tubes and incubated in 1 ml DI water with agitation at 37C. After 24 hours, specimens were centrifuged to pellet the crushed particles and the aqueous phase removed. The pellet was then re-agitated with 1 ml DI water and incubated an additional 24 hours to remove residual protein. Protein concentration was determined using fluorescence spectroscopy (Tecan Infinite 200 Pro) by referencing a standard 10-point calibration curve prepared by measuring fluorescence of known concentrations of BSA-FITC. The concentration of BSA-FITC successfully encapsulated in the microsphere was then calculated and compared to the theoretical concentration loaded into the primary emulsion.

### *4.2.5. In Vitro Release Kinetics of Model Protein*

Microspheres containing BSA-FITC were placed in 2 mL centrifuge tubes and incubated in 1 mL DI water with agitation at 37C. At specified time points over 21 days, microsphere releasates were collected and replaced with 1 mL of fresh DI water. Daily protein release was determined using fluorescence spectroscopy (Tecan Infinite 200 Pro) by referencing a standard 10-point calibration curve prepared by measuring fluorescence of known concentrations of BSA-FITC. Cumulative release was determined by

normalizing each cumulative time point to the total amount released over the experiment period.

*4.2.6. Preparation of rhBMP-2 Loaded Microspheres*

Similar to BSA-FITC microsphere fabrication, an aqueous solution containing rhBMP-2 (E. coli expressed, R&D systems) was emulsified with EGDMA and surfactant to yield the primary HIPE. The rhBMP-2 HIPE was then polymerized and immersed in 0.5 mL release medium (DMEM containing 0.1% FBS) and allowed to release for 4 days. Releasates were collected and diluted to a concentration of 100 ng/mL for testing of bioactivity.

*4.2.7. Bioactivity Retention of Encapsulated rhBMP-2 with Reporter Cells*

A rapid assessment of bioactivity retention of rhBMP-2 loaded into polyHIPE scaffolds was performed by monitoring luciferase activity of a BMP responsive immortalized reporter (BRITER) cell line. Reporter cells were seeded at a density of 100,000 cells/$cm^2$ and cultured in growth media (DMEM + 10% FBS) containing 1 uM 4-hydroxytamoxifen to minimize endogenous BMP expression. After 24 hours, culture media was removed and replaced with polyHIPE releasate (100 ng/mL rhBMP-2) or indicated concentration of stock rhBMP-2 solution (100, 60, 20, 0 ng/mL rhBMP-2). After 3 hours, cells were lysed and luciferase activity measured using a Dual Luciferase Reporter Assay System (Promega). Relative luciferase activity was determined by normalizing BMP-2 dependent firefly luciferase activity to an internal cell density control via renilla luciferase activity.

*4.2.8. Osteogenic Differentiation of Human Mesenchymal Stem Cells*

Bone marrow-derived hMSCs were obtained as passage 1 from the Center for the Preparation and Distribution of Adult Stem Cells at Texas A&M Health Science Center College of Medicine, Institute for Regenerative Medicine at Scott & White through NIH Grant # P40RR017447. Cells were cultured to 80% confluency on tissue-culture polystyrene flasks in standard growth media containing Minimum Essential Media α (MEM α, Life Technologies) supplemented with 16.5% fetal bovine serum (FBS, Atlanta Biologicals) and 1% L-glutamine (Life Technologies) prior to passaging. All experiments were performed with cells at passage 3.

Alkaline phosphatase activity of hMSCs cultured with polyHIPE releasate was determined by monitoring the conversion of p-nitrophenyl phosphate (PNPP, Thermo Scientific) to p-nitrophenol. hMSCs were seeded at a density of 15,000 cells/cm$^2$ in standard growth media and allowed to adhere. After 24 hours, polyHIPE releasate or fresh rhBMP-2 as positive control (100 ng/mL) was added and changed every 3 days for 14 days following measurement of ALP activity. Samples were lysed using thermal shock and incubated with PNPP Substrate for 30 min. ALP activity was determined as the rate of PNPP conversion to p-nitrophenyl by measuring the absorbance at 405 nm (Tecan Infinite M200Pro) and normalized to cell number obtained from dsDNA quantification (PicoGreen, Life Technologies).

*4.2.9. Composite Scaffold Fabrication and Characterization*

Composite microsphere/polyHIPE scaffolds were fabricated by loading microspheres into redox initiated polyHIPEs prior to cure. Briefly, redox HIPEs were fabricated

according to established protocols with an organic phase comprised of 10 wt% PGPR and 1 wt% benzoyl peroxide (BPO) initiator or trimethylaniline (TMA) as reducing agent.[128] Microspheres were added at 0, 5, 10, or 20 wt% (dried microsphere/ HIPE polymer phase) to both initiating and reducing emulsions and mixed to facilitate crosslinking. HIPEs were placed in a 37°C aluminum bead bath to facilitate crosslinking overnight.

The effect of microsphere incorporation on polyHIPE compressive modulus and yield strength was investigated following ASTM D1621-04a. PolyHIPEs were sectioned into disks with a 3:1 diameter to height ratio (15 mm diameter, 5 mm thick) using an Isomet® saw. PolyHIPE specimens were compressed using an Instron 3300 at a strain rate of 50 mm/s. The compressive modulus was calculated from the slope of the linear region and the compressive yield strength was identified, after correcting for zero strain, as the stress at the yield point or 10% strain.

*4.2.10. Statistical Analysis*

The data are displayed as mean ± standard deviation for each composition. An analysis of variance (ANOVA) comparison was used for multiple composition comparisons with a Tukey's multiple comparison to analyze the significance of the data. A Student's t-test was performed to determine any statistically significant differences if only two compositions were present. All tests were carried out at a 95% confidence interval ($p<0.05$).

## 4.3. Results and Discussion

### *4.3.1. Fabrication and Characterization of PolyHIPE Microspheres*

To establish polyHIPE microspheres as a platform for sustained delivery of bioactive factors, the role of particle diameter and architecture on encapsulation efficiency and release kinetics of the model protein, BSA-FITC, was determined. We previously determined that a strict balance of fabrication parameters including external flow velocity and emulsion injection rates is necessary to ensure laminar flow and uniform particle generation.[262] Prior to investigation of encapsulation efficiency and release kinetics, particle diameter and pore architecture was characterized to ensure there were no negative effects on emulsion stability after loading of the protein. A factorial design of two particle diameters and two pore sizes was utilized to fabricate four distinct compositions utilizing the parameters outlined in **Table 4.1**.

First, control over external flow velocity was modulated to generate two distinct particle diameters. Tubing diameter of 1.6 mm was used with a flow rate of 1.2 ml/min to yield a flow velocity of 15 cm/min and large particles approximately 900 microns in size. An elevated flow velocity of 298 cm/min was achieved by decreasing tubing diameter to 0.8 mm and increasing flow rate to 6.0 ml/min. As a result of the increased shear forces at the injection site, small diameter particles approximately 300 microns in diameter were formed. A significant advantage of polyHIPE microsphere fabrication is the facile modulation of particle size and architecture independent of each other. We have previously discussed the role of surfactant concentration on internal droplet size and resultant pore diameter in polyHIPE scaffolds. Using this knowledge, two particle

diameters ~45 microns to ~15 microns were fabricated by increasing surfactant concentrations from 10 wt% and 30 wt%. Representative micrographs particle diameter and pore size are provided in **Figure 4.2** with quantification of particle and pore size provided in **Table 4.2**.

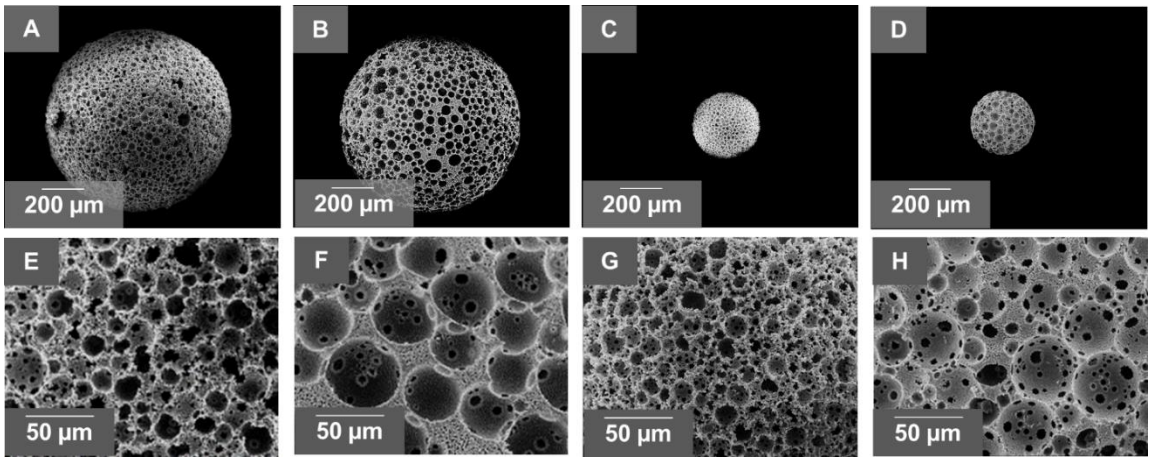


**Figure 4.2.** Modulated particle diameter of model compositions with representative SEM micrographs (A-D). Modulated pore diameter of model compositions with representative SEM micrographs (E-H). From left to right: large particle-small pore, large particle-large pore, small particle-small pore, small particle-large pore.

**Table 4.2.** Summary table of properties for model compositions including particle diameter (n=25), pore size (n=100), and loading efficiency (n=12). All data represents average ± standard deviation.

| Composition | Particle Size (µm) | Pore Size (µm) | Loading Efficiency |
|---|---|---|---|
| Part L-Pore S | 908 ± 67 | 19 ± 5 | 92% ± 5% |
| Part L-Pore L | 933 ± 76 | 46 ± 11 | 85% ± 4% |
| Part S-Pore S | 282 ± 48 | 16 ± 5 | 83% ± 2% |
| Part S-Pore L | 333 ± 41 | 42 ± 12 | 71% ± 5% |

### *4.3.2. Improved Loading Efficiency with In-Line Encapsulation*

A significant drawback to growth factor incorporation is elevated production costs associated with inefficient loading of these therapeutics during the manufacturing process. Microsphere delivery systems fabricated using traditional emulsion-solvent evaporation methods often report encapsulation efficiencies below 70%.[266, 267] Other systems, such as post-loaded scaffolds soaked in concentrated growth factor solutions, require elevated soak times and growth factor concentrations.[113] Therefore, a fabrication method with the ability to efficiently load bioactive factor into delivery vehicles would overcome a significant barrier to clinical translation. A major advantage of combining emulsion templating with controlled fluidics is the ability to in-line load growth factor directly into the microsphere vehicle during fabrication. This is achieved through incorporation of a concentrated protein solution as the internal droplet phase during formation of the primary emulsion. After injection into the external phase, the continuous phase is then photopolymerized, trapping the protein within the porous structure of the microsphere. Encapsulation efficiency of the model protein, BSA-FITC, was determined in each composition by crushing and extracting the protein. Particles with large diameters had exceptionally high encapsulation efficiencies with 92% and 85% for small and large pore sizes, respectively (**Table 4.2)**. The rapid polymerization of the prepolymer phase during fabrication trapped the in-line loaded protein, which combined with the lack of additional purification processes allowed for high encapsulation efficiency. Microspheres with small particle diameter experienced a minor decrease in encapsulation efficiency to 83% and 71% for small and large pore sizes, respectively. It is hypothesized that the increased

surface area/volume ratio of small diameter particles allowed for more rapid diffusion of protein trapped in surface pores during fabrication. It is important to note that the fabrication setup was optimized over several iterations to achieve this high encapsulation efficiency. Specifically, microsphere collection was adjusted to minimize flow of the external aqueous phase over microspheres that had already exited the tubing, minimizing undesirable washout of protein after cure. Overall, the ability to achieve high encapsulation efficiency of a model protein within a multitude of particle and pore diameters demonstrates the versatility of the polyHIPE microsphere platform.

*4.3.3. Effect of Microsphere Composition on Release Kinetics*

A primary aim of this work was to identify key relationships between microsphere property and release kinetics of a model protein. Achieving physiologically relevant delivery profiles of osteogenic factors is a critical design criterion that has yet to be sufficiently addressed in clinically available systems. Although some level of burst release, or rapid diffusion of factor out of the vehicle immediately following implantation, can be desirable and initiate fracture healing, it has been demonstrated that sustained delivery of osteogenic factor is also needed to allow appropriate time for osteoprogenitor cell recruitment and differentiation.[243] To this end, delivery profiles of polyHIPE microspheres were monitored over 21 days to assess levels of burst and sustained release, **Figure 4.3**. Unlike traditional delivery of small, hydrophobic compounds, release of growth factors from polymeric systems most often proceeds through diffusion of the protein through water filled pores.[268] Due to high molecular weight, growth factor release is not achieved by diffusion through the hydrophobic polymer phase. Passive diffusion of

protein out of water filled pores is referred to as the 'intrinsic' or 'true-release' mechanism of porous polymeric systems.[268] To further understand release kinetics, extensive study has been performed to identify rate-controlling mechanisms in these systems.[268] In this study we investigate the role of several rate-controlling mechanisms on model protein release including surface area-to-volume ratio, path length/tortuosity, and protein adsorption. The use of a double emulsion, controlled fluids fabrication system, allows for independent modulation of microsphere property and more systematic study of these mechanisms. The effect of surface area-to-volume ratio on release kinetics was first assessed by fabricating two distinct sets of microspheres, each set containing a large and small diameter particle of similar pore size. As expected small microspheres had a higher level of burst release after 24 hours, ranging from ~65% to ~78%, **Figure 4.3B**. Microspheres with a reduced surface area-to-volume ratio (large diameter) experienced a decreased 24 hour burst ranging from ~25% to ~47%. We attribute this difference in burst profile to the 3-fold increase in relative surface area for smaller particles, allowing for more rapid diffusion of protein away from the particle surface. Furthermore, the increased path length of large diameter particles resulted in ~80% of protein released after 7 days as opposed to ~95% protein release for small diameter particles.

In addition to characterizing the effect of particle diameter on release kinetics, the effect of pore architecture and tortuosity was assessed, **Figure 4.3C**. Tortuosity, a unit-less measure of path length through a porous medium relative to the end-to-end path length, is hypothesized to act as a primary tool in modulating release kinetics. Specifically, as pore size decreases, the subsequent increase in tortuosity is predicted to reduce protein

diffusion out of the microsphere. To investigate this mechanism, two distinct sets of microspheres were fabricated, each set containing two unique pore sizes for particles of similar diameter. For both particle diameters, a decrease in pore size resulted in more sustained release. Release after 72 hours decreased from ~80% to ~60% for large particles. A smaller change in protein release was observed after 72 hours for small particles with varied pore size. This was attributed to the high level of burst release discussed previously. However, increased tortuosity delayed 95% release of the protein from day 5 to day 9 for small diameter particles. In addition to increased tortuosity, it was hypothesized that a decreased pore size resulted in increased protein adsorption as a result of larger surface area present in the particle. Although protein adsorption may lead to incomplete release, protein-material interactions have been demonstrated as a potent rate-controlling mechanism in polymeric delivery systems.[269]

These studies were designed to provide introductory investigation into the potential of polyHIPE microspheres as controlled delivery vehicles. Additional methods can be explored to further modulate release kinetics. Given the slow degradation rates of EGDMA scaffolds, degradation-based release was not hypothesized to play significant role in these studies. However, selection of alternative biodegradable prepolymers fabricated with a closed-pore architecture would allow for introduction of yet another rate-controlling mechanism, further enhancing the tunability of this system. We have previously demonstrated that closed pore morphologies can be achieved with this system by changing to an aqueous initiator.[130]

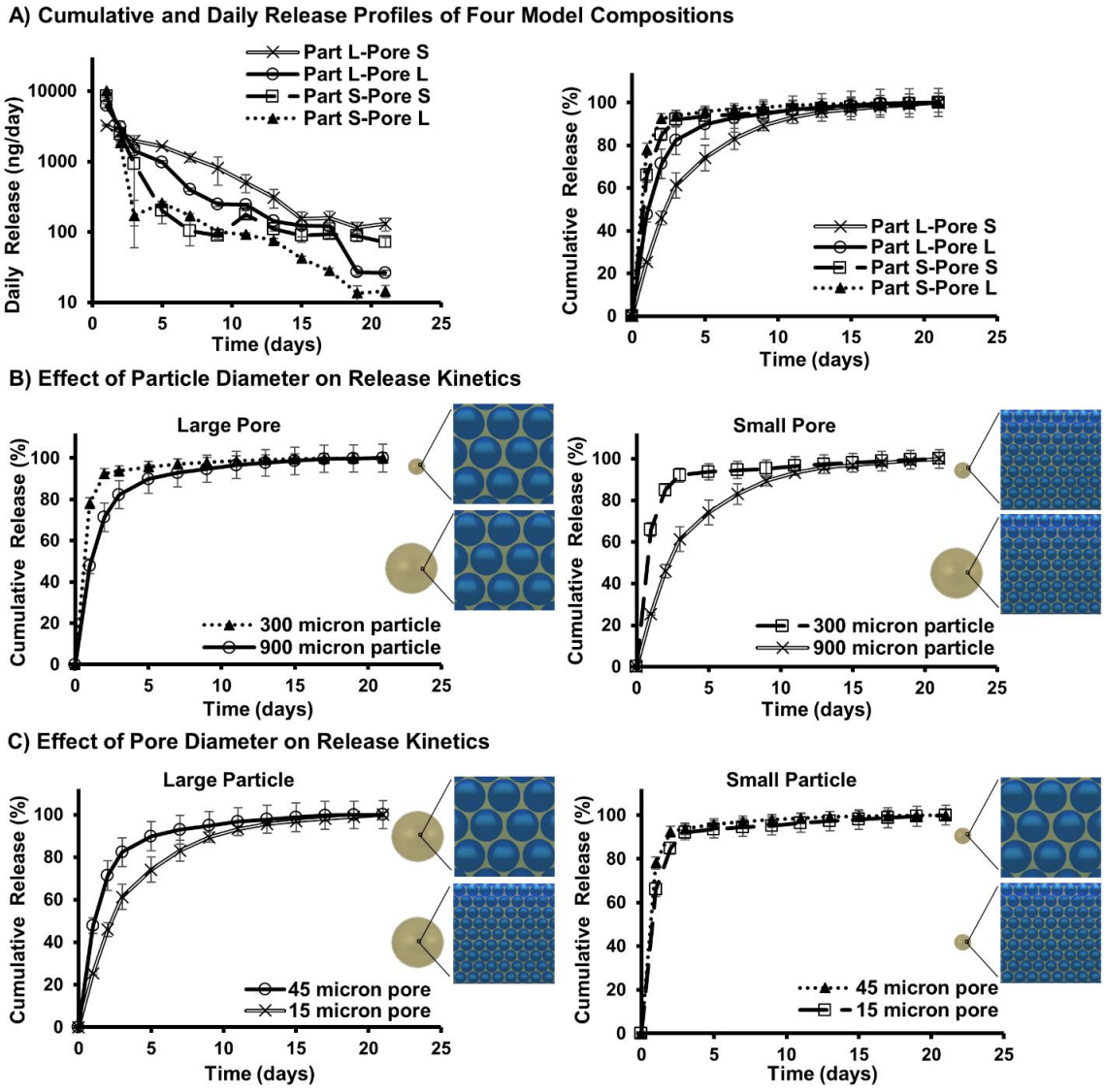


**Figure 4.3.** Tuning release profiles of BSA-FITC from polyHIPE microspheres. Daily and cumulative release profiles for all model compositions (A). Effect of particle size on release kinetics for large (45um) and small (15um) pore size (B). Effect of pore diameter on release kinetics for large (900um) and small (300um) particle size (C). All data represents average ± standard deviation for n = 3.

*4.3.4. Bioactivity Retention of Encapsulated rhBMP-2*

A significant hurdle to translation of BMP-2 loaded scaffolds is developing a fabrication method that retains therapeutic activity of encapsulated factors. Processes that require extensive purification, exposure to heat, or interaction with toxic solvents are prone to reduced bioactivity retention.[270] The photopolymerization method utilized here crosslinks the continuous phase of the primary emulsion within minutes at room temperature and eliminates the need for additional purification. The lack of organic solvents in this process provides the advantage of eliminating toxic leachables that may denature rhBMP-2 and raise concerns over biocompatibility. A significant step in the investigation of polyHIPE microspheres as a viable growth factor delivery system is to confirm growth factor loaded into the primary emulsion retains therapeutic activity after fabrication. To this end, a BMP responsive reporter cell was utilized as an initial test of bioactivity, **Figure 4.4**. Abbreviated BRITER, these immortalized calvarial osteoblasts are modified with a BMP responsive dual luciferase reporter construct.[271] Upon exposure to exogenous BMP-2, these cell exhibit a prompt and robust response, allowing for rapid detection of BMP activity. Luciferase activity was first determined in response to selected concentrations of non-encapsulated rhBMP-2 and utilized to determine a reference activity profile. rhBMP-2 was then encapsulated in high internal phase emulsion and photopolymerized. Encapsulated factor was extracted from the scaffold over 4 days and exposed to reporter cells for 3h followed my measurement of luciferase activity. Protein concentration extracted from primary emulsions was determined using established CBQCA quantification assays and normalized to a concentration of 100 ng/mL (data not

shown). As shown in **Figure 4.4**, encapsulated rhBMP-2 retained ~60% activity compared to non-encapsulated BMP-2 of equal concentration. BRITER cells with no exogenous BMP-2 exposure were used as negative control and demonstrated negligible activity.

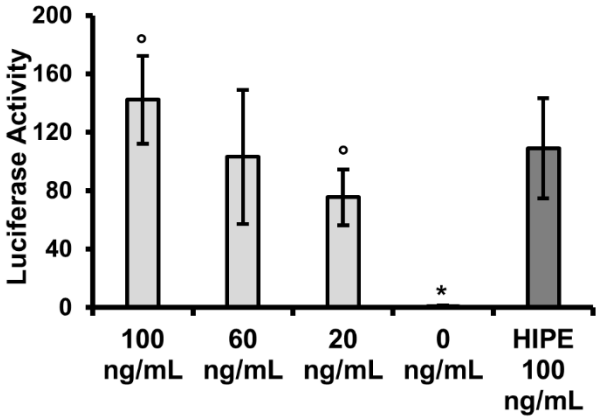


**Figure 4.4.** Normalized FFLuc activity of BRITER cell line treated with releasates taken from rhBMP-2 loaded microspheres. Percent bioactivity retention determined by comparison to FFLuc of known rhBMP-2 stocks.

### *4.3.5. Osteoblastic Differentiation of hMSCs Induced by rhBMP-2 Release*

Next, an additional measure of bioactivity was performed to investigate if extracted rhBMP-2 could elicit osteoblastic differentiation of human mesenchymal stem cells. In this study, alkaline phosphatase activity was characterized as an early marker of osteoblastic differentiation, **Figure 4.5**. The upregulation of ALP, an enzyme active in mineral formation and dephosphorylation processes of osteoblasts, is a well-established response to exposure of exogenous BMPs.[235] hMSCs were cultured with rhBMP-2 encapsulated and released form polyHIPE scaffolds, with non-encapsulated rhBMP-2 or

osteogenic media used as positive controls. Additionally, cells cultured in standard growth media without an osteoinductive agent were used as a negative control. After 2-week exposure, encapsulated rhBMP-2 promoted a similar osteoblastic response as hMSCs cultured in osteogenic (dexamethasone supplemented) conditions. Non-encapsulated rhBMP-2 had the highest activity with a ~4 fold increase over standard growth conditions. There are several mechanisms that may explain the observed difference in bioactivity for factor released from polyHIPEs compared to stock rhBMP-2. Most likely, early degradation of the factor occurred during the incubation period utilized for protein extraction. Bone morphogenetic proteins have been shown to possess low stability with therapeutic half-life being a function of incubation conditions such as solvent, temperature, and time in solution.[272-274] Stabilizing saccharides such as trehalose and heparin are often utilized to improve bioactivity retention in microsphere delivery systems studied for bone tissue engineering. Trehalose, a non-reducing disaccharide, serves as thermal protectant and improves stability under lyophilization and storage conditions.[275] Furthermore, Zhao *et al.* and Bramono *et al.* demonstrated heparin, a sulfated polysaccharide, could be used to limit degradation and prolong half-life of BMP-2 in media, up to 20-fold in cases.[276, 277] Although this study suggests that there is some reduction in bioactivity, the ability of encapsulated factor to promote measurable osteoblastic differentiation after release from polyHIPE scaffolds in the absence of additional stabilization demonstrates the utility of the polyHIPE microspheres. In addition, exposure of polyHIPE releaseate had no deleterious effects on cell density during the culture period, confirming no toxic leachable are present after microsphere fabrication. As

these preliminary studies indicate the ability to retain bioactivity of encapsulated factor after HIPE fabrication, current focus will be placed on extending therapeutic activity during duration of the targeted release profiles through investigation of stabilizing molecules.

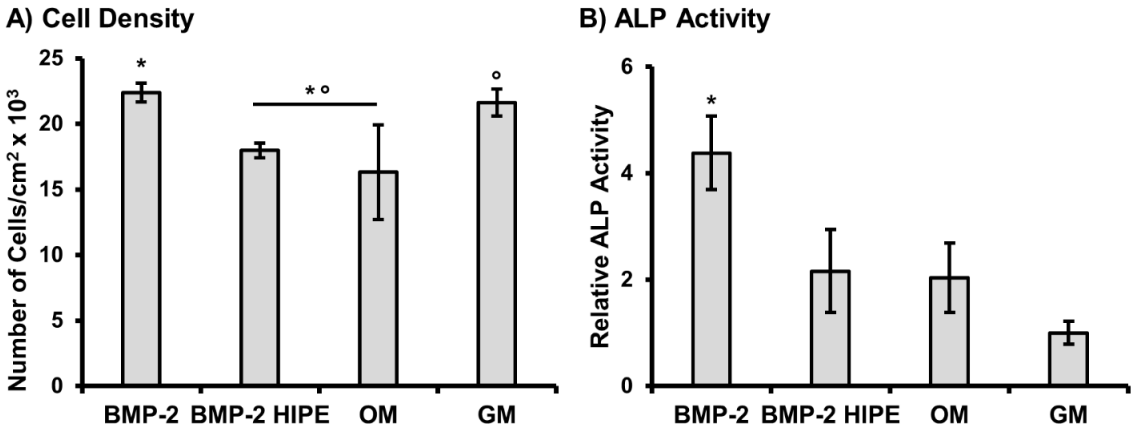


**Figure 4.5.** Effect of rhBMP-2 loaded polyHIPE releasate on cell density (A) and alkaline phosphatase activity (B) of hMSCs cultured with releasate for 14 days. Cells were cultured in fresh solution of stock rhBMP-2 (BMP-2) and osteogenic media (OM) as positive control, and growth media (GM) as negative control. All data represents average ± standard deviation for n = 4. The * and ° represent significant difference ($p<0.05$) between BMP-2 or GM and indicated compositions for density or ALP activity.

### *4.3.6. Effect of Microsphere Incorporation on Composite PolyHIPE Properties*

Ideally, an injectable bone graft contains a porous architecture to facilitate cellular infiltration, and compressive properties sufficient to stabilize the injury and provide mechanical stimuli to encourage regeneration.[20, 27] PolyHIPE scaffolds are unique in their ability to combine high porosities with uniform pore structures with mechanical properties that approach those of cancellous bone. Therefore, it is critical that any platform utilized

to provide targeted bioactivity not compromise load bearing potential of the graft. To this end, the effect of microsphere incorporation on compressive modulus and strength of injectable scaffold was characterized as a function of microsphere structure and percent incorporation. It was hypothesized that providing similar chemistry and pore architecture to that of the polyHIPE monoliths would limit effects on mechanical properties. An initial study of polyHIPE compressive modulus and strength was performed after adding 5 wt% of each of the four model compositions to assess potential effects of particle and pore size. At this level of incorporation, no statistical were differences observed between the blank polyHPE and any microsphere loaded composition, **Figure 4.6A**. This is promising as it demonstrates the ability to tune release profiles without impacting scaffold mechanical properties. To further highlight the range of this system, additional studies were performed to identify the compressive modulus and strength for increasing amounts of particle incorporation. Microspheres with surfactant concentration matched to that of the neat polyHIPE scaffold were added at increased amounts of 10 and 20 wt%, **Figure 4.6B**. A non-significant decrease in compressive properties was observed for 10 wt%, with ~50% reduction in compressive properties observed at 20 wt% incorporation. It is hypothesized that as the number of particles increased, non-uniform dispersion within the emulsion resulted in the formation of aggregates and limited proper integration with the surrounding, curing HIPE. Uniform dispersion within the scaffold is critical as it has been observed that a lack of interfacial interactions between scaffold and microsphere can result in a decrease of composite mechanical properties.[258] Kempen *et al.* demonstrated that increasing amounts of both PLGA and PPF microspheres added into a porous PPF scaffold

resulted in a significant decrease in compressive properties. Although a decrease was observed with increasing incorporation of PPF microspheres, the availability of covalent, interfacial interactions between scaffold and microsphere of matching chemistry resulted in increased compressive properties over PLGA microspheres. From this, it is anticipated that if uniform dispersion within our scaffold is maintained, allowing for appropriate interfacial bonding between methacrylate functional groups of sphere and emulsion, mechanical effects will be reduced. Current studies are exploring modified double barrel syringes that allow for more homogenous mixing and distribution of microspheres in the injectable HIPE. Furthermore, it is not anticipated that 20 wt% microsphere incorporation will be needed to promote an osteogenic response. Microsphere incorporation ranging 1-10 wt% has been demonstrated suitable to promote new bone formation utilizing loaded protein concentrations similar to those presented here.[118, 119, 259, 278] If a more robust response is desired, BMP-2 concentration loaded into the primary emulsion can be easily modulated to improve activity as has been observed in similar microsphere delivery systems.[278]

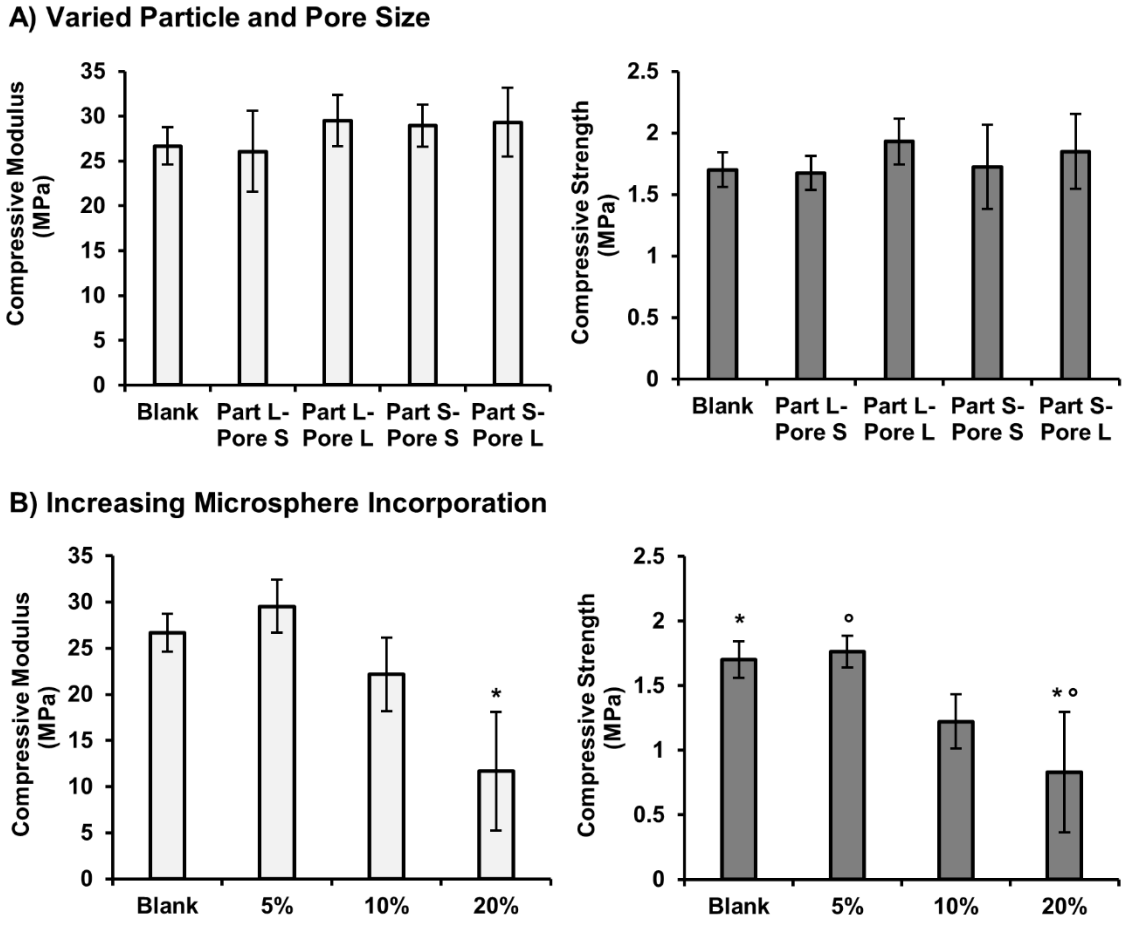


**Figure 4.6.** Effect of microsphere particle size and pore size on composite scaffold compressive modulus and strength for 5 wt% incorporation using four model compositions (A). Effect of increasing microsphere incorporation (5, 10 and 20 wt%) on composite scaffold compressive modulus and strength (B). All data represents average ± standard deviation for n = 3. The * and ° represent significant difference ($p<0.05$) for 20 wt% compressive modulus or strength and other indicated compositions.

In addition, incorporation of microspheres into the polyHIPE scaffold will provide an additional variable to tune release of osteoinductive factors in our system. Multiple studies have reported on the ability to improve sustained release profiles of growth factor delivered from microsphere vehicles by imbedding into secondary scaffolds.[119, 239] These

studies have reported success in promoting osteogenic activity *in vitro* and *in vivo*. Subsequent studies will assess the ability of polyHIPE scaffolds embedded with rhBMP-2 loaded microspheres to promote osteoblastic differentatin of mesenchymal stem cells cultured on the scaffold surface.

## 4.4. Conclusions

The aim of this study was to improve the osteoinductive potential of polyHIPE grafts by utilizing a new polyHIPE microsphere-based growth factor delivery system and establish the key relationships between microsphere properties and resultant protein release kinetics. The independent and combined effects of particle and pore size on burst and sustained release of proteins was determined. Bioactivity retention of the encapsulated BMP-2 growth after emulsion fabrication and photopolymerization processes was confirmed with demonstrated ability of the released BMP-2 to induce osteogenic differentiation of hMSCs. Finally, microsphere loaded composites were characterized to demonstrate that microsphere incorporation did not have deleterious effects on compressive properties. Overall, this investigation provides key insights critical to the design of an osteoinductive polyHIPE system capable of providing physiologically relevant delivery profiles.

# CHAPTER V

# CONCLUSIONS

## 5.1. Summary

The work presented here aims to develop an improved bone replacement based on the emulsion templating platform. These studies detail methods of fabricating injectable and porous grafts with improved function in clinically relevant environments, cell delivery platforms for improved loading of polyHIPE scaffolds, and porous microspheres for targeted growth factor delivery. Together, these advancements address limitations of current standards of care, including autologous and allogenic grafts, by providing a readily available bone replacement that has been optimized to actively guide bone regeneration.

Injectable polyHIPEs with improved resistance to oxygen inhibition were fabricated utilizing the thiol monomer pentaerythritol tetrakis(3-mercaptoproprionate), and the biodegradable macomer, propylene fumarate dimethacrylate. Thiol-methacrylate polyHIPEs exhibited rapid cure and improved network formation under oxygen rich conditions and retained the ability to modulate key properties including porosity, architecture, and compressive properties. Furthermore, thiol-methacrylate polymerization introduced a potent tool to tune the hydrolytic degradation rates of these injectable scaffolds. Matching the degradation profile of a tissue engineered scaffold with the healing rate of the native tissue is critical component of improving defect regeneration.

To improve the regenerative capacity of polyHIPE grafts, poly(ethylene glycol)-dithiothreitol hydrogels were utilized to improve seeding and distribution of human

mesenchymal stem cells (hMSCs) within 3D printed polyHIPEs. These *in situ* cell carriers, fabricated from biodegradable, redox initiated hydrogels, exhibited tunable polymerization rates, uniform cell distribution, and viable release of encapsulated stem cells. Regenerative potential of these composite, cell-laden polyHIPEs was demonstrated by characterizing osteoblastic differentiation of hMSCs released onto 3D printed polyHIPEs. This *in situ* approach to cell seeding permits facile use of patient specific cells that can be incorporated in tissue engineered scaffolds with minimal processing in the surgical suite.

Finally, additional osteoinductive character was added to the graft through the solvent-free fabrication of porous, in-line loaded microspheres capable of efficiently delivering osteoinductive factors. Modulation of polyHIPE microsphere property provided tools for tuning release kinetics without compromising compressive properties. Methods were developed to characterize bioactivity retention of encapsulated BMP-2 factor using a luminescence based reporter cell line and functional MSC differentiation assays. These studies demonstrate the strong potential of polyHIPE microspheres to improve bone regeneration through growth factor delivery and decrease manufacturing costs through utilization of more efficient fabrication and loading techniques.

Collectively, these studies highlight the strong potential of polyHIPE scaffolds to serve as an improved bone replacement with the ability to actively guide bone regeneration. Although the technologies developed in this work hold advantages in bone tissue engineering, the platforms utilized here are tunable in nature and be easily applied to the engineering of other target tissues.

## 5.2. Significance of Work

To date, no system has been able to fully match the healing potential that autologous tissue possesses due to its unique combination of osteoconductive (collagen-based ECM), osteoinductive (growth factors and cytokines), and osteogenic (stem and osteoprogenitor cells) properties. This work aimed to develop a polyHIPE graft that was capable of actively guiding bone regeneration by modeling these natural processes that make autologous grafting the current standard of care. Specifically, this work investigated PFDMA polyHIPE scaffolds as a porous and osteoconductive substrate to support bone repair. Furthermore, platforms to induce osteoinductive and osteogenic activity were investigated through development of polymeric delivery vehicles that allow for incorporation of bone morphogenetic proteins and mesenchymal stem cells. Combined, these technologies provide the foundation for developing novel, patient specific polyHIPE bone replacements with improved healing potential.

In Chapter 2, an alternative polymerization mechanism was explored to improve polymerization times and network formation in clinically relevant, oxygen rich enviornments. Redox initiated polyHIPEs have demonstrated a host of properties that are advantageous for bone repair. However, these studies were performed in a controlled environment that does not adequately represent all the challenges that are present *in vivo*. Retaining established properties, including rapid cure, uniform pore architecture, and load bearing potential, is dependent on the ability to obtain uniform high network formation in oxygen rich environments. Addressing the problem of oxygen inhibition has been discussed extensively in photopolymerized systems, however it has not been addressed

sufficiently in injectable systems.[155] Development of an injectable, highly porous graft that undergoes rapid polymerization *in vivo* is a major challenge in bone tissue engineering. This work demonstrated a thiol-methacrylate polymerization route that would be better immune to oxygen inhibition and provide an additional tool for modulating scaffold degradation rate. Differences in patient demographics, including age, health, and severity of injury, make developing a single graft capable of matching healing rate extremely difficult. As a result, modulating thiol concentration is a critical tool as it allows for rapid tuning of ester-based hydrolysis of the polyHIPE scaffold.

In Chapter 3, a platform for improved seeding of stem cells in tissue engineered grafts was developed. Mesenchymal stem cells play a significant role in regeneration of musculoskeletal tissues through recruitment and direction of progenitor cells, promotion of angiogenesis, and modulation of immune response.[192] Designing a biomaterial carrier that improves placement, retention, and survival of transplanted stem cells is currently a major focus in regenerative medicine as the hostile environment of injured tissue often yields the direct injection of stem cells into the defect site ineffective.[81] This work provided a method of encapsulating stem cells in biodegradable hydrogel, protecting them from early removal and subsequently improving the number and placement of stem cells seeded in a 3D printed polyHIPE graft. Development of a composite polyHIPE-hydrogel graft has the additional advantage of retaining requisite mechanical properties that are often lacking in hydrogel carriers alone. In addition to the direct effect this platform could have on improving regeneration, methods were developed to better characterize osteogenic activity on polyHIPE grafts through characterization of ALP and

mineralization markers. These methods can be used and further adapted to investigate osteogenic potential as additional technologies are introduced into polyHIPE grafts. Furthermore, this work provides a platform that can be further adapted (e.g. bioactivity, degradation profiles, and cell type) for incorporation of stem cells therapies into engineering strategies for other target tissues, including cardiac and nerve applications.

In Chapter 4, growth factor delivery was explored as a means to improve the osteoinductive character of our grafts. Through this work, a solvent-free method for generating porous, growth factor loaded microspheres was established via combination of emulsion templating and controlled fluidics fabrication techniques. Development of a cost-efficient growth factor delivery system that has high loading efficiency and tunable release kinetics is a significant challenge in tissue engineering. The improvements this system presents in processing and purification offer the potential to maximize loading efficiency while simultaneously minimizing scale up concerns. These studies produced methods to characterize and modulate protein release, as well as assess bioactivity retention of encapsulated factor, all protocols that can be easily adapted to a wide range of bioactive factors. Furthermore, this system provides a baseline fabrication method that can be further modified to deliver multiple growth factors simultaneously. Numerous studies have probed the benefits of multiple factor delivery and worked to design systems that better mimic the complex chemical environment of native tissue.[253]

Overall, this work demonstrates the ability to tune polyHIPE grafts to achieve desired physical and mechanical properties in clinically relevant settings. Furthermore, the tunable nature of the emulsion templating platform allows it to be easily tuned for the

incorporation of stem cells and bioactive factors. Although each component of this work aimed to provide a specific advantage to our polyHIPE bone graft, the broader impact of this work lies in the development of platforms and methods that can be easily modified to achieve regeneration in any target tissue.

### 5.3. Challenges and Future Directions

This work details the development of tunable polyHIPE scaffolds with improved healing potential through incorporation of stem cells and osteoinductive factors. Despite the demonstrated improvements in scaffold function and osteogenic potential *in vitro*, additional studies are needed to further optimize scaffold composition and assess bone formation *in vivo*.

A primary focus of this work was the modification of polyHIPE scaffolds, and development of assaying techniques, to better probe hMSC-polyHIPE interactions. It was demonstrated that polyHIPE scaffolds support desired markers of stem cell attachment, viability, and osteoblastic differentiation. However, these studies were performed in a highly controlled *in vitro* setting that relied on the adsorption of serum proteins to facilitate cell attachment. It is probable that cellular infiltration and migration would be reduced *in vivo* due to a lack of native binding sites for host cells, a phenomenon observed in other synthetic polymer systems.[94] Developing a hybrid polyHIPE scaffold with ECM-like surface modifiers would present an intriguing approach to encouraging native cell infiltration, as well as a potent tool to controlling cell fate. Integrin-mediated control of osteoblastic differentiation has been explored previously as a means of improving bone regeneration.[185] The work presented here demonstrated proof of principle protocols that

allow for facile incorporation of functionalized protein into polyHIPE scaffolds. Pore surfaces of modified scaffolds stained positive for gelatin incorporation and promoted cell attachment in serum free culture. This same approach could be utilized to crosslink a multitude of ECM-like proteins to the pore surface. Streptococcal collagen-like proteins are engineered proteins that form a triple helix similar to mammalian collagen, but with the added advantage of being able to provide precise control over presented integrin binding domains. Systematic investigation must first be completed to identify integrin-mediated signaling pathways most active in osteoblastic differentiation, followed by synthesis of the corresponding designer protein. Common methods for identification include antibody blocking targeted integrin receptors and monitoring the effect on gene expression using the osteoblastic markers, alkaline phosphatase, RUNX2, osteopontin, osteocalcin, and collagen I. Next, attachment, viability, and differentiation protocols discussed in this work could be implemented to ensure improvements in desired cell markers over a two week culture period.

The ability to delivery cells within a polyHIPE scaffold was a key advancement presented in this work. *In vitro* studies demonstrated significant improvement in cell distribution and retention over standard suspension seeding methods. Despite these improvements, it is critical that *in vivo* improvements be investigated as implantation into diseased or injured tissue is known to pose significant challenges to cell retention.[82] A proof of principle study investigating cell retention could be performed utilizing a subcutaneous model in Sprague-Dawley rats. A primary advantage of the *in situ* cell carrier developed here is that it allows for facile incorporation of host specific cells in the

surgical setting. As such, bone marrow derived stromal cells can be isolated from femoral limbs, expanded *in vitro*, and injected into a 3D printed polyHIPE. Monitoring retention and migration of transplanted cells can be performed through RT-PCR analysis of gender specific genes, fluorescent tagging using standard immunostaining protocols, or magnetic resonance imaging of magnetically labelled cells. It is probable that *in vivo* application may alter degradation profiles over those observed *in vitro*. If accelerated degradation were to occur, it is possible that transplanted cells may be removed before they have substantial time to adjust the regenerative microenvironment of damaged tissue. If necessary, degradation rate can be adjusted by modulating the number of DTT linkages present in the macromer backbone. This would allow for retention of established hydrogel properties while ensuring cells remained protected and present long enough to produce a robust trophic effect.

Treatment of musculoskeletal defects is a unique challenge in tissue engineering as these injuries are often accompanied by large volumetric tissue loss, compromising native vasculature and nutrient transport systems. As a result, it is necessary to engineer systems that promote both osteo-and angiogenesis. BMP-2 delivery is a potent method for improving osteogenic activity and has been shown to upregulate production of angiogenic factors in osteoblasts, however direct delivery of angiogenic factors, such as vascular endothelial growth factor, has been shown to provide synergistic improvements in bone healing.[253] Controlled co-delivery of these factors would provide a platform that could better explore the complex feedback loops present in bone healing and vascularization signaling pathways. The emulsion templating based-controlled fluidics fabrication method

would allow for development of microsphere delivery systems capable of co-delivery of these factors. Core-shell systems allow for controlled, sequential delivery of multiple therapeutic agents by encapsulating them in distinct spatial locations of the delivery system and providing unique temporal release profiles.[279] The present fluidics system would be modified with a coaxial needle to allow dual injection of two primary emulsions, each containing a distinct bioactive factor. These emulsions could be fabricated with unique pore architectures to allow for independent control over release kinetics. Although modulation of particle and pore size provides independent tools to control protein release kinetics, it is probable that a more sustained release profiles will be desired. To extend release, closed pore microspheres could be investigated to change the release mechanism from solely passive diffusion, to degradation mediated release. Upon degradation of the pore walls, encapsulated protein would be allowed to diffuse out into the surrounding scaffold. Modulation of internal phase volume fraction, or use of a water soluble initiator could facilitate formation of closed pore polyHIPEs. Although the methacrylated macromer utilized for microsphere fabrication here does not degrade in a suitable time frame, other systems explored here, such as thiol-methacrylate systems, could provide more rapid and controlled degradation rates.

Finally, to fully assess the clinical potential of the polyHIPE system developed in this work, *in vivo* osteogenesis must be monitored. The rabbit femoral condyle plug model provides a rapid, high throughput method for investigation of biocompatibility, host response and osteogenesis.[280] It is hypothesized that the platforms developed in this work would provide synergistic improvements in bone regeneration. To confirm this

hypothesis, a factorial study design must be implemented to investigate the individual and synergistic effects of scaffold surface modification, stem cell delivery, and growth factor delivery. MicroCT radiographic analysis would be used to monitor temporal changes in mineralized tissue formation over 8 and 16 weeks. Next, histological analysis using H&E and trichrome stains would be used to evaluate inflammation, vascularization, and bone formation across various regions of each defect. Sections would be subjectively scored, evaluated, and compared to blank defect controls and clinical calcium phosphate controls. Finally, microscale integration of the scaffold with the host tissue will be assessed by measuring peak loads of mechanical push out testing. Completion of this study would be invaluable in the development of selection criteria needed to balance improvements in healing with potential scale up and manufacturing costs.

Although additional investigation is required to confirm polyHIPE grafts are a viable bone grafting option, the technologies detailed in this work provide a promising platform that can be built upon to ensure all necessary criteria are met to support *in vivo* regeneration. The methods established here allow for characterization of all major tenets the tissue engineering paradigm, including scaffold properties, cell-material interactions, and bioactive factor delivery. In summary, the presented work, combined with these proposed studies, will provide knowledge critical to the development of a polyHIPE graft capable of actively guiding bone regeneration.

# REFERENCES


1. Bose, S. & Tarafder, S. Calcium phosphate ceramic systems in growth factor and drug delivery for bone tissue engineering: a review. *Acta biomaterialia* **8**, 1401-1421 (2012).

2. Praemer, A., Furner, S., Rice, D.P. & Kelsey, J.L. Musculoskeletal conditions in the United States. (1992).

3. Rodriguez-Merchan, E.C. & Forriol, F. Nonunion: general principles and experimental data. *Clinical orthopaedics and related research* **419**, 4-12 (2004).

4. Bosch, C., Melsen, B. & Vargervik, K. Importance of the critical-size bone defect in testing bone-regenerating materials. *The Journal of craniofacial surgery* **9**, 310-316 (1998).

5. Key, J.A. The effect of a local calcium depot on osteogenesis and healing of fractures. *JBJS* **16**, 176-184 (1934).

6. Hollinger, J.O. & Kleinschmidt, J.C. The critical size defect as an experimental model to test bone repair materials. *The Journal of craniofacial surgery* **1**, 60-68 (1990).

7. Sommerfeldt, D. & Rubin, C. Biology of bone and how it orchestrates the form and function of the skeleton. *European Spine Journal* **10**, S86-S95 (2001).

8. Coombes, A.G.A. & Meikle, M.C. Resorbable synthetic polymers s replacements for bone graft. *Clinical Materials* **17**, 35-67 (1994).

9. Kalfas, I.H. Principles of bone healing. *Neurosurgical Focus* **10**, 1-4 (2001).

10. Yaszemski, M.J., Payne, R.G., Hayes, W.C., Langer, R. & Mikos, A.G. Evolution of bone transplantation: molecular, cellular and tissue strategies to engineer human bone. *Biomaterials* **17**, 175-185 (1996).

11. Dimitriou, R., Tsiridis, E. & Giannoudis, P.V. Current concepts of molecular aspects of bone healing. *Injury* **36**, 1392-1404 (2005).

12. Bostrom, M.P.G. Expression of bone morphogenetic proteins in fracture healing. *Clinical Orthopaedics and Related Research*, S116-S123 (1998).

13. Carano, R.A. & Filvaroff, E.H. Angiogenesis and bone repair. *Drug discovery today* **8**, 980-989 (2003).

14. Hoerth, R.M. et al. Mechanical and structural properties of bone in non-critical and critical healing in rat. *Acta biomaterialia* **10**, 4009-4019 (2014).

15. Chamay, A. & Tschantz, P. Mechanical influences in bone remodeling. Experimental research on Wolff's law. *Journal of Biomechanics* **5**, 173-180 (1972).

16. Gutta, R. & Waite, P.D. Cranial bone grafting and simultaneous implants: a submental technique to reconstruct the atrophic mandible. *British Journal of Oral and Maxillofacial Surgery* **46**, 477-479 (2008).

17. Samartzis, D. et al. Comparison of allograft to autograft in multilevelanterior cervical discectomy and fusion with rigid plate fixation. *The Spine Journal* **3**, 451-459 (2003).

18. Chau, A. & Mobbs, R. Bone graft substitutes in anterior cervical discectomy and fusion. *European Spine Journal* **18**, 449-464 (2009).

19. Bauer, T.W. & Muschler, G.F. Bone graft materials - An overview of the basic science. *Clinical Orthopaedics and Related Research*, 10-27 (2000).

20. Kretlow, J.D., Young, S., Klouda, L., Wong, M. & Mikos, A.G. Injectable biomaterials for regenerating complex craniofacial tissues. *Advanced Materials* **21**, 3368-3393 (2009).

21. Dumas, J.E. et al. Synthesis and characterization of an injectable allograft bone/polymer composite bone void filler with tunable mechanical properties. *Tissue Engineering: Part A* **16**, 2505-2518 (2010).

22. Katti, K.S. Biomaterials in total joint replacement. *Colloids and Surfaces B: Biointerfaces* **39**, 133-142 (2004).

23. Haas, S.S., Brauer, G.M. & Dickson, G. A characterization of polymethylmethacrylate bone cement. *Journal Article* **57**, 380-391 (1975).

24. Zhang, J., Liu, W., Schnitzler, V., Tancret, F. & Bouler, J.-M. Calcium phosphate cements for bone substitution: Chemistry, handling and mechanical properties. *Acta Biomaterialia* **10**, 1035-1049 (2014).

25. Rose, F.R. & Oreffo, R.O. Bone tissue engineering: hope vs hype. *Biochemical and biophysical research communications* **292**, 1-7 (2002).

26. Langer, R. & Vacanti, J.P. Tissue engineering. *Science* **260**, 920-926 (1993).

27. Karageorgiou, V. & Kaplan, D. Porosity of 3D biomaterial scaffolds and osteogenesis. *Biomaterials* **26**, 5474-5491 (2005).

28. Ishaug-Riley, S.L., Crane-Kruger, G.M., Yaszemski, M.J. & Mikos, A.G. Three-dimensional culture of rat calvarial osteoblasts in porous biodegradable polymers. *Biomaterials* **19**, 1405-1412 (1998).

29. Marcacci, M. et al. Stem cells associated with macroporous bioceramics for long bone repair: 6-to 7-year outcome of a pilot clinical study. *Tissue Engineering* **13**, 947-955 (2007).

30. Taylor, D. Fatigue of bone and bones: An analysis based on stressed volume. *Journal of Orthopaedic Research* **16**, 163-169 (1998).

31. Huiskes, R., Weinans, H. & Van Rietbergen, B. The relationship between stress shielding and bone resorption around total hip stems and the effects of flexible materials. *Clinical orthopaedics and related research* **274**, 124-134 (1992).

32. Temenoff, J.S. & Mikos, A.G. Injectable biodegradable materials for orthopedic tissue engineering. *Biomaterials* **21**, 2405-2412 (2000).

33. Dumas, J. et al. Balancing the rates of new bone formation and polymer degradation enhances healing of weight-bearing allograft/polyurethane composites in rabbit femoral defects. *Tissue engineering. Part A* **20**, 115-129 (2014).

34. Pham, Q.P., Sharma, U. & Mikos, A.G. Electrospinning of polymeric nanofibers for tissue engineering applications: a review. *Tissue engineering* **12**, 1197-1211 (2006).

35. Nezarati, R.M., Eifert, M.B. & Cosgriff-Hernandez, E. Effects of humidity and solution viscosity on electrospun fiber morphology. *Tissue Engineering Part C: Methods* **19**, 810-819 (2013).

36. Kim, T.K., Yoon, J.J., Lee, D.S. & Park, T.G. Gas foamed open porous biodegradable polymeric microspheres. *Biomaterials* **27**, 152-159 (2006).

37. Harris, L.D., Kim, B.-S. & Mooney, D.J. Open pore biodegradable matrices formed with gas foaming. *Journal of biomedical materials research* **42**, 396-402 (1998).

38. Hacker, M. et al. Solid lipid templating of macroporous tissue engineering scaffolds. *Biomaterials* **28**, 3497-3507 (2007).

39. Mistry, A.S. et al. Fabrication and in vitro degradation of porous fumarate-based polymer/alumoxane nanocomposite scaffolds for bone tissue engineering. *Journal of Biomedical Materials Research Part A* **89**, 68-79 (2009).

40. Lin-Gibson, S., Cooper, J.A., Landis, F.A. & Cicerone, M.T. Systematic investigation of porogen size and content on scaffold morphometric parameters and properties. *Biomacromolecules* **8**, 1511-1518 (2007).

41. Guan, J., Fujimoto, K.L., Sacks, M.S. & Wagner, W.R. Preparation and characterization of highly porous, biodegradable polyurethane scaffolds for soft tissue applications. *Biomaterials* **26**, 3961-3971 (2005).

42. Day, R.M. et al. In vivo characterisation of a novel bioresorbable poly(lactide-co-glycolide) tubular foam scaffold for tissue engineering applications. *Journal of Materials Science: Materials in Medicine* **15**, 729-734 (2004).

43. Busby, W., Cameron, N.R. & Jahoda, C.A.B. Emulsion-derived foams (polyHIPEs) containing poly(ε-caprolactone) as matrixes for tissue engineering. *Biomacromolecules* **2**, 154-164 (2001).

44. Busby, W., Cameron, N.R. & Jahoda, C.A.B. Tissue engineering matrixes by emulsion templating. *Polymer International* **51**, 871-881 (2002).

45. Barbetta, A. et al. Scaffolds based on biopolymeric foams. *Adv Funct Mater* **15**, 118-124 (2005).

46. Bokhari, M.A., Birch, M.A. & Akay, G. Polyhipe polymer: a novel scaffold for in vitro bone tissue engineering. *Experimental Medical Biology: Tissue Engineering, Stem Cells, and Gene Therapies* **534**, 247-254 (2003).

47. Cameron, N.R., Barbetta, A. & Cooper, S.J. High internal phase emulsions (HIPEs) containing divinylbenzene and 4-vinylbenzyl chloride and the morphology of the resulting PolyHIPE materials. *Chemical Communications*, 221–222 (2000).

48. Cameron, N.R. & Sherrington, D.C. Synthesis and characterisation of poly(aryl ether sulfone) polyHIPE materials. *Macromolecules* **30**, 5860-5869 (1997).

49. Hayman, M.W., Smith, K.H., Cameron, N.R. & Przyborskia, S.A. Growth of human stem cell-derived neurons on solid three-dimensional polymers. *J Biochem Biophys Methods* **62**, 231-240 (2005).

50. Decker, C. Effect of UV radiation on polymers. *Marcel Dekker, Handbook of Polymer Science and Technology.* **3**, 541-608 (1989).

51. Decker, C. & Jenkins, A.D. Kinetic approach of oxygen inhibition in ultraviolet- and laser-induced polymerizations. *Macromolecules* **18**, 1241-1244 (1985).

52. O'Brien, A.K., Cramer, N.B. & Bowman, C.N. Oxygen inhibition in thiol–acrylate photopolymerizations. *Journal of Polymer Science Part A: Polymer Chemistry* **44**, 2007-2014 (2006).

53. Murphy, M.B., Moncivais, K. & Caplan, A.I. Mesenchymal stem cells: environmentally responsive therapeutics for regenerative medicine. *Experimental & molecular medicine* **45**, e54 (2013).

54. Friedenstein, A., Piatetzky-Shapiro, I. & Petrakova, K. Osteogenesis in transplants of bone marrow cells. *Development* **16**, 381-390 (1966).

55. Caplan, A.I. Mesenchymal stem cells. *Journal of orthopaedic research* **9**, 641-650 (1991).

56. Owen, M. Marrow stromal stem cells. *J Cell Sci* **1988**, 63-76 (1988).

57. Pittenger, M.F. et al. Multilineage potential of adult human mesenchymal stem cells. *science* **284**, 143-147 (1999).

58. Dominici, M. et al. Minimal criteria for defining multipotent mesenchymal stromal cells. The International Society for Cellular Therapy position statement. *Cytotherapy* **8**, 315-317 (2006).

59. DiGirolamo, C.M. et al. Propagation and senescence of human marrow stromal cells in culture: a simple colony-forming assay identifies samples with the greatest potential to propagate and differentiate. *British journal of haematology* **107**, 275-281 (1999).

60. Murphy, J.M. et al. Reduced chondrogenic and adipogenic activity of mesenchymal stem cells from patients with advanced osteoarthritis. *Arthritis & Rheumatology* **46**, 704-713 (2002).

61. Barry, F.P. & Murphy, J.M. Mesenchymal stem cells: clinical applications and biological characterization. *The international journal of biochemistry & cell biology* **36**, 568-584 (2004).

62. Schäffler, A. & Büchler, C. Concise review: adipose tissue-derived stromal cells—basic and clinical implications for novel cell-based therapies. *Stem cells* **25**, 818-827 (2007).

63. Yoshimura, H. et al. Comparison of rat mesenchymal stem cells derived from bone marrow, synovium, periosteum, adipose tissue, and muscle. *Cell and tissue research* **327**, 449-462 (2007).

64. Lee, O.K. et al. Isolation of multipotent mesenchymal stem cells from umbilical cord blood. *Blood* **103**, 1669-1675 (2004).

65. Caplan, Arnold I. & Correa, D. The msc: an injury drugstore. *Cell Stem Cell* **9**, 11-15 (2011).

66. Haynesworth, S.E., Baber, M.A. & Caplan, A.I. Cytokine expression by human marrow-derived mesenchymal progenitor cells in vitro: Effects of dexamethasone and IL-1α. *Journal of cellular physiology* **166**, 585-592 (1996).

67. Caplan, A.I. & Bruder, S.P. Mesenchymal stem cells: building blocks for molecular medicine in the 21st century. *Trends in molecular medicine* **7**, 259-264 (2001).

68. Sorrell, J.M., Baber, M.A. & Caplan, A.I. Influence of adult mesenchymal stem cells on in vitro vascular formation. *Tissue Engineering Part A* **15**, 1751-1761 (2009).

69. Chen, L., Tredget, E.E., Wu, P.Y. & Wu, Y. Paracrine factors of mesenchymal stem cells recruit macrophages and endothelial lineage cells and enhance wound healing. *PloS one* **3**, e1886 (2008).

70. Tateishi-Yuyama, E. et al. Therapeutic angiogenesis for patients with limb ischaemia by autologous transplantation of bone-marrow cells: a pilot study and a randomised controlled trial. *The Lancet* **360**, 427-435 (2002).

71. Aggarwal, S. & Pittenger, M.F. Human mesenchymal stem cells modulate allogeneic immune cell responses. *Blood* **105**, 1815-1822 (2005).

72. Ren, G. et al. Mesenchymal stem cell-mediated immunosuppression occurs via concerted action of chemokines and nitric oxide. *Cell stem cell* **2**, 141-150 (2008).

73. Selmani, Z. et al. Human leukocyte antigen-G5 secretion by human mesenchymal stem cells is required to suppress T lymphocyte and natural killer function and to induce CD4+ CD25highFOXP3+ regulatory T cells. *Stem cells* **26**, 212-222 (2008).

74. Cselenyák, A., Pankotai, E., Horváth, E.M., Kiss, L. & Lacza, Z. Mesenchymal stem cells rescue cardiomyoblasts from cell death in an in vitro ischemia model via direct cell-to-cell connections. *BMC Cell Biology* **11**, 29 (2010).

75. Uccelli, A., Moretta, L. & Pistoia, V. Mesenchymal stem cells in health and disease. *Nature reviews immunology* **8**, 726 (2008).

76. Gonzalez-Rey, E., Gonzalez, M.A., Rico, L., Buscher, D. & Delgado, M. Human adult stem cells derived from adipose tissue protect against experimental colitis and sepsis. *Gut* (2009).

77. Connolly, J.F., Guse, R., Tiedeman, J. & Dehne, R. Autologous marrow injection as a substitute for operative grafting of tibial nonunions. *Clinical orthopaedics and related research*, 259-270 (1991).

78. Hernigou, P., Poignard, A., Beaujean, F. & Rouard, H. Percutaneous autologous bone-marrow grafting for nonunions: influence of the number and concentration of progenitor cells. *JBJS* **87**, 1430-1437 (2005).

79. Bruder, S.P., Kraus, K.H., Goldberg, V.M. & Kadiyala, S. The effect of implants loaded with autologous mesenchymal stem cells on the healing of canine segmental bone defects. *JBJS* **80**, 985-996 (1998).

80. Bruder, S.P. et al. Bone regeneration by implantation of purified, culture-expanded human mesenchymal stem cells. *Journal of orthopaedic research* **16**, 155-162 (1998).

81. Horwitz, E.M. et al. Transplantability and therapeutic effects of bone marrow-derived mesenchymal cells in children with osteogenesis imperfecta. *Nature medicine* **5**, 309 (1999).

82. Burdick, J.A., Mauck, R.L. & Gerecht, S. To serve and protect: hydrogels to improve stem cell-based therapies. *Cell stem cell* **18**, 13-15 (2016).

83. Nicodemus, G.D. & Bryant, S.J. Cell encapsulation in biodegradable hydrogels for tissue engineering applications. *Tissue Engineering Part B: Reviews* **14**, 149-165 (2008).

84. Marquardt, L.M. & Heilshorn, S.C. Design of injectable materials to improve stem cell transplantation. *Current stem cell reports* **2**, 207-220 (2016).

85. Awad, H.A., Wickham, M.Q., Leddy, H.A., Gimble, J.M. & Guilak, F. Chondrogenic differentiation of adipose-derived adult stem cells in agarose, alginate, and gelatin scaffolds. *Biomaterials* **25**, 3211-3222 (2004).

86. Nichol, J.W. et al. Cell-laden microengineered gelatin methacrylate hydrogels. *Biomaterials* **31**, 5536-5544 (2010).

87. Nuttelman, C.R., Tripodi, M.C. & Anseth, K.S. In vitro osteogenic differentiation of human mesenchymal stem cells photoencapsulated in PEG hydrogels. *Journal of Biomedical Materials Research Part A* **68**, 773-782 (2004).

88. Burdick, J.A. & Anseth, K.S. Photoencapsulation of osteoblasts in injectable RGD-modified PEG hydrogels for bone tissue engineering. *Biomaterials* **23**, 4315-4323 (2002).

89. Nuttelman, C.R., Tripodi, M.C. & Anseth, K.S. Synthetic hydrogel niches that promote hMSC viability. *Matrix biology* **24**, 208-218 (2005).

90. Temenoff, J.S. et al. Thermally cross-linked oligo (poly (ethylene glycol) fumarate) hydrogels support osteogenic differentiation of encapsulated marrow stromal cells in vitro. *Biomacromolecules* **5**, 5-10 (2004).

91. Qiu, Y. et al. PEG-based hydrogels with tunable degradation characteristics to control delivery of marrow stromal cells for tendon overuse injuries. *Acta biomaterialia* **7**, 959-966 (2011).

92. Simmons, C.A., Alsberg, E., Hsiong, S., Kim, W.J. & Mooney, D.J. Dual growth factor delivery and controlled scaffold degradation enhance in vivo bone formation by transplanted bone marrow stromal cells. *Bone* **35**, 562-569 (2004).

93. Zhao, L., Weir, M.D. & Xu, H.H. An injectable calcium phosphate-alginate hydrogel-umbilical cord mesenchymal stem cell paste for bone tissue engineering. *Biomaterials* **31**, 6502-6510 (2010).

94. Guo, R. et al. A transient cell-shielding method for viable MSC delivery within hydrophobic scaffolds polymerized in situ. *Biomaterials* **54**, 21-33 (2015).

95. Barnes, G.L., Kostenuik, P.J., Gerstenfeld, L.C. & Einhorn, T.A. Growth factor regulation of fracture repair. *Journal of Bone and Mineral Research* **14**, 1805-1815 (1999).

96. Lieberman, J.R., Daluiski, A. & Einhorn, T.A. The role of growth factors in the repair of bone: biology and clinical applications. *JBJS* **84**, 1032-1044 (2002).

97. Heldin, C.-H., Miyazono, K. & Ten Dijke, P. TGF-β signalling from cell membrane to nucleus through SMAD proteins. *Nature* **390**, 465 (1997).

98. Ferguson, C., Alpern, E., Miclau, T. & Helms, J.A. Does adult fracture repair recapitulate embryonic skeletal formation? *Mechanisms of development* **87**, 57-66 (1999).

99. Urist, M.R. Bone: formation by autoinduction. *Science* **150**, 893-899 (1965).

100. Wozney, J.M. et al. Novel regulators of bone formation: molecular clones and activities. *Science* **242**, 1528-1534 (1988).

101. Cheng, H. et al. Osteogenic activity of the fourteen types of human bone morphogenetic proteins (BMPs). *JBJS* **85**, 1544-1552 (2003).

102. Tsuji, K. et al. BMP2 activity, although dispensable for bone formation, is required for the initiation of fracture healing. *Nature genetics* **38**, 1424 (2006).

103. Fiedler, J., Röderer, G., Günther, K.P. & Brenner, R.E. BMP-2, BMP-4, and PDGF-bb stimulate chemotactic migration of primary human mesenchymal progenitor cells. *Journal of cellular biochemistry* **87**, 305-312 (2002).

104. Deckers, M.M. et al. Bone morphogenetic proteins stimulate angiogenesis through osteoblast-derived vascular endothelial growth factor A. *Endocrinology* **143**, 1545-1553 (2002).

105. Zhang, F. et al. Sustained BMP signaling in osteoblasts stimulates bone formation by promoting angiogenesis and osteoblast differentiation. *Journal of Bone and Mineral Research* **24**, 1224-1233 (2009).

106. Zhang, W. et al. VEGF and BMP-2 promote bone regeneration by facilitating bone marrow stem cell homing and differentiation. *Eur Cell Mater* **27**, 1-11 (2014).

107. McKay, W.F., Peckham, S.M. & Badura, J.M. A comprehensive clinical review of recombinant human bone morphogenetic protein-2 (INFUSE® Bone Graft). *International orthopaedics* **31**, 729-734 (2007).

108. Burkus, J.K., Gornet, M.F., Dickman, C.A. & Zdeblick, T.A. Anterior lumbar interbody fusion using rhBMP-2 with tapered interbody cages. *Clinical Spine Surgery* **15**, 337-349 (2002).

109. Vaccaro, A.R. et al. A pilot study evaluating the safety and efficacy of OP-1 Putty (rhBMP-7) as a replacement for iliac crest autograft in posterolateral lumbar arthrodesis for degenerative spondylolisthesis. *Spine* **29**, 1885-1892 (2004).

110. Friedlaender, G.E. et al. Osteogenic protein-1 (bone morphogenetic protein-7) in the treatment of tibial nonunions: a prospective, randomized clinical trial comparing rhOP-1 with fresh bone autograft. *The Journal of bone and joint surgery. American volume* **83**, S151 (2001).

111. Carragee, E.J., Hurwitz, E.L. & Weiner, B.K. A critical review of recombinant human bone morphogenetic protein-2 trials in spinal surgery: emerging safety concerns and lessons learned. *The Spine Journal* **11**, 471-491 (2011).

112. Shields, L.B. et al. Adverse effects associated with high-dose recombinant human bone morphogenetic protein-2 use in anterior cervical spine fusion. *Spine* **31**, 542-547 (2006).

113. Geiger, M., Li, R. & Friess, W. Collagen sponges for bone regeneration with rhBMP-2. *Advanced drug delivery reviews* **55**, 1613-1629 (2003).

114. Gokmen, M.T. & Du Prez, F.E. Porous polymer particles—A comprehensive guide to synthesis, characterization, functionalization and applications. *Progress in Polymer Science* **37**, 365-405 (2012).

115. Makadia, H.K. & Siegel, S.J. Poly lactic-co-glycolic acid (PLGA) as biodegradable controlled drug delivery carrier. *Polymers* **3**, 1377-1397 (2011).

116. Anderson, J.M. & Shive, M.S. Biodegradation and biocompatibility of PLA and PLGA microspheres. *Advanced drug delivery reviews* **28**, 5-24 (1997).

117. Cohen, S., Yoshioka, T., Lucarelli, M., Hwang, L.H. & Langer, R. Controlled delivery systems for proteins based on poly (lactic/glycolic acid) microspheres. *Pharmaceutical research* **8**, 713-720 (1991).

118. Lee, J.W. et al. Bone regeneration using a microstereolithography-produced customized poly (propylene fumarate)/diethyl fumarate photopolymer 3D scaffold incorporating BMP-2 loaded PLGA microspheres. *Biomaterials* **32**, 744-752 (2011).

119. Li, B. et al. The effects of rhBMP-2 released from biodegradable polyurethane/microsphere composite scaffolds on new bone formation in rat femora. *Biomaterials* **30**, 6768-6779 (2009).

120. Lee, J., Oh, Y.J., Lee, S.K. & Lee, K.Y. Facile control of porous structures of polymer microspheres using an osmotic agent for pulmonary delivery. *Journal of Controlled Release* **146**, 61-67 (2010).

121. Nam, Y.S., Yoon, J.J. & Park, T.G. A novel fabrication method of macroporous biodegradable polymer scaffolds using gas foaming salt as a porogen additive. *Journal of biomedical materials research* **53**, 1-7 (2000).

122. Jain, R.A. The manufacturing techniques of various drug loaded biodegradable poly (lactide-co-glycolide)(PLGA) devices. *Biomaterials* **21**, 2475-2490 (2000).

123. Berkland, C., Pollauf, E., Pack, D.W. & Kim, K.K. Uniform double-walled polymer microspheres of controllable shell thickness. *Journal of controlled release* **96**, 101-111 (2004).

124. Middleton, J.C. & Tipton, A.J. Synthetic biodegradable polymers as orthopedic devices. *Biomaterials* **21**, 2335-2346 (2000).

125. Akay, G., Birch, M.A. & Bokhari, M.A. Microcellular polyHIPE polymer supports osteoblast growth and bone formation in vitro. *Biomaterials* **25**, 3991-4000 (2004).

126. Moglia, R.S. et al. Injectable PolyHIPEs as High-Porosity Bone Grafts. *Biomacromolecules* **12**, 3621-3628 (2011).

127. Moglia, R.S. et al. Injectable polyMIPE scaffolds for soft tissue regeneration. *Polymer* **55**, 426-434 (2014).

128. Moglia, R.S. et al. Injectable Polymerized High Internal Phase Emulsions with Rapid in Situ Curing. *Biomacromolecules* **15**, 2870-2878 (2014).

129. Robinson, J.L. et al. Osteoinductive PolyHIPE Foams as Injectable Bone Grafts. *Tissue Engineering Part A* **22**, 403-414 (2016).

130. Robinson, J.L., Moglia, R.S., Stuebben, M.C., McEnery, M.A. & Cosgriff-Hernandez, E. Achieving interconnected pore architecture in injectable polyHIPEs for bone tissue engineering. *Tissue Engineering Part A* **20**, 1103-1112 (2014).

131. Barbetta, A., Dentini, M., Zannoni, E.M. & De Stefano, M.E. Tailoring the Porosity and Morphology of Gelatin-Methacrylate PolyHIPE Scaffolds for Tissue Engineering Applications. *Langmuir* **21**, 12333-12341 (2005).

132. Peter, S.J., Miller, M.J., Yasko, A.W., Yaszemski, M.J. & Mikos, A.G. Polymer concepts in tissue engineering. *Journal of Biomedical Materials Research* **43**, 422-427 (1998).

133. Rueggeberg, F. & Margeson, D. The effect of oxygen inhibition on an unfilled/filled composite system. *Journal of Dental Research* **69**, 1652-1658 (1990).

134. Cramer, N.B. & Bowman, C.N. Kinetics of thiol–ene and thiol–acrylate photopolymerizations with real-time fourier transform infrared. *Journal of Polymer Science Part A: Polymer Chemistry* **39**, 3311-3319 (2001).

135. Morgan, C.R., Magnotta, F. & Ketley, A.D. Thiol/ene photocurable polymers. *Journal of Polymer Science: Polymer Chemistry Edition* **15**, 627-645 (1977).

136. O'Brien, A.K. & Bowman, C.N. Modeling the effect of oxygen on photopolymerization kinetics. *Macromolecular Theory and Simulations* **15**, 176-182 (2006).

137. Caldwell, S. et al. Degradable emulsion-templated scaffolds for tissue engineering from thiol-ene photopolymerisation. *Soft Matter* **8**, 10344-10351 (2012).

138. Lovelady, E., Kimmins, S.D., Wu, J. & Cameron, N.R. Preparation of emulsion-templated porous polymers using thiol-ene and thiol-yne chemistry. *Polym Chem* **2**, 559-562 (2011).

139. Langford, C., Johnson, D. & Cameron, N. Chemical functionalization of emulsion-templated porous polymers by thiol–ene "click" chemistry. *Polymer Chemistry* **5**, 6200-6206 (2014).

140. Hynes, R.O. Integrins: bidirectional, allosteric signaling machines. *Cell* **110**, 673-687 (2002).

141. Giancotti, F.G. & Ruoslahti, E. Integrin signaling. *Science* **285**, 1028-1033 (1999).

142. Chastain, S.R., Kundu, A.K., Dhar, S., Calvert, J.W. & Putnam, A.J. Adhesion of mesenchymal stem cells to polymer scaffolds occurs via distinct ECM ligands and controls their osteogenic differentiation. *Journal of Biomedical Materials Research Part A* **78**, 73-85 (2006).

143. Bokhari, M.A., Akay, G., Zhang, S. & Birch, M.A. The enhancement of osteoblast growth and differentiation in vitro on a peptide hydrogel—polyHIPE polymer hybrid material. *Biomaterials* **26**, 5198-5208 (2005).

144. Chen, G., Sato, T., Ushida, T., Ochiai, N. & Tateishi, T. Tissue engineering of cartilage using a hybrid scaffold of synthetic polymer and collagen. *Tissue Engineering* **10**, 323-330 (2004).

145. Timmer, M.D., Horch, A.R., Ambrose, C.G. & Mikos, A.G. Effect of physiological temperature on the mechanical properties and network structure of biodegradable poly(propylene fumarate)-based networks. *J Biomat Sci Polym Ed* **14**, 369-382 (2003).

146. Whitely, M.E. et al. Prevention of Oxygen Inhibition of PolyHIPE Radical Polymerization Using a Thiol-Based Cross-Linker. *ACS biomaterials science & engineering* **3**, 409-419 (2017).

147. Foudazi, R., Gokun, P., Feke, D.L., Rowan, S.J. & Manas-Zloczower, I. Chemorheology of Poly(high internal phase emulsions). *Macromolecules* **46**, 5393-5396 (2013).

148. Barbetta, A. & Cameron, N.R. Morphology and surface area of emulsion-derived (PolyHIPE) solid foams prepared with oil-phase soluble porogenic solvents: Span 80 as surfactant. *Macromolecules* **37**, 3188-3201 (2004).

149. Gregory, T.R. Nucleotypic effects without nuclei: genome size and erythrocyte size in mammals. *Genome* **43**, 895-901 (2000).

150. Kloosterboer, J.G. in Electronic applications 1-61 (Springer, 1988).

151. Gou, L., Coretsopoulos, C.N. & Scranton, A.B. Measurement of the dissolved oxygen concentration in acrylate monomers with a novel photochemical method. *Journal of Polymer Science Part A: Polymer Chemistry* **42**, 1285-1292 (2004).

152. Rydholm, A.E., Bowman, C.N. & Anseth, K.S. Degradable thiol-acrylate photopolymers: polymerization and degradation behavior of an in situ forming biomaterial. *Biomaterials* **26**, 4495-4506 (2005).

153. Bowman, C.N. & Kloxin, C.J. Toward an enhanced understanding and implementation of photopolymerization reactions. *AIChE Journal* **54**, 2775-2795 (2008).

154. Decker, C. UV-curing chemistry: past, present, and future. *JCT, Journal of coatings technology* **59**, 97-106 (1987).

155. Studer, K., Decker, C., Beck, E. & Schwalm, R. Overcoming oxygen inhibition in UV-curing of acrylate coatings by carbon dioxide inerting, Part I. *Progress in Organic Coatings* **48**, 92-100 (2003).

156. Ligon, S.C., Husár, B., Wutzel, H., Holman, R. & Liska, R. Strategies to reduce oxygen inhibition in photoinduced polymerization. *Chemical reviews* **114**, 557-589 (2013).

157. Murphy, C.M., Haugh, M.G. & O'Brien, F.J. The effect of mean pore size on cell attachment, proliferation and migration in collagen–glycosaminoglycan scaffolds for bone tissue engineering. *Biomaterials* **31**, 461-466 (2010).

158. Barbetta, A. et al. in Macromolecular Symposia, Vol. 226 203-212 (Wiley Online Library, 2005).

159. Hainey, P., Huxham, I., Rowatt, B., Sherrington, D. & Tetley, L. Synthesis and ultrastructural studies of styrene-divinylbenzene polyhipe polymers. *Macromolecules* **24**, 117-121 (1991).

160. Lee, T., Guymon, C., Jönsson, E.S. & Hoyle, C. The effect of monomer structure on oxygen inhibition of (meth) acrylates photopolymerization. *Polymer* **45**, 6155-6162 (2004).

161. Peter, S.J., Lu, L., Kim, D.J. & Mikos, A.G. Marrow stromal osteoblast function on a poly (propylene fumarate)/β-tricalcium phosphate biodegradable orthopaedic composite. *Biomaterials* **21**, 1207-1213 (2000).

162. Peter, S.J. et al. In vitro degradation of a poly (propylene fumarate)/β-tricalcium phosphate composite orthopaedic scaffold. *Tissue Engineering* **3**, 207-215 (1997).

163. Yaszemski, M.J. et al. The ingrowth of new bone tissue and initial mechanical properties of a degrading polymeric composite scaffold. *Tissue engineering* **1**, 41-52 (1995).

164. Stańczyk, M. & Van Rietbergen, B. Thermal analysis of bone cement polymerisation at the cement–bone interface. *Journal of biomechanics* **37**, 1803-1810 (2004).

165. Cole, M.A., Jankousky, K.C. & Bowman, C.N. Redox initiation of bulk thiol–ene polymerizations. *Polymer chemistry* **4**, 1167-1175 (2013).

166. Fouassier, J.-P. & Rabek, J.F. Radiation curing in polymer science and technology: Practical aspects and applications, Vol. 4. (Springer Science & Business Media, 1993).

167. Mistry, A. et al. *In vivo* bone biocompatibility and degradation of porous fumarate-based polymer/alumoxane nanocomposites for bone tissue engineering. *J Biomed Mater Res A* **92A**, 451-462 (2010).

168. Patel, Z.S. et al. Dual delivery of an angiogenic and an osteogenic growth factor for bone regeneration in a critical size defect model. *Bone* **43**, 931-940 (2008).

169. Kim, S.-S., Park, M.S., Jeon, O., Choi, C.Y. & Kim, B.-S. Poly (lactide-co-glycolide)/hydroxyapatite composite scaffolds for bone tissue engineering. *Biomaterials* **27**, 1399-1409 (2006).

170. Dumas, J.E. et al. Injectable reactive biocomposites for bone healing in critical-size rabbit calvarial defects. *Biomedical Materials* **7**, 024112 (2012).

171. Kim, C.W. et al. Characterization of porous injectable poly-(propylene fumarate)-based bone graft substitute. *Journal of Biomedical Materials Research Part A* **85**, 1114-1119 (2008).

172. P. Fisher, J., Holland, T.A., Dean, D., Engel, P.S. & Mikos, A.G. Synthesis and properties of photocross-linked poly (propylene fumarate) scaffolds. *Journal of Biomaterials Science, Polymer Edition* **12**, 673-687 (2001).

173. Dumas, J.E. et al. Synthesis and characterization of an injectable allograft bone/polymer composite bone void filler with tunable mechanical properties. *Tissue Engineering Part A* **16**, 2505-2518 (2010).

174. Gorna, K. & Gogolewski, S. Biodegradable porous polyurethane scaffolds for tissue repair and regeneration. *Journal of Biomedical Materials Research Part A* **79**, 128-138 (2006).

175. Graham, N.B. & Cameron, A. Nanogels and microgels: The new polymeric materials playground. *Pure Appl Chem* **70**, 1271-1275 (1998).

176. Schoenmakers, R.G., van de Wetering, P., Elbert, D.L. & Hubbell, J.A. The effect of the linker on the hydrolysis rate of drug-linked ester bonds. *J Control Release* **95**, 291-300 (2004).

177. Timmer, M.D., Shin, H., Horch, R.A., Ambrose, C.G. & Mikos, A.G. In vitro cytotoxicity of injectable and biodegradable poly (propylene fumarate)-based networks: unreacted macromers, cross-linked networks, and degradation products. *Biomacromolecules* **4**, 1026-1033 (2003).

178. Peter, S.J., Miller, S.T., Zhu, G., Yasko, A.W. & Mikos, A.G. In vivo degradation of a poly(propylene fumarate)/β-tricalcium phosphate injectable composite scaffold. *J Biomed Mater Res* **41**, 1-7 (1998).

179. He, S. et al. Synthesis of biodegradable poly (propylene fumarate) networks with poly (propylene fumarate)–diacrylate macromers as crosslinking agents and characterization of their degradation products. *Polymer* **42**, 1251-1260 (2001).

180. Shi, X.e.a. Fabrication of porous ultra-short single-walled carbon nanotube nanocomposite scaffolds for bone tissue engineering. *Biomaterials* **28**, 4078-4090 (2007).

181. Roberts, J.J. & Bryant, S.J. Comparison of photopolymerizable thiol-ene PEG and acrylate-based PEG hydrogels for cartilage development. *Biomaterials* **34**, 9969-9979 (2013).

182. Ruoslahti, E. & Pierschbacher, M.D. New perspectives in cell adhesion: RGD and integrins. *Science* **238**, 491-497 (1987).

183. Cosgriff-Hernandez, E. et al. Bioactive hydrogels based on designer collagens. *Acta biomaterialia* **6**, 3969-3977 (2010).

184. Clover, J., Dodds, R. & Gowen, M. Integrin subunit expression by human osteoblasts and osteoclasts in situ and in culture. *Journal of cell science* **103**, 267-271 (1992).

185. Schneider, G.B., Zaharias, R. & Stanford, C. Osteoblast integrin adhesion and signaling regulate mineralization. *Journal of dental research* **80**, 1540-1544 (2001).

186. Artico, M. et al. Bone autografting of the calvaria and craniofacial skeleton: historical background, surgical results in a series of 15 patients, and review of the literature. *World Neurosurgery* **60**, 71-79 (2003).

187. Lanza, R., Langer, R. & Vacanti, J.P. Principles of tissue engineering. (Academic press, 2011).

188. Vacanti, J.P. & Langer, R. Tissue engineering: the design and fabrication of living replacement devices for surgical reconstruction and transplantation. *The lancet* **354**, S32-S34 (1999).

189. Sears, N., Dhavalikar, P., Whitely, M. & Cosgriff-Hernandez, E. Fabrication of biomimetic bone grafts with multi-material 3D printing. *Biofabrication* **9**, 025020 (2017).

190. Sears, N.A., Dhavalikar, P.S. & Cosgriff-Hernandez, E.M. Emulsion inks for 3D printing of high porosity materials. *Macromolecular rapid communications* **37**, 1369-1374 (2016).

191. Caplan, A. Why are MSCs therapeutic? New data: new insight. *Journal of Pathology* **217**, 318-324 (2009).

192. Caplan, A.I. Review: mesenchymal stem cells: cell-based reconstructive therapy in orthopedics. *Tissue engineering* **11**, 1198-1211 (2005).

193. Caplan, A.I. & Dennis, J.E. Mesenchymal stem cells as trophic mediators. *Journal of Cellular Biochemistry* **98**, 1076-1084 (2006).

194. Templin, C., Lüscher, T.F. & Landmesser, U. Cell-based cardiovascular repair and regeneration in acute myocardial infarction and chronic ischemic cardiomyopathy–current status and future developments. *International journal of developmental biology* **55**, 407-417 (2011).

195. Gómez-Barrena, E. et al. Bone regeneration: stem cell therapies and clinical studies in orthopaedics and traumatology. *Journal of cellular and molecular medicine* **15**, 1266-1286 (2011).

196. Loebel, C. & Burdick, J.A. Engineering Stem and Stromal Cell Therapies for Musculoskeletal Tissue Repair. *Cell stem cell* (2018).

197. Hoffman, M.D., Van Hove, A.H. & Benoit, D.S. Degradable hydrogels for spatiotemporal control of mesenchymal stem cells localized at decellularized bone allografts. *Acta biomaterialia* **10**, 3431-3441 (2014).

198. Park, H., Temenoff, J.S., Tabata, Y., Caplan, A.I. & Mikos, A.G. Injectable biodegradable hydrogel composites for rabbit marrow mesenchymal stem cell and growth factor delivery for cartilage tissue engineering. *Biomaterials* **28**, 3217-3227 (2007).

199. Zhou, H. & Xu, H.H. The fast release of stem cells from alginate-fibrin microbeads in injectable scaffolds for bone tissue engineering. *Biomaterials* **32**, 7503-7513 (2011).

200. Vo, T. et al. Injectable dual-gelling cell-laden composite hydrogels for bone tissue engineering. *Biomaterials* **83**, 1-11 (2016).

201. Man, Y. et al. Angiogenic and osteogenic potential of platelet-rich plasma and adipose-derived stem cell laden alginate microspheres. *Biomaterials* **33**, 8802-8811 (2012).

202. Yao, R., Zhang, R., Luan, J. & Lin, F. Alginate and alginate/gelatin microspheres for human adipose-derived stem cell encapsulation and differentiation. *Biofabrication* **4**, 025007 (2012).

203. Benoit, D.S., Schwartz, M.P., Durney, A.R. & Anseth, K.S. Small functional groups for controlled differentiation of hydrogel-encapsulated human mesenchymal stem cells. *Nature materials* **7**, 816 (2008).

204. Williams, C.G. et al. In vitro chondrogenesis of bone marrow-derived mesenchymal stem cells in a photopolymerizing hydrogel. *Tissue engineering* **9**, 679-688 (2003).

205. Griffin, D.R. & Kasko, A.M. Photodegradable macromers and hydrogels for live cell encapsulation and release. *Journal of the American Chemical Society* **134**, 13103-13107 (2012).

206. Mawad, D., Martens, P.J., Odell, R.A. & Poole-Warren, L.A. The effect of redox polymerisation on degradation and cell responses to poly (vinyl alcohol) hydrogels. *Biomaterials* **28**, 947-955 (2007).

207. Sarac, A. Redox polymerization. *Progress in Polymer Science* **24**, 1149-1204 (1999).

208. Johnson, L.M., Fairbanks, B.D., Anseth, K.S. & Bowman, C.N. Enzyme-mediated redox initiation for hydrogel generation and cellular encapsulation. *Biomacromolecules* **10**, 3114-3121 (2009).

209. Anseth, K.S. et al. In situ forming degradable networks and their application in tissue engineering and drug delivery. *Journal of controlled release* **78**, 199-209 (2002).

210. Metters, A., Anseth, K. & Bowman, C. Fundamental studies of a novel, biodegradable PEG-b-PLA hydrogel. *Polymer* **41**, 3993-4004 (2000).

211. Williams, C.G., Malik, A.N., Kim, T.K., Manson, P.N. & Elisseeff, J.H. Variable cytocompatibility of six cell lines with photoinitiators used for polymerizing hydrogels and cell encapsulation. *Biomaterials* **26**, 1211-1218 (2005).

212. Fedorovich, N.E. et al. The effect of photopolymerization on stem cells embedded in hydrogels. *Biomaterials* **30**, 344-353 (2009).

213. Hudalla, G.A., Eng, T.S. & Murphy, W.L. An approach to modulate degradation and mesenchymal stem cell behavior in poly (ethylene glycol) networks. *Biomacromolecules* **9**, 842-849 (2008).

214. Temenoff, J.S., Shin, H., Conway, D.E., Engel, P.S. & Mikos, A.G. In vitro cytotoxicity of redox radical initiators for cross-linking of oligo (poly (ethylene glycol) fumarate) macromers. *Biomacromolecules* **4**, 1605-1613 (2003).

215. Jongpaiboonkit, L. et al. An adaptable hydrogel array format for 3-dimensional cell culture and analysis. *Biomaterials* **29**, 3346-3356 (2008).

216. Van De Wetering, P., Metters, A.T., Schoenmakers, R.G. & Hubbell, J.A. Poly (ethylene glycol) hydrogels formed by conjugate addition with controllable swelling, degradation, and release of pharmaceutically active proteins. *Journal of Controlled Release* **102**, 619-627 (2005).

217. Malliaras, K., Kreke, M. & Marban, E. The stuttering progress of cell therapy for heart disease. *Clinical Pharmacology & Therapeutics* **90**, 532-541 (2011).

218. Kim, K., Dean, D., Lu, A., Mikos, A.G. & Fisher, J.P. Early osteogenic signal expression of rat bone marrow stromal cells is influenced by both hydroxyapatite nanoparticle content and initial cell seeding density in biodegradable nanocomposite scaffolds. *Acta biomaterialia* **7**, 1249-1264 (2011).

219. Xu, H.H., Takagi, S., Quinn, J.B. & Chow, L.C. Fast-setting calcium phosphate scaffolds with tailored macropore formation rates for bone regeneration. *Journal of Biomedical Materials Research Part A* **68**, 725-734 (2004).

220. Arinzeh, T.L. et al. Allogeneic mesenchymal stem cells regenerate bone in a critical-sized canine segmental defect. *JBJS* **85**, 1927-1935 (2003).

221. Ball, A.N. et al. The Challenges of Promoting Osteogenesis in Segmental Bone Defects and Osteoporosis. *Journal of Orthopaedic Research* (2017).

222. Mygind, T. et al. Mesenchymal stem cell ingrowth and differentiation on coralline hydroxyapatite scaffolds. *Biomaterials* **28**, 1036-1047 (2007).

223. Jaiswal, N., Haynesworth, S.E., Caplan, A.I. & Bruder, S.P. Osteogenic differentiation of purified, culture-expanded human mesenchymal stem cells in vitro. *Journal of cellular biochemistry* **64**, 295-312 (1997).

224. Maeno, S. et al. The effect of calcium ion concentration on osteoblast viability, proliferation and differentiation in monolayer and 3D culture. *Biomaterials* **26**, 4847-4855 (2005).

225. Marie, P.J. The calcium-sensing receptor in bone cells: a potential therapeutic target in osteoporosis. *Bone* **46**, 571-576 (2010).

226. Hoppe, A., Güldal, N.S. & Boccaccini, A.R. A review of the biological response to ionic dissolution products from bioactive glasses and glass-ceramics. *Biomaterials* **32**, 2757-2774 (2011).

227. Lan, P.X., Lee, J.W., Seol, Y.-J. & Cho, D.-W. Development of 3D PPF/DEF scaffolds using micro-stereolithography and surface modification. *Journal of Materials Science: Materials in Medicine* **20**, 271-279 (2009).

228. Chen, X. et al. Effect of surface roughness of Ti, Zr, and TiZr on apatite precipitation from simulated body fluid. *Biotechnology and bioengineering* **101**, 378-387 (2008).

229. Chen, X.-B., Li, Y.-C., Du Plessis, J., Hodgson, P.D. & Wen, C.e. Influence of calcium ion deposition on apatite-inducing ability of porous titanium for biomedical applications. *Acta biomaterialia* **5**, 1808-1820 (2009).

230. Burchardt, H. The biology of bone graft repair. *Clinical orthopaedics and related research*, 28-42 (1983).

231. Khan, Y., Yaszemski, M.J., Mikos, A.G. & Laurencin, C.T. Tissue engineering of bone: material and matrix considerations. *JBJS* **90**, 36-42 (2008).

232. Chen, D., Zhao, M. & Mundy, G.R. Bone morphogenetic proteins. *Growth factors* **22**, 233-241 (2004).

233. Wozney, J.M. & Rosen, V. Bone morphogenetic protein and bone morphogenetic protein gene family in bone formation and repair. *Clinical orthopaedics and related research*, 26-37 (1998).

234. Kanczler, J. & Oreffo, R. Osteogenesis and angiogenesis: the potential for engineering bone. *Eur Cell Mater* **15**, 100-114 (2008).

235. Rawadi, G., Vayssiere, B., Dunn, F., Baron, R. & Roman-Roman, S. BMP-2 controls alkaline phosphatase expression and osteoblast mineralization by a Wnt autocrine loop. *Journal of Bone and Mineral Research* **18**, 1842-1853 (2003).

236. Lee, K., Silva, E.A. & Mooney, D.J. Growth factor delivery-based tissue engineering: general approaches and a review of recent developments. *Journal of the Royal Society Interface* **8**, 153-170 (2011).

237. Young, S., Wong, M., Tabata, Y. & Mikos, A.G. Gelatin as a delivery vehicle for the controlled release of bioactive molecules. *Journal of controlled release* **109**, 256-274 (2005).

238. Li, C., Vepari, C., Jin, H.-J., Kim, H.J. & Kaplan, D.L. Electrospun silk-BMP-2 scaffolds for bone tissue engineering. *Biomaterials* **27**, 3115-3124 (2006).

239. Kempen, D.H. et al. Retention of in vitro and in vivo BMP-2 bioactivities in sustained delivery vehicles for bone tissue engineering. *Biomaterials* **29**, 3245-3252 (2008).

240. Kretlow, J.D., Klouda, L. & Mikos, A.G. Injectable matrices and scaffolds for drug delivery in tissue engineering. *Advanced drug delivery reviews* **59**, 263-273 (2007).

241. Uludag, H., D'Augusta, D., Palmer, R., Timony, G. & Wozney, J. Characterization of rhBMP-2 pharmacokinetics implanted with biomaterial carriers in the rat ectopic model. *Journal of Biomedical Materials Research: An Official Journal of The Society for Biomaterials, The Japanese Society for Biomaterials, and The Australian Society for Biomaterials* **46**, 193-202 (1999).

242. Seeherman, H. & Wozney, J.M. Delivery of bone morphogenetic proteins for orthopedic tissue regeneration. *Cytokine & growth factor reviews* **16**, 329-345 (2005).

243. Cho, T.J., Gerstenfeld, L.C. & Einhorn, T.A. Differential temporal expression of members of the transforming growth factor β superfamily during murine fracture healing. *Journal of Bone and Mineral Research* **17**, 513-520 (2002).

244. Celeste, A.J. et al. Identification of transforming growth factor beta family members present in bone-inductive protein purified from bovine bone. *Proceedings of the National Academy of Sciences* **87**, 9843-9847 (1990).

245. Uludag, H., Gao, T., Porter, T.J., Friess, W. & Wozney, J.M. Delivery systems for BMPs: factors contributing to protein retention at an application site. *JBJS* **83**, S128-S135 (2001).

246. Vo, T.N., Kasper, F.K. & Mikos, A.G. Strategies for controlled delivery of growth factors and cells for bone regeneration. *Advanced drug delivery reviews* **64**, 1292-1309 (2012).

247. Brazel, C.S. & Peppas, N.A. Mechanisms of solute and drug transport in relaxing, swellable, hydrophilic glassy polymers. *Polymer* **40**, 3383-3398 (1999).

248. Jeon, O., Powell, C., Solorio, L.D., Krebs, M.D. & Alsberg, E. Affinity-based growth factor delivery using biodegradable, photocrosslinked heparin-alginate hydrogels. *Journal of Controlled Release* **154**, 258-266 (2011).

249. Bhakta, G. et al. Hyaluronic acid-based hydrogels functionalized with heparin that support controlled release of bioactive BMP-2. *Biomaterials* **33**, 6113-6122 (2012).

250. Crouzier, T. et al. The performance of BMP-2 loaded TCP/HAP porous ceramics with a polyelectrolyte multilayer film coating. *Biomaterials* **32**, 7543-7554 (2011).

251. Kuboki, Y. et al. BMP-induced osteogenesis on the surface of hydroxyapatite with geometrically feasible and nonfeasible structures: topology of osteogenesis. *Journal of Biomedical Materials Research: An Official Journal of The Society for Biomaterials, The Japanese Society for Biomaterials, and the Australian Society for Biomaterials* **39**, 190-199 (1998).

252. Crotts, G. & Park, T.G. Protein delivery from poly (lactic-co-glycolic acid) biodegradable microspheres: release kinetics and stability issues. *Journal of microencapsulation* **15**, 699-713 (1998).

253. Kempen, D.H. et al. Effect of local sequential VEGF and BMP-2 delivery on ectopic and orthotopic bone regeneration. *Biomaterials* **30**, 2816-2825 (2009).

254. Arnold, M.M., Gorman, E.M., Schieber, L.J., Munson, E.J. & Berkland, C. NanoCipro encapsulation in monodisperse large porous PLGA microparticles. *Journal of Controlled Release* **121**, 100-109 (2007).

255. Yang, Y. et al. Development of highly porous large PLGA microparticles for pulmonary drug delivery. *Biomaterials* **30**, 1947-1953 (2009).

256. Cai, Y., Chen, Y., Hong, X., Liu, Z. & Yuan, W. Porous microsphere and its applications. *International journal of nanomedicine* **8**, 1111 (2013).

257. Gentile, P., Chiono, V., Carmagnola, I. & Hatton, P.V. An overview of poly (lactic-co-glycolic) acid (PLGA)-based biomaterials for bone tissue engineering. *International journal of molecular sciences* **15**, 3640-3659 (2014).

258. Kempen, D.H. et al. Controlled drug release from a novel injectable biodegradable microsphere/scaffold composite based on poly (propylene fumarate). *Journal of Biomedical Materials Research Part A* **77**, 103-111 (2006).

259. Brown, K.V. et al. Improving bone formation in a rat femur segmental defect by controlling bone morphogenetic protein-2 release. *Tissue Engineering Part A* **17**, 1735-1746 (2011).

260. Cleland, J.L., Powell, M.F. & Shire, S.J. The development of stable protein formulations: a close look at protein aggregation, deamidation, and oxidation. *Critical reviews in therapeutic drug carrier systems* **10**, 307-377 (1993).

261. Schliephake, H. Application of bone growth factors—the potential of different carrier systems. *Oral and maxillofacial surgery* **14**, 17-22 (2010).

262. Moglia, R. et al. Solvent-Free Fabrication of polyHIPE Microspheres for Controlled Release of Growth Factors. *Macromolecular rapid communications* **35**, 1301-1305 (2014).

263. Freiberg, S. & Zhu, X. Polymer microspheres for controlled drug release. *International journal of pharmaceutics* **282**, 1-18 (2004).

264. Santoro, M., Tatara, A.M. & Mikos, A.G. Gelatin carriers for drug and cell delivery in tissue engineering. *Journal of controlled release* **190**, 210-218 (2014).

265. Tan, H., Huang, D., Lao, L. & Gao, C. RGD modified PLGA/gelatin microspheres as microcarriers for chondrocyte delivery. *Journal of Biomedical Materials Research Part B: Applied Biomaterials* **91**, 228-238 (2009).

266. Yang, Y.-Y., Chia, H.-H. & Chung, T.-S. Effect of preparation temperature on the characteristics and release profiles of PLGA microspheres containing protein fabricated by double-emulsion solvent extraction/evaporation method. *Journal of Controlled Release* **69**, 81-96 (2000).

267. Kirby, G.T. et al. PLGA-based microparticles for the sustained release of BMP-2. *Polymers* **3**, 571-586 (2011).

268. Fredenberg, S., Wahlgren, M., Reslow, M. & Axelsson, A. The mechanisms of drug release in poly (lactic-co-glycolic acid)-based drug delivery systems—a review. *International journal of pharmaceutics* **415**, 34-52 (2011).

269. Crotts, G., Sah, H. & Park, T.G. Adsorption determines in-vitro protein release rate from biodegradable microspheres: quantitative analysis of surface area during degradation. *Journal of controlled release* **47**, 101-111 (1997).

270. van de Weert, M., Hennink, W.E. & Jiskoot, W. Protein instability in poly (lactic-co-glycolic acid) microparticles. *Pharmaceutical research* **17**, 1159-1167 (2000).

271. Yadav, P.S., Prashar, P. & Bandyopadhyay, A. BRITER: a BMP responsive osteoblast reporter cell line. *PloS one* **7**, e37134 (2012).

272. Hsieh, C.-Y., Hsieh, H.-J., Liu, H.-C., Wang, D.-M. & Hou, L.-T. Fabrication and release behavior of a novel freeze-gelled chitosan/γ-PGA scaffold as a carrier for rhBMP-2. *Dental Materials* **22**, 622-629 (2006).

273. Takada, T. et al. Sulfated polysaccharides enhance the biological activities of bone morphogenetic proteins. *Journal of Biological Chemistry* **278**, 43229-43235 (2003).

274. Seto, S.P., Miller, T. & Temenoff, J.S. Effect of selective heparin desulfation on preservation of bone morphogenetic protein-2 bioactivity after thermal stress. *Bioconjugate chemistry* **26**, 286-293 (2015).

275. Zhao, J. et al. Trehalose maintains bioactivity and promotes sustained release of BMP-2 from lyophilized CDHA scaffolds for enhanced osteogenesis in vitro and in vivo. *PLoS One* **8**, e54645 (2013).

276. Bramono, D.S. et al. Bone marrow-derived heparan sulfate potentiates the osteogenic activity of bone morphogenetic protein-2 (BMP-2). *Bone* **50**, 954-964 (2012).

277. Zhao, B. et al. Heparin potentiates the in vivo ectopic bone formation induced by bone morphogenetic protein-2. *Journal of Biological Chemistry* **281**, 23246-23253 (2006).

278. Kempen, D.H. et al. Effect of autologous bone marrow stromal cell seeding and bone morphogenetic protein-2 delivery on ectopic bone formation in a microsphere/poly (propylene fumarate) composite. *Tissue Engineering Part A* **15**, 587-594 (2008).

279. Perez, R.A. & Kim, H.-W. Core–shell designed scaffolds for drug delivery and tissue engineering. *Acta biomaterialia* **21**, 2-19 (2015).

280. Link, D.P. et al. Bone response and mechanical strength of rabbit femoral defects filled with injectable CaP cements containing TGF-β1 loaded gelatin microparticles. *Biomaterials* **29**, 675-682 (2008).